TIMING, GROWTH AND HOMEOSTASIS: AN ANTHOLOGY OF THREE NOVEL PLAYERS IN *DROSOPHILA MELANOGASTER*

A DISSERTATION
SUBMITTED TO THE FACULTY OF THE GRADUATE SCHOOL
OF THE UNIVERSITY OF MINNESOTA
BY

ARPAN GHOSH

IN PARTIAL FULFILLMENT OF THE REQUIREMENTS
FOR THE DEGREE OF
DOCTOR OF PHILOSOPHY

MICHAEL B. O'CONNOR, ADVISOR

AUGUST 2013

ACKNOWLEDGEMENTS

I would like to acknowledge and thank the members of the O'Connor lab, particularly MaryJane O'Connor, Aidan Peterson and Naoki Yamanaka for their assistance and guidance in the preparation of this work. I would like to thank my advisor Dr. Michael O'Connor for giving me the opportunity to work on the projects presented in this thesis, for his valuable advise and also for providing an environment that encourages independent thinking during the course of my graduate studies. I would also like to show my appreciation for my committee members Dr. Anna Petryk, Dr. Do-Hyung Kim, Dr. Hiroshi Nakato and Dr. Sean Conner for their valuable suggestions and guidance. I thank MaryJane O'Connor for generating the *kri* mutants and Emma Leof for characterizing the *kri* mutants. This work was supported by grants from the NIH, HHMI and the Ordway foundation. I would also like to thank the American Heart Association for supporting me with the AHA pre-doctoral fellowship from January-2011 to December-2012. Lastly I want to extend my gratitude to my family, friends and past mentors; without their support, encouragement and guidance I would not have been able to finish this graduation study.

TABLE OF CONTENTS

LIST OF TABLES

CHAPTER 3

APPENDIX I

APPENDIX II

LIST OF FIGURES

CHAPTER 1:

CHAPTER 2:

CHAPTER 1

INTRODUCTION

Developmental timing, growth and homeostasis form the cornerstones that shape the genesis and subsequent maintenance of a healthy adult for all multicellular organisms. Understanding the mechanisms that regulate these processes has important implications both from the perspective of our understanding of basic biology and also for our understanding of complex biological disorders involving these processes. For instance, the age of onset of human puberty has advanced significantly in the last few decades and precocious puberty has been shown to cause lasting psychological and physical complications (Kaplowitz and Oberfield, 1999; Lazar and Phillip, 2012; Sonis et al., 1985; Walvoord, 2010). An in-depth understanding of the mechanisms that regulate developmental transitions can help us better evaluate the causes of precocious puberty and possibly devise strategies to prevent them. Similarly, deregulation of homeostatic mechanisms leads to disorders like obesity and diabetes, that have become a worldwide health concern and combating these multifaceted disorders will require an extensive understanding of the regulatory networks that regulate homeostasis (Bruce and Hanson; Kirk and Klein, 2009; Tseng et al., 2010). Understanding growth, on the other hand, has significant applications in translational research involving cancer biology and regeneration (Tennessen et al., 2011).

My thesis work explores the mechanisms regulating developmental timing, homeostasis and growth using the model organism *Drosophila melanogaster*.

The fast generation time of this model organism and presence of defined developmental transitions, that manifest as clear physiological events like molting and metamorphosis, make *Drosophila* an excellent model to study developmental timing (Thummel, 2001; Yamanaka et al., 2013). Additionally, the exceptional growth observed during the larval stages, along with the fact that the larva grows in close contact with its environment necessitating robust homeostatic mechanisms, provides a unique opportunity to use these animals to study growth and homeostasis. The fruit fly is also highly amenable to genetic, biochemical and cell biological manipulations allowing easy experimental investigations. This chapter briefly discusses the mechanisms that are known to regulate timing, growth and homeostasis in *Drosophila* and parallels that exist between *Drosophila* and vertebrates.

1.1 Life cycle of *Drosophila melanogaster*

Life cycle of *Drosophila* starts as an egg that is produced by sexual reproduction involving two healthy adults. *Drosophila* eggs develop into first instar larvae that, after hatching, undergo two molting stages to give rise to second and third instar larvae. During the larval stages the larvae feed constantly and undergo a remarkable 150-200 fold growth. At the end of the feeding stage larvae start wandering out of the food and enter metamorphosis by forming pupae. The animals undergo metamorphosis inside the pupal case and eclose as adults, thereby completing the life cycle. Post eclosion adult flies need to reach

sexual maturity before they can reproduce. Timing of the transitions between the various developmental stages in *Drosophila* is sensitive to both internal and external factors (Tennessen and Thummel, 2011; Thummel, 2001). External factors like humidity, length of day light and temperature can all significantly effect developmental timing with temperature affecting timing most profoundly. Under lab culture conditions of 25^{O}C embryonic development is completed in about 24 hours (Figure 1). First and second instar larval stages last about 24 hours each, and the third instar stage lasts about 48 hours. Subsequently, the larvae wander for about 12 hours and enter pupal stage. Pupal stage then lasts about three and a half days and is followed by eclosion of adults. The entire developmental cycle is thereby completed in a total of 9 days from egg to adult.

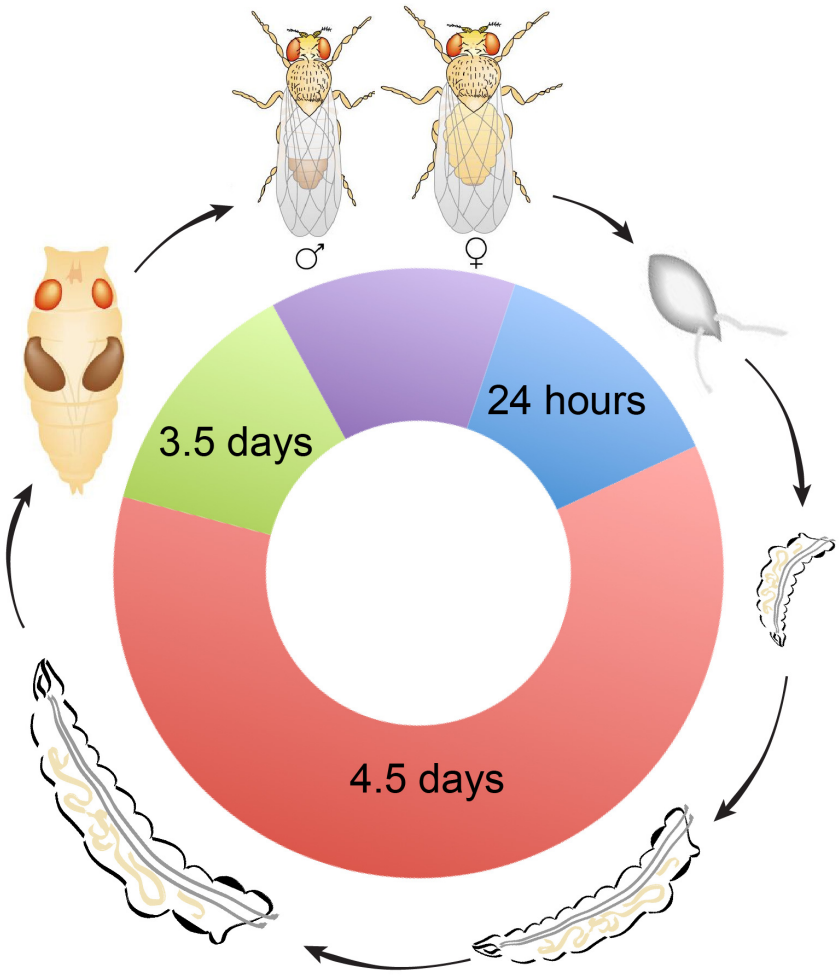

Figure 1: A schematic showing the life cycle of *Drosophila melanogaster*

A schematic of the *Drosophila* life cycle showing the various developmental stages and the estimated time spent at each stage. The duration of each stage shown here is for animals that are grown at 25^{O}C. The three larval stages are demarcated by molting events at the end of each instar. First instar and second instar larval stages last about 24 hours each. Third instar stage is about 48 hours long and the larvae spend another 12 hours wandering before entering pupal stage.

1.2 Regulation of developmental transitions in *Drosophila melanogaster*

Internally, a number of hormonal and neuropeptidergic signals regulate the various developmental transitions (Figure 2 and 3). The most important among these signals is the insect steroid hormone ecdysone (E) (Yamanaka et al., 2013). E is produced primarily by the larval prothoracic glands (PGs), a pair of endocrine organs located in the ring gland, and is released into the hemolymph in response to multiple environmental cues that converge on the PGs to regulate developmental transitions (Yamanaka et al., 2013). Once released in the hemolymph, E is taken up by the peripheral tissues where it is converted to its active form 20-hydroxyecdysone (20E) by the action of a P450 monooxygenase expressed in the non-endocrine tissues (Petryk et al., 2003). 20E ultimately acts as the primary developmental hormonal signal that leads to manifestation of various physiological, morphological and behavioral changes by initiating necessary gene expression cascades (Thummel, 2001). Consistent with this understanding, ecdysone titers peak ahead of each of the developmental transitions and dictate progression from the embryonic stage to eclosion of an adult fly (Figure 2). The intensity of these peaks, along with additional regulatory mechanisms including, but not limited to, differential expression of receptor isoforms and primary ecdysone inducible factors, dictate the spatio-temporal effect of ecdysone signaling at the various developmental stages. While ecdysone is the primary effector of developmental transitions, production and

release of ecdysone from the PGs is regulated by mechanisms that integrate various environmental, metabolic and homeostatic cues that are conducive for healthy development (Yamanaka et al., 2013).

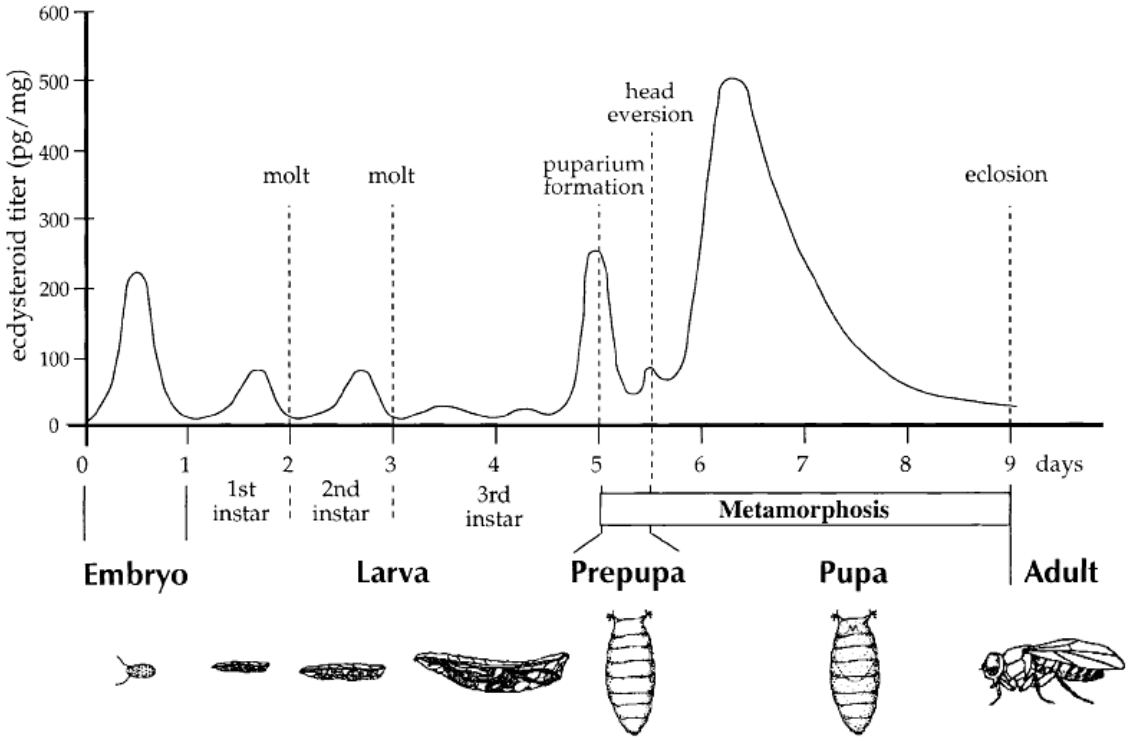

Figure 2: A schematic representation of the ecdysone pulses that trigger each of the major developmental transitions in *Drosophila*

The profile is depicted as 20E (the active form of ecdysone) equivalents in whole body homogenates (Riddiford, 1993). Dotted lines mark the major developmental transitions. From (Thummel, 2001).

Among the various mechanisms that regulate the production and release of ecdysone in *Drosophila*, the role of the insect neuropeptide regulator, prothoracicotropic hormone (PTTH), is most well understood (Mcbrayer et al.,

2007; Rewitz et al., 2009). PTTH is produced by a pair of bilaterally-symmetric peptidergic neurons in the larval brain called the PG neurons. The PG neurons innervate the Prothoracic glands (PGs) and are thought to regulate timing by regulating the release of PTTH that ultimately induces ecdysone biosynthesis by activating a MAP kinase pathway in the PGs (Mcbrayer et al., 2007; Rewitz et al., 2009; Siegmund and Korge, 2001). The PTTH-producing PG neurons have been long believed to be the master regulators of timing that integrate and evaluate multiple developmental cues. However, this view may not present the complete picture of the regulatory network that dictates developmental transitions and has been challenged based on two observations. First, an increasing body of evidence shows that the only developmental cue that the PG neurons respond to is photoperiod (Mcbrayer et al., 2007; Truman and Riddiford, 1974). Second, ablation of the neurons or knocking down the PTTH receptor "*torso*" in the PGs do not block developmental progression but rather only delays developmental transitions (Mcbrayer et al., 2007; Rewitz et al., 2009). Moreover, this delay primarily affects the timing of entering metamorphosis while prior developmental transitions remain mostly un-affected. Therefore, it can be predicted that mechanisms, independent of the PG neurons and PTTH, exist to sense additional developmental parameters and ensure progression of developmental transitions.

The PGs themselves have been proposed to serve as a major regulatory node and have been shown to integrate tropic signals, particularly nutritional signals that relay the metabolic state of the larvae, to induce ecdysteroidogenesis (Figure 3) (Gibbens et al., 2011; Huang et al., 2008). A number of recent publicaitons point to Insulin-Insulin-like growth factor signaling (IIS) as a major regulator of ecdysone synthesis in the PGs (Caldwell et al., 2005; Colombani et al., 2005; Mirth et al., 2005). Since IIS is known to induce tissue growth in *Drosophila* larvae, it was proposed that IIS, via PI3K, regulates growth of the PGs allowing them to reach a mature stage competent for ecdysone production and release. This view is credible in light of the fact that the prothoracicotropic hormone purified from lepidopterans was an insulin family peptide and was later named bombyxin (Ishizaki and Suzuki, 1994). However, artificially inducing over-growth of PG cells does not accelerate developmental transitions indicating that physical cellular growth may not be the mechanism by which IIS regulates ecdysone titers (Cáceres et al., 2011). An alternate hypothesis that has been proposed is that IIS integrates the nutritional status of the animal by cross communicating with the MAPK pathway in the PGs thereby making the PG cells competent to respond to PTTH and produce ecdysone (Yamanaka et al., 2013). Apart from PTTH and IIS, a number of other signaling pathways including TGF-β signaling, nitrous oxide signaling and TOR signaling can affect ecdysone production in the PGs. These signals allow integration of multiple physiological

inputs in the PGs when deciding the right time for transitioning to the next developmental state (Reviewed in (Yamanaka et al., 2013)).

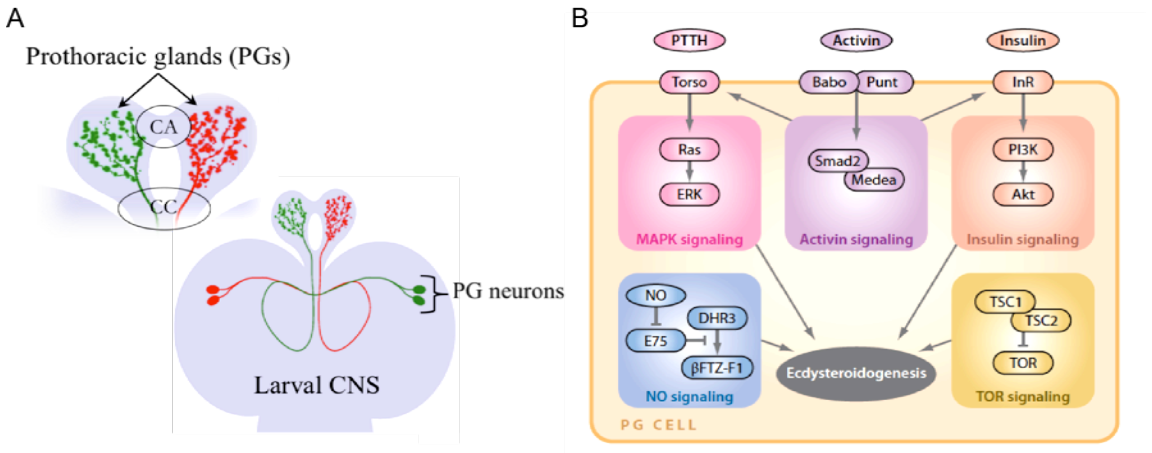

Figure 3: Regulation of ecdysone production and release in *Drosophila*

(A) A schematic of the PG neurons that contralaterally innervated the PGs and stimulated ecdysone release. (B) Schematic of the various signaling pathways that has been shown to influence ecdysteroidogenesis in the *Drosophila* PGs (Yamanaka et al., 2013).

While juvenile-to-adult transitions in holometabolous insects like *Drosophila* seem quite different from mammals, significant parallels can be drawn in terms of mechanistic similarities in induction of hormonal cascades and physiological setups that induce these cascades. Similar to insects, vertebrates attain sexual maturity by undergoing juvenile-to-adult transition through puberty. The timing of pubertal transition in vertebrates is also regulated by a brain-endocrine axis that is similar to insects. Pubertal transition is initiated by the

Kisspeptin-producing neurons in the brain that produce kisspeptin and directly stimulate the gonadotropin-releasing hormone (GnRH)-producing neurons resulting in the release of GnRH (Oakley et al.). GnRH subsequently signals to the pituitary gland through a G-protein coupled receptor and induces release of lutenizing hormone (LH) and follicle-stimulating hormone (FSH) (Ebling and Cronin, 2000). LH and FSH finally stimulate production of sex steroids in the gonads which leads to sexual maturity (LeMaire, 1989). This conservation in the hormonal regulation of developmental transitions along with the advantage of a short life cycle make insects an attractive model system to study the mechanisms involved in regulating developmental transitions and hormonal signaling.

1.3 Mechanisms regulating growth in *Drosophila melanogaster*

Much like other higher animals the final size of the *Drosophila* adult is determined by the amount of growth achieved during juvenile stages. For flies the juvenile stage consists of the three larval instars during which the animal's mass increases a remarkable 200 fold. At the end of the third instar stage, as metamorphosis begins, the larvae cease to grow and the mass of the larvae at this point determines the final body size of the adult (Tennessen and Thummel, 2011). Therefore, the final body size of the adult is linked to the timing of entering metamorphosis. Under circumstances when food is not scarce and the larvae continue to grow at a normal rate, delayed entry into metamorphosis will lead to a larger animal, whereas precocious initiation of metamorphosis will lead to a

smaller animal. In addition to developmental timing, nutrient availability plays a major role in determining the rate of growth and therefore final body size (Tennessen and Thummel, 2011).

Nutrient availability in larvae is sensed by the larval fatbody (FB), a functional homologue of both adipose tissue and the mammalian liver, and is then linked to tissue growth through systemic hormonal signals (Colombani et al., 2003; Géminard et al., 2009; Kim et al., 2008). The nutrient sensing mechanism of the FB primarily relies on amino acid transporters, like slimfast and minidiscs, which allow absorption of amino acids from the hemolymph (Colombani et al., 2003; Martin et al., 2000). Inside FB cells, amino acids activate the highly conserved TOR pathway via poorly understood mechanisms involving Rag GTPases (Kim et al., 2008) leading to secretion of a yet unknown regulatory molecule from the FB that induces growth by primarily targeting the insulin insulin-like growth factor signaling (IIS) pathway (Géminard et al., 2009). The FB thus senses the nutritional state of the animal by amino acid levels via the TOR signaling pathway and remotely regulates growth by linking nutrient availability to insulin signaling (Figure 4).

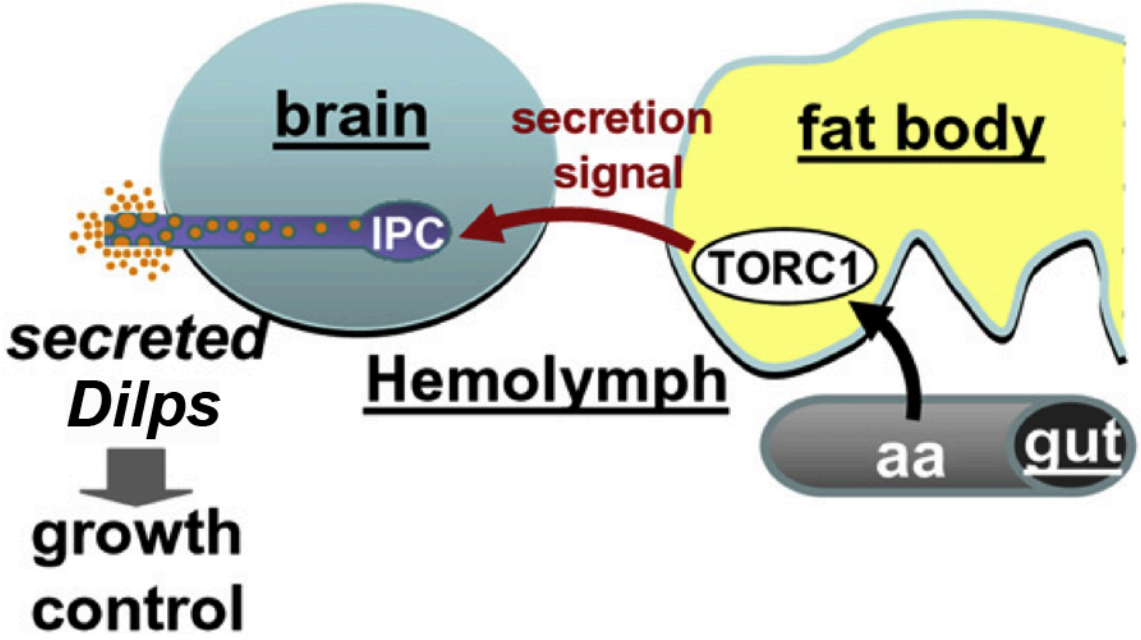

Figure 4: Larval FB remotely regulates Dilp release in response to amino acid availability.

A model showing the remote control of brain Dilp release by the FB. Amino acids, delivered by the gut into circulation, are taken up by the larval FB cells. In the FB cells amino acids activate the TOR pathway, which generates a secreted positive messenger. This messenger signals to the *Drosophila* insulin producing cells (IPCs) in the brain and induces Dilp release. From (Géminard et al., 2009).

Insulin signaling (IIS) in *Drosophila* is mediated by *Drosophila* Insulin-like peptides, and the fly genome encodes 7 of these peptides (Dilp1-7). Three of these peptides, Dilp 2, 3, and 5, are expressed in two clusters of neurosecretory cells located in the larval brain (Brogiolo et al., 2001; Ikeya et al., 2002). These cells are analogous to vertebrate β-cells and release Dilps into circulation in response to nutrient availability (Géminard et al., 2009). Interestingly, despite

being expressed in the same cell, each of these Dilps are regulated differently by nutrients and may have independent functions with respect to growth and nutrient homeostasis. Nutrient availability affects Dilp 3 and 5 at the transcriptional level with starvation significantly down-regulating the mRNA level of these genes (Ikeya et al., 2002). On the contrary, Dilp2 is expressed all the time, and the peptides produced are stored in dense granules in the IPCs until nutritional signals perceived by the FB induce secretion of this peptide into the hemolymph (Géminard et al., 2009). Once in the hemolymph, Dilp peptides bind and activate the sole *Drosophila* insulin receptor (Inr) in the peripheral tissue which in turn, via a complex network of interactions with cellular nutrient sensors, growth promoting pathways and cellular homeostatic regulators, promotes cellular growth (Figure 5) (reviewed in (Teleman, 2010)).

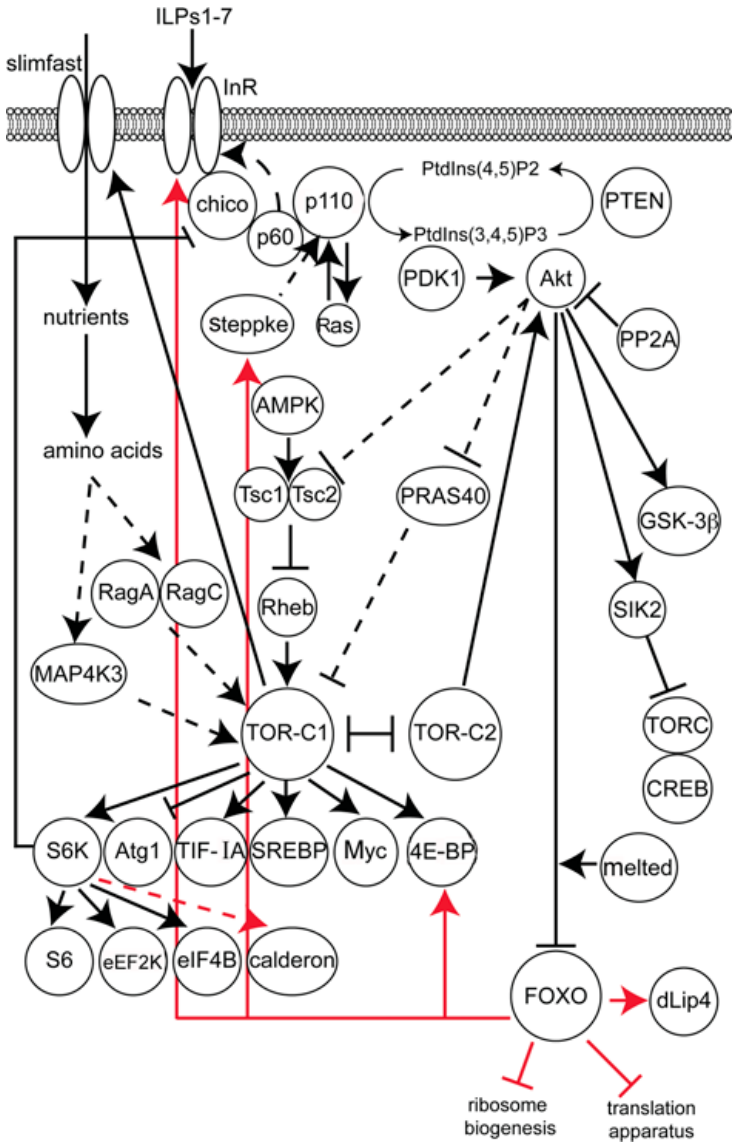

Figure 5: Intracellular insulin signaling pathway in *Drosophila*

Functional relationship between IIS and other intracellular signaling components is indicated. Arrows show activation, but may not necessarily indicate direct interaction. Bar-ended lines indicate inhibitory interaction. Broken lines indicate either indirect interactions or interactions that need further verification. Red lines indicate transcriptional regulation. From (Teleman, 2010).

1.4 *Drosophila* as a model to study physiological homeostasis

Homeostasis (Greek: “homois”, “similar” and “stasis”, “standing still”) is one of the most remarkable properties of complex multicellular organisms and refers to their ability to maintain a constant internal environment in response to changing environmental conditions like temperature, salt concentration and nutrient availability. Physiological homeostasis thus is critical for survival of multicellular organisms, and not surprisingly most organisms have evolved robust networks of multiple sensors, effectors and feedback mechanisms to maintain and regulate homeostasis. Deciphering how components of these networks function to achieve homeostasis is essential for understanding the underlying mechanisms behind complex diseases such as metabolic syndrome and diabetes. While a significant body of work has been generated using vertebrate models of homeostasis, understanding the genetic basis of the complex regulatory network and the functional interactions between the various pathways that regulate homeostasis can be very challenging to study in higher organisms. However, the fruit fly has emerged in recent years as an attractive model system to understand the genetic basis of homeostatic regulation (Baker and Thummel, 2007; Léopold and Perrimon, 2007). These studies have also revealed surprising similarities in homeostatic mechanisms between vertebrates and insects.

1.5 Regulation of metabolic homeostasis in *Drosophila melanogaster*

While the term homeostasis can encompass a wide range of physiological processes including regulation of cell number, temperature and salt and water content, for the purpose of this study we will focus on the regulation of metabolic homeostasis. Metabolic homeostasis in *Drosophila* is regulated by a number of players. First, a number of less understood nutrient and energy sensing mechanisms, including amino acid sensors like dRagA/B, Path and energy sensors like AMPK, detect the nutrient and energy state of the animals (Kim et al., 2008; Long, 2006; Pan and Hardie, 2002; Sancak et al., 2008). Most of these sensory mechanisms have been shown to converge on the TOR pathway, which regulates both cellular growth, and in case of *Drosophila* larvae, helps generate diffusible signals from metabolic tissues like the FB. These signals then induce the release of systemic metabolic regulators like Dilps that coordinate systemic metabolic homeostasis or can lead to induction of tissue growth (Géminard et al., 2009; Sousa-Nunes et al., 2011).

In *Drosophila* the Insulin-like growth factors play a dual role as regulators of both growth and nutrient homeostasis. Dilps, especially Dilp2, which is closest to human insulin in sequence similarity, play a vital role in regulating cellular nutrient uptake and consequently homeostasis of nutrients in circulation (Teleman, 2010). Consistently, knocking down *dilp2* or ablating the IPCs leads to a diabetic phenotype similar to vertebrates, characterized by a higher

concentration of circulating sugar (Broughton et al., 2008; Rulifson et al., 2002). The physiological consequences of high circulating sugar concentration are still not understood. However, it must be noted that, unlike vertebrates high circulating sugar in larvae has not yet been shown to cause any tissue damage. Loss of IIS in the larvae also leads to increased accumulation of glycogen and obesity, characterized by higher triacylglycerol (TAG) content (Böhni et al., 1999; Broughton et al., 2005; Grönke et al., 2010; Tatar, 2001). Increase in total glycogen upon loss of IIS may be a unique characteristic of holometabolous insect larvae as Bombyxin, the insulin homologue in *Bombyx mori*, has also been shown to induce glycogen breakdown and mobilization in the major nutrient storage tissues (Satake et al., 1997). Apart from IIS, the *Drosophila* glucagon homologue AKH (adipokinetic hormone) also plays an important role in nutrient homeostasis. AKH has been proposed to be released in response to low circulating nutrient conditions and has been shown to induce nutrient mobilization from tissues like the FB (Kim and Rulifson, 2004; Lee and Park, 2004)(Figure 6). In addition to signals like Dilp and AKH that systemically regulate nutrient homeostasis, a considerable amount of cross talk between metabolically important tissues also exists in *Drosophila*. For instance, larval oenocytes, cells that have been shown to facilitate nutrient mobilization, have been proposed to interact closely with the FB to regulate nutrient mobilization upon starvation (Gutierrez et al., 2007). Similarly, signaling by microbial metabolites in the gut

has been shown to affect systemic insulin signaling via an unknown pathway (Shin et al., 2011). Taken together, these studies demonstrate that metabolic homeostasis requires a concerted interaction between various metabolic pathways and metabolic tissues in an animal (Figure 6). However, metabolic regulators discussed so far represent only a fraction of the robust network that would be necessary for metabolic homeostasis. Deciphering novel regulators of metabolism therefore is essential for obtaining a complete picture of systemic homeostatic networks and for understanding the mechanisms involved in metabolic disorders. In line with this goal, in Chapter 3 I describe our study exploring the role of TGF-β/Activin signaling in regulating metabolism and homeostasis.

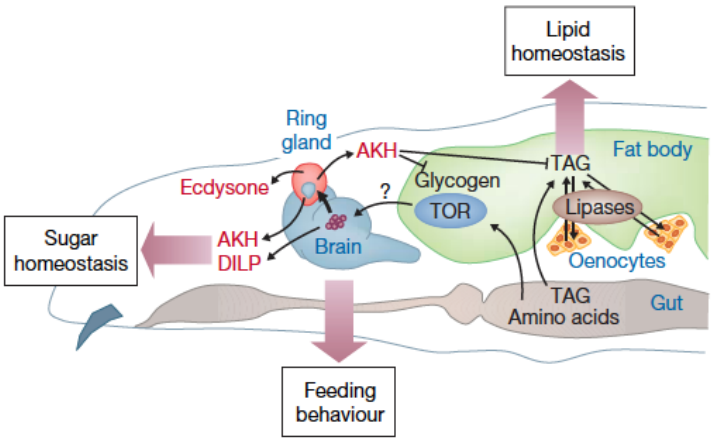

Figure 6: A schematic showing the major regulators of nutrient homeostasis in *Drosophila* larvae

Hormone names are shown in red, tissue names in blue. DILP, Drosophila insulin-like peptides; TAG: triacylglycerol. From (Léopold and Perrimon, 2007).

1.6 The TGF-β signaling paradigm

The TGF-β superfamily forms the largest group of secreted polypeptide growth factors in the animal kingdom and, in vertebrates, consists of more than 30 ligands (Schmierer and Hill, 2007). Based on similarities in sequence and signaling mechanism, these signaling molecules can be divided into two large subgroups that include the TGF-β/Activin and the bone morphogenetic protein (BMP) family. These ligands bind and activate a heteromeric receptor complex containing type I and type II serine/threonine kinases. The activated receptor complex then phosphorylates the R-Smad family of transcription factors. Canonical BMP signaling results in the phosphorylation of R-Smads1/5/8 while Activin/TGF-β ligands signal through R-Smads2/3. Phosphorylation of R-Smads facilitates their association with a common co-Smad in a heterotrimeric complex that is retained in the nucleus where it regulates transcription of target genes in association with a wide variety of cofactors. Additional layers of complexity are provided by extracellular molecules, like chordin, noggin and follistatin, that can bind and regulate ligand availability, and by inhibitory Smads that can negatively regulate activated R-Smads inside the cell (Balemans and Van Hul, 2002; Itoh and Dijke, 2007; Thompson et al., 2005). Moreover, a considerable amount of crosstalk exists between the TGF-β ligands and the various combinations of type I and type II receptors. Based on the receptor used, TGF-β ligands can have different physiological effects on target tissues (Feng and Derynck, 2005).

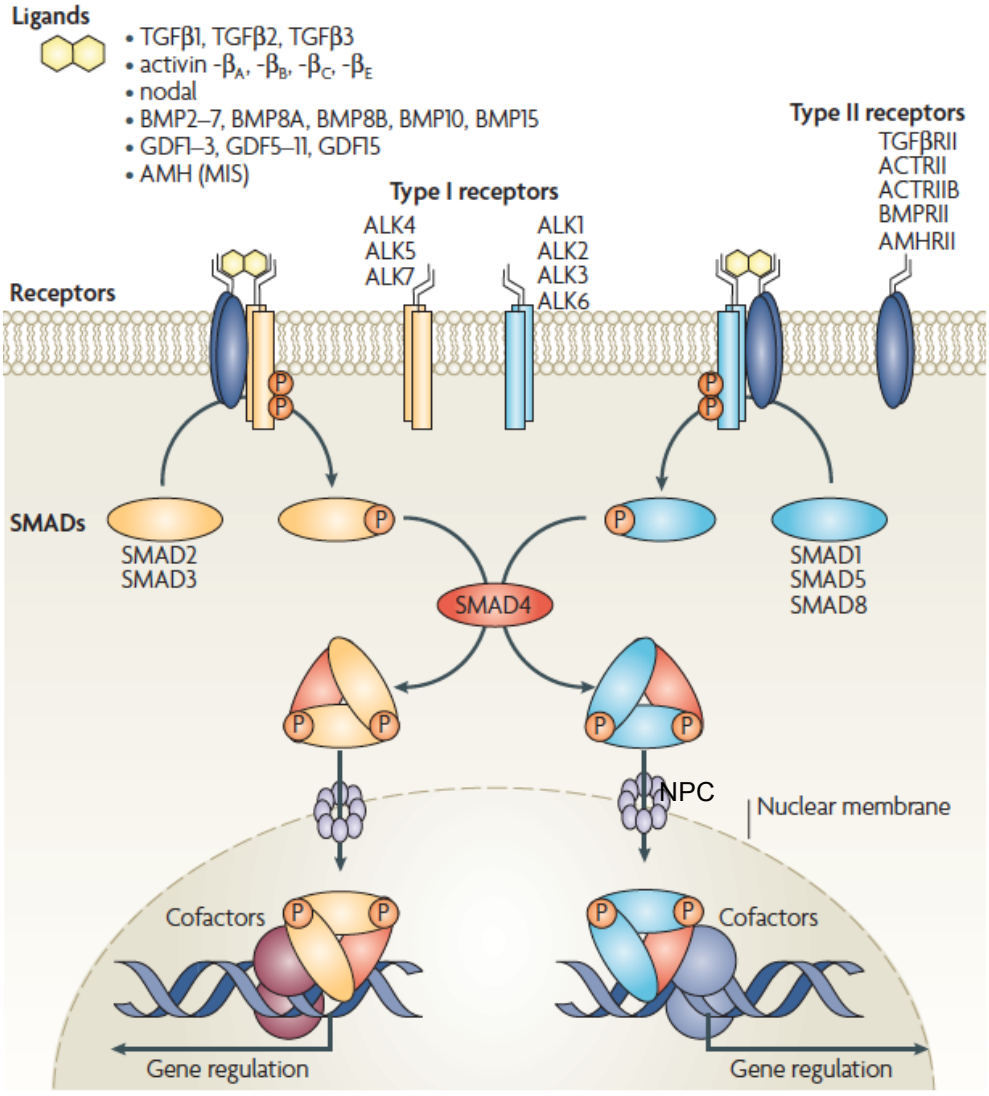

Figure 7: TGF-β signaling in vertebrates

The signaling pathway is initiated when TGF-β ligands bind to the heterodimeric receptor complex consisting of a type I receptor and a type II receptor. Upon ligand binding the constitutively active type II receptor phosphorylates the type I receptor and activates it. Activated type I receptor then phosphorylates an intracellular R-Smad that, upon activation, binds an intracellular Co-Smad (SMAD4). The active R-Smad/Co-Samd complex translocates to the nucleus and regulates gene expression. From (Schmierer and Hill, 2007).

1.7 TGF-β signaling in the *Drosophila melanogaster*

Canonical TGF-β signaling is strikingly conserved in the fruit fly *Drosophila melanogaster.* However, *Drosophila* has fewer ligands and receptors and therefore provides a much simpler system to study (Figure 8). There are only 7 ligands of which *dActivin* (*dAct*) and *dawdle* (*daw*) represent the TGF-β/Activin branch of TGF-β signaling (Figure 8 and 9) (Brummel et al., 1994; Parker et al., 2004; 2006; Serpe and O'Connor, 2006). Of the remaining ligands, three are clear BMP homologues and two novel ligands are too divergent to be definitively assigned to a particular TGF-β subfamily (Parker et al., 2004). The TGF-β/Activin pathway in *Drosophila* is initiaited by ligand binding to the type I receptor, Baboon, that functions with either of the two type II receptors, Wit or Punt (Figure 9) (Brummel et al., 1994; Serpe and O'Connor, 2006). There are three Baboon (Babo) isoforms in *Drosophila* that most likely bind different TGF-β/Activin ligands and signal through the single intracellular transducer dSmad2 (also called Smox) (Das et al., 1999; Jensen et al., 2009; Serpe and O'Connor, 2006; Shimmi et al., 2005). BMP signaling on the other hand is mediated by the type I receptors Tkv or Sax in combination with Wit or Punt. For both BMP and TGF-β/Activin pathways, the product of the *medea* locus has been shown to function as the common co-Smad (Brummel et al., 1994; Letsou et al., 1995; Ruberte et al., 1995; Shimmi et al., 2005). The relative simplicity of TGF-β signaling in the fly, along with the availability of powerful genetic approaches, makes *Drosophila* an

attractive system to study the role of TGF-β signaling in various physiological processes.

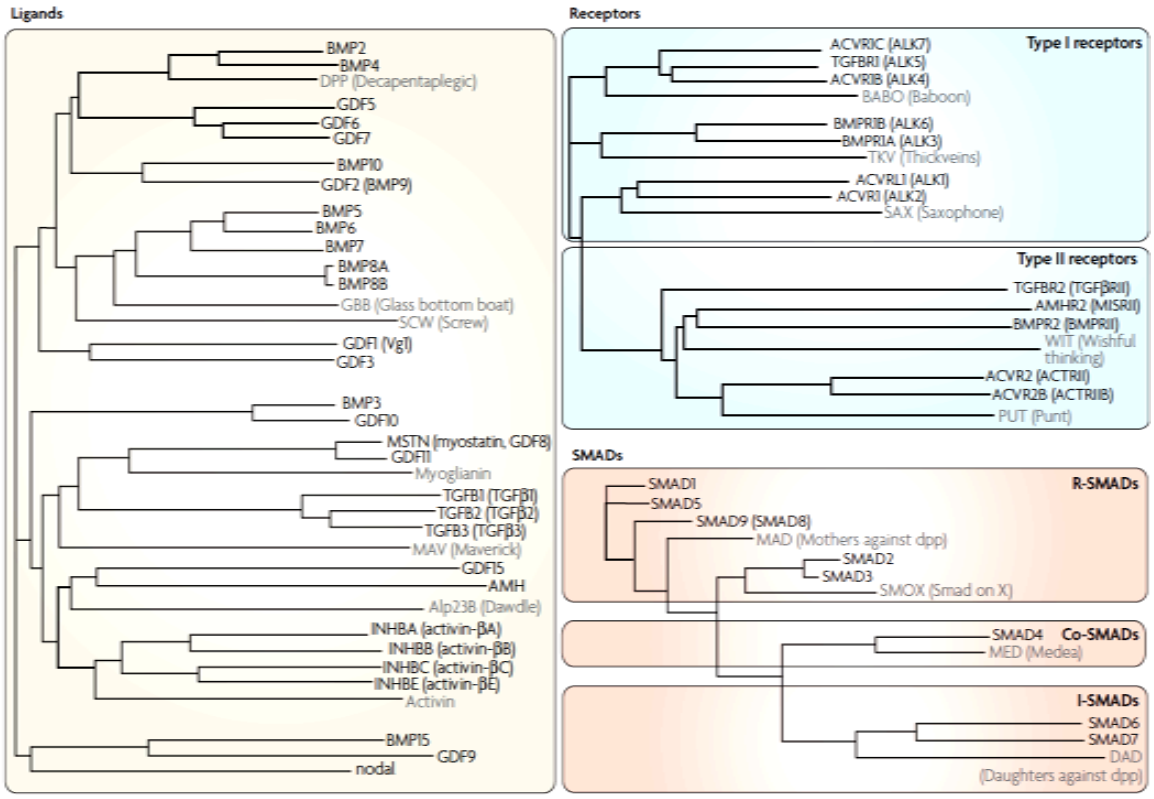

Figure 8: A phylogenetic tree of the various components of the TGF-β superfamily

A phylogenetic tree derived from alignment of protein sequences of the components of the TGF signaling superfamily. Mammalian proteins are shown in black whereas *Drosophila* homologues are shown in grey. Protein symbols are given with alternative names in parentheses. For the ligands, the putative, mature, fully processed forms were used to construct the tree. ACVR, activin receptor; ALK, activin receptor-like kinase; AMH, anti-Muellerian hormone; AMHR2, AMH receptor-2; BMP, bone morphogenetic protein; BMPR, BMP receptor; GDF, growth and differentiation factor; I-SMAD, inhibitory

SMAD; R-SMAD, receptor-regulated SMAD; TGF, transforming growth factor; TGFBR, TGF receptor. From (Schmierer and Hill, 2007).

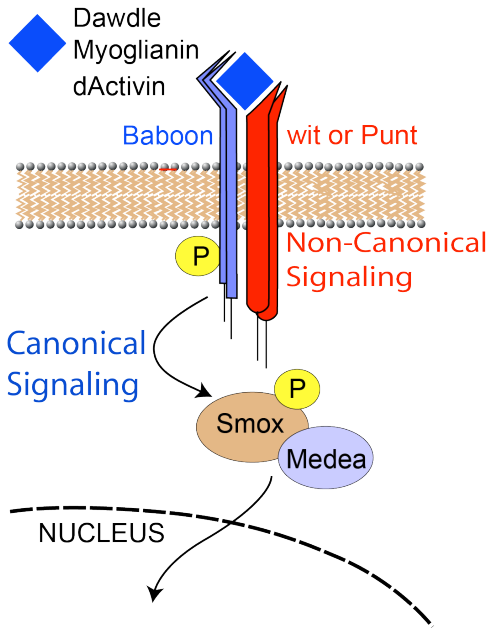

Figure 9: TGF-β/Activin signaling in *Drosophila*

TGF-β/Activin signaling is mediated by the three known ligands, Daw, Myoglianin and Activin-β. The mechanism of signaling is similar to vertebrates where the ligand binds a heterodimeric receptor complex consisting of a type I receptor (Babo) and a type II receptor (Wit or Punt). Upon ligand binding the constitutively active type II receptor phosphorylates and activates Babo. Activated Babo then phosphorylates an intracellular R-Smad homologue Smox, which upon activation binds an intracellular Co-Smad homologue Medea. The Smox/Medea complex translocates to the nucleus and regulates gene expression.

My thesis work explores the role of novel players in regulation of developmental timing, growth and homeostasis in *Drosophila melanogaster*. Chapter 2 of my thesis shows how a developmental gap gene, *giant,* is involved in regulating developmental timing. Chapter 3 explores the role of *Drosophila* TGF-β ligand Daw in regulating metabolism, sugar and pH homeostasis and energy homeostasis in the larvae. Lastly chapter 4 shows the role of a pyrimidine salvage pathway enzyme, uracil phosphorybosiltransferase in regulating larval growth.

CHAPTER 2

The *Drosophila* gap gene *giant* regulates ecdysone production through specification of PTTH-producing PG neurons.

2.1 INTRODUCTION

The *giant* (*gt*) locus, located on the *Drosophila* X chromosome, codes for a zinc finger transcription factor that is widely known for its role in specifying early anterior/posterior pattern in the blastoderm embryo (Capovilla et al., 1992; Eldon and Pirrotta, 1991; Reinitz and Levine, 1990; Stanojevic et al., 1991). Amorphic *gt* alleles lead to embryonic lethality due to the loss of posterior abdominal segments 5-7 and sometimes 8, as well as labral and labial structures in the head region (Gergen and Wieschaus, 1985; Mohler et al., 1989; Petschek et al., 1987). However, the original *gt* alleles were discovered and partially characterized as mutations that produced large third instar larvae as a result of developmental delay (Bridges, 1928). These mutants played an important role in the early history of *Drosophila* genetics because they also produced larger than normal polytene chromosomes that aided early cytogenetic studies (Bridges, 1935).

The viable *gt* alleles exhibit variable penetrance (~25% females, 13% males) that can be enhanced in females when placed over a deficiency, suggesting that they are hypomorphic mutations that enable some mutant larvae to survive past the early essential embryonic requirement for *gt* (Schwartz et al., 1984). These larvae exhibit pronounced developmental delay especially during the third instar stage and pupate approximately 5 days later than wildtype (Schwartz et al., 1984). Post-embryonic development in holometabolous insects

is characterized by defined molting periods followed by metamorphosis. The precise timing of these events is regulated at a systemic level in response to multiple cues like nutritional status, body size, organ development and environmental conditions (Edgar, 2006; Menut et al., 2007; Mirth and Riddiford, 2007; Nijhout, 2003). While these cues may regulate developmental timing in several ways, the primary mechanism involves production and secretion of the insect steroid hormone ecdysone. In *gt* hypomorphic larvae, the protracted third instar stage appears to result from a delay in the rise of ecdysone titer that precedes the initiation of metamorphosis. Consistent with this view, feeding these animals 20-hydroxecdysone (20-E) reverts the delay phenotype leading to normal size larvae that pupate at the appropriate time (Schwartz et al., 1984).

The molecular mechanism by which *gt* controls ecdysone production has been a long-standing mystery. In many insects, the regulation of ecdysone production in larvae involves two major components: a pair of bilaterally symmetric neurons (PG neurons) located in the cebral labrum portion of the brain, and the prothoracic gland, the endocrine organ that actually produces and secretes ecdysone (Gilbert et al., 2002). In *Drosophila,* the PG neurons directly innervate the prothoracic gland (Siegmund and Korge, 2001) and induce production and secretion of ecdysone by releasing an adenotropic peptide hormone called prothoracicotropic hormone (PTTH) (Mcbrayer et al., 2007). PTTH signals through the receptor tyrosine kinase Torso to activate a RAS/ERK

cascade that ultimately stimulates transcription of ecdysone biosynthetic enzymes (Rewitz et al., 2009). Intriguingly, attenuation of PTTH signaling delays the rise in ecdysone titer and the onset of pupation by approximately 5 days resulting in large pupae and adults, similar to those produced by *gt* hypomorphs (Mcbrayer et al., 2007; Rewitz et al., 2009). The similarity in phenotype between *gt* hypomorphs and attenuation of PTTH signaling prompted us to investigate the role of PTTH in the *gt* phenotype further. Here we report that rather than directly regulating PTTH production in the PG neurons, *gt* indirectly controls PTTH and subsequent ecdysone production by influencing the developmental fate of the PTTH-producing PG neurons.

2.2 RESULTS

2.2.1 Hypomorphic mutations in *giant* show stochastic elimination of ptth expression in PG neurons.

The phenotypes seen in *gt* hypomorphic alleles (Schwartz et al., 1984), although less penetrant, are remarkably similar to those described for loss of the PTTH-producing PG neurons or PTTH signal transduction components (Mcbrayer et al., 2007; Rewitz et al., 2009). These include developmental delay and low ecdysone titers during the prolonged third instar stage, production of large larvae, pupa and adults, and the ability to rescue these phenotypes by feeding larvae 20-E (Figure 10 A and B, (Mcbrayer et al., 2007; Rewitz et al., 2009; Schwartz et al., 1984)). To examine if loss of *gt* affected the expression of

PTTH in the PG neurons, we carried out *in situ* hybridization using a *ptth* probe on brains prepared from wandering third instar hypomorphic *gt* alleles gt^{1} or gt^{E6}. Similar *in situ* hybridization experiments with wild type CNSs show four distinct *ptth*-producing PG neurons, two in each brain lobe (Mcbrayer et al., 2007). However, *gt* hypomorphic alleles revealed varying degrees of abnormal *ptth* expression in different larvae and mutant backgrounds. The gt^{1} mutants display the most variability with approximately one third of the larvae showing either one or no cell expressing *ptth* (Figure 10C and D). Other gt^{1} larvae exhibit relatively normal *ptth* expression (Figure 10E). Individuals containing the gt^{E6} allele consistently exhibited expression within only one cell of the pair of bilateral PTTH-expressing neurons within each brain hemisphere instead of the usual two (Figure 10F). We conclude that the similarity in phenotype between ablation of PG neurons and the *gt* hypomorphic mutants and the semi-penetrant phenotype of the *gt* hypomorphic allele is likely caused by the partial loss of *ptth* expression in the PG neurons.

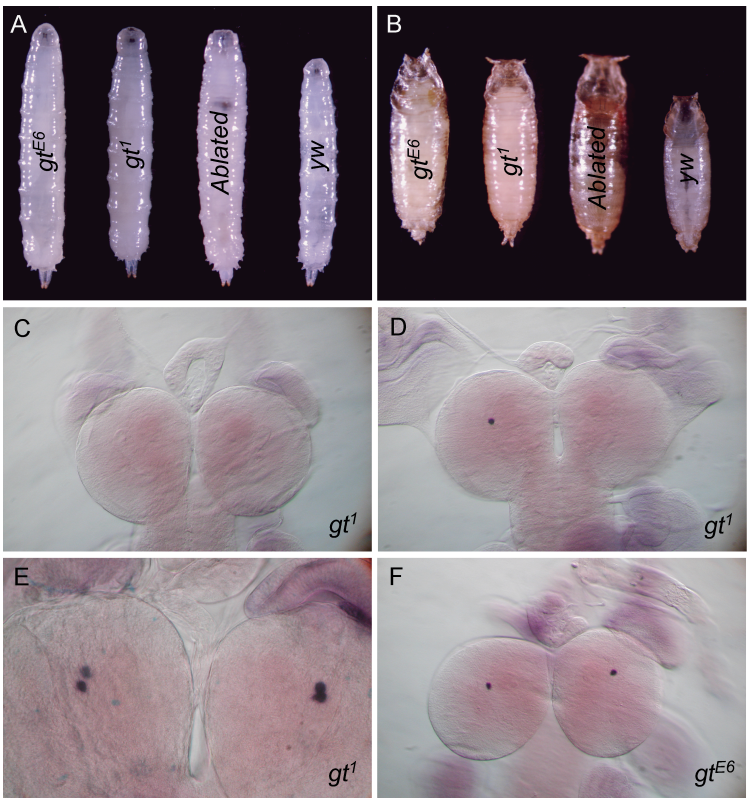

Figure 10: Hypomorphic *giant* mutants are phenotypically similar to PG neuron ablated flies and show variable loss of PTTH expression in the PG neurons

(A and B) gt^{1} and gt^{E6} larvae exhibit a prolonged third instar stage in about 25% of females and 13% of males. This phenotype, although much less penetrant, is similar to PG neuron ablated larvae (*ptth*>Gal4/UAS-*grim*). This prolonged third instar stage gives rise to larvae and pupae that are significantly larger than *yw* control animals (pictures were taken at same magnification and settings and fused using Photoshop). (C) Consistently *ptth* expression, as observed by *in situ* hybridization, is lost from all four PG neurons in the developmentally delayed gt^{1} larvae. (D-E) Normally developing *gt* hypomorphic larvae show a variable stochastic loss of *ptth* expression ranging from one-three of the four PG neurons. Many of them express *ptth* in all four PG neurons similar to wild type animals.

2.2.2 Gt is not expressed in PTTH-producing neurons or the prothoracic gland.

Since *gt* encodes a zinc finger-containing DNA binding transcription factor, one possible explanation for loss of *ptth* expression in the PG neurons of *gt* hypomorphic mutants is that Gt directly controls *ptth* transcription. To address this possibility, we used immuno-staining to examine Gt expression in both larvae and embryos. We found no evidence for Gt expression in larval or embryonic PG neurons. In the embryo we detected dynamic expression of Gt in various portions of the developing brain (Figure 11A,B and D). At stage 14 we observed two prominent Gt-expressing neurons in the lateral portion of each brain hemisphere that could be either the PG neurons or perhaps their precursors (Figure 11B and C, yellow arrows). To examine this issue, we attempted to double stain embryonic brains for Gt and PTTH using a transgenic line that expresses an HA-tagged form of PTTH (Mcbrayer et al., 2007). However, embryonic expression of PTTH-HA in the PG neurons does not begin until approximately stage 17 -18, and at this time we no longer detect consistent Gt expression in the brain. However, in a few rare embryos we observed simultaneous Gt and PTTH staining within the brain but they were in adjacent non-overlapping cells (Figure 11D, red arrowheads showing Gt expressing cells and green arrowheads showing the PG neurons). These results indicate that it is unlikely that Gt directly regulates *ptth* transcription in the PG neurons.

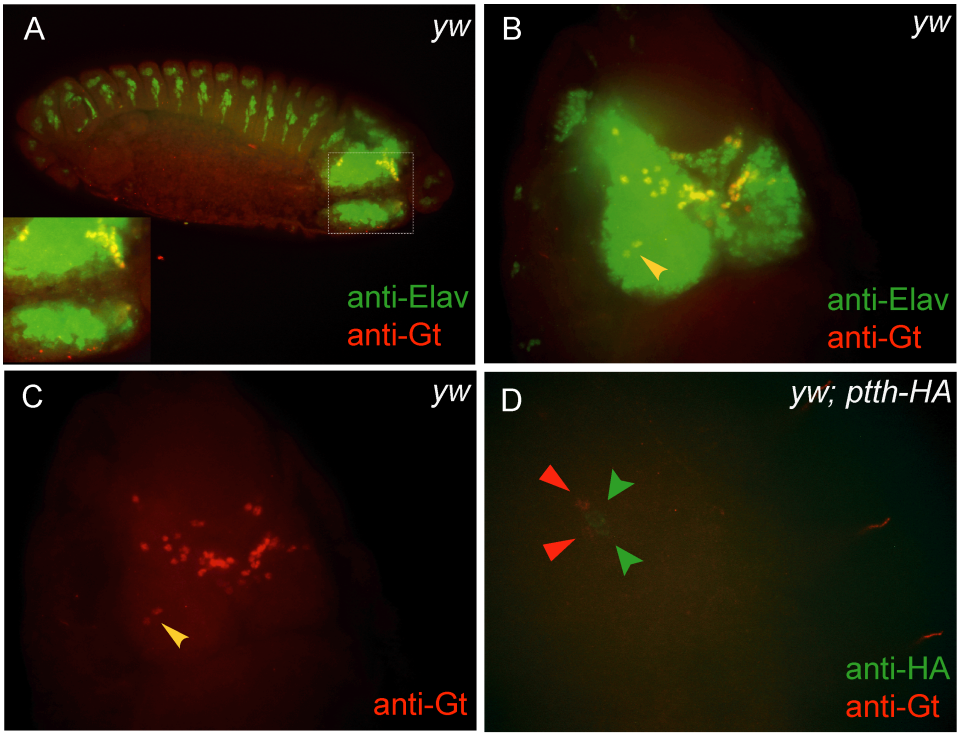

Figure 11: Giant is expressed in the embryonic brain including two neurons adjacent to the PG neurons

(A) Co-staining wild-type embryos with anti-Elav (a pan-neuronal marker) and anti-Gt show that Gt is expressed in the developing embryonic brain even at late embryonic stages. (B-C) At stage 14 there are two prominent Gt-expressing neurons in the lateral portion of each brain lobe, positioned ideally to be either the PG neurons themselves or precursors to PG neurons (B and C (red channel from B), yellow arrowheads). (D) To check if the PG neurons in the embryo express Gt, PTTH-HA expressing embryos were co-stained with anti-HA and anti-Gt antibodies. PTTH-HA expression is seen very late during embryogenesis by which time Gt expression fades. However, on rare occasions two Gt expressing cells (red arrowheads) could be seen right next to the PTTH-HA expressing PG neurons (green arrowheads).

2.2.3 *gt*^{1} affects the fate of PTTH-producing PG neurons

In the absence of any evidence supporting a role for Gt in regulating *ptth* transcription, we sought to determine if loss of Gt affects the specification of PG neurons. Besides *ptth*, the only other described marker for PG neuron fate is the Feb211-Gal4 enhancer trap line (Siegmund and Korge, 2001) that contains an insertion into an unknown gene on chromosome 3. Analysis of expression from this enhancer line in *gt*^{1} mutant larvae revealed a similar stochastic loss of GFP expression in different numbers of PG neurons as seen for *ptth* expression itself (Figure 12A and B). The all or none response observed for both *ptth* and Feb211-Gal4 expression in *gt* hypomorphs is consistent with a stochastic loss of PG neurons in these mutants.

The *gt*^{1} mutation has been shown to be associated with two spontaneous insertions, one near the 5' region of the gene and the other in the 3' region (Mohler et al., 1989). We predict that these insertions likely affect *gt* expression levels during embryogenesis, and altered *gt* expression may affect the fating of different regions of the brain including precursors that give rise to the PG neurons. To examine this issue in more detail, we sought to determine if Gt expression is reduced or if fewer cells express Gt in *gt*^{1} mutant animals compared to wild type embryos. Figure 12 (C-F) shows a comparison between control and *gt*^{1} stage 13 embryos. We observe that under identical staining and exposure conditions, Gt staining intensity in the control embryo is stronger

compared to the *gt*^{1} embryo (Figure 12C and D). We also note a prominent cluster of approximately 5 bilateral posterior midline neurons that express Gt in stage 13 embryos (Figure 12E, yellow arrowheads). In equivalently staged *gt*^{1} mutant embryos (Figure 12F), the number of cells in this cluster that express Gt is reduced to two to four cells (Figure 12F, yellow arrowheads). Similarly, staining of a cluster of three cells positioned anteriorly on the midline axis (Figure 12E and F, blue arrows) is also dramatically reduced in the *gt*^{1} sample.

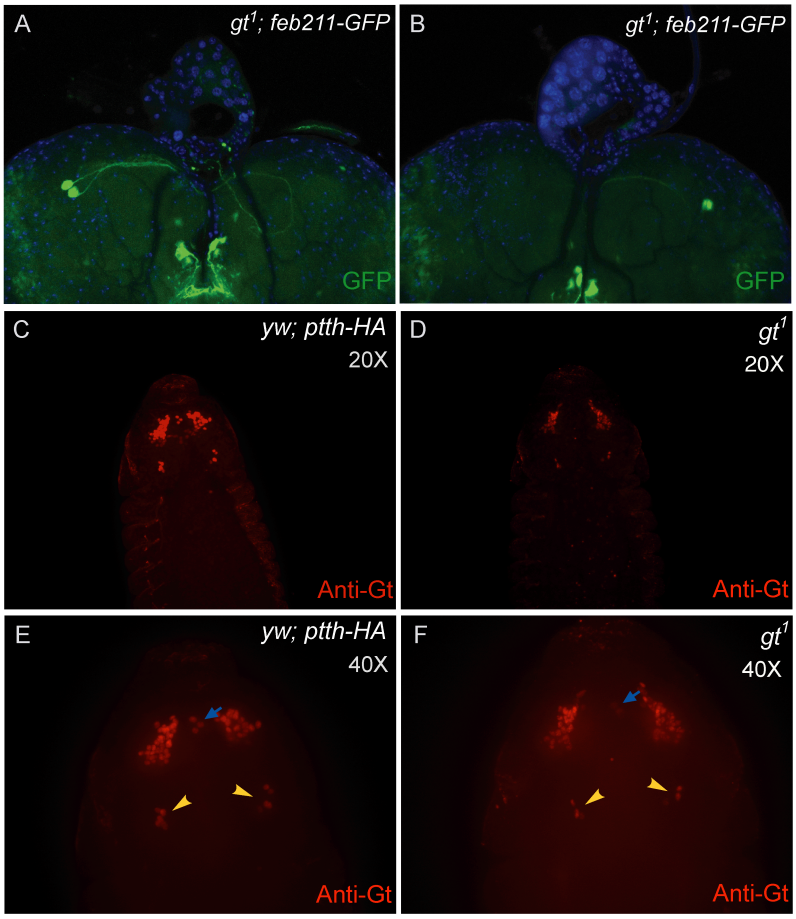

Figure 12: *gt*^{1} affects expression of an independent PG neuron marker Feb211-GFP and may affect PG neuron development by expression threshold effect

(A and B) In a *gt*^{1} background Feb211-GFP expression is lost in a stochastic manner identical to *ptth* in figure 1 indicating that the fate of the PG neurons may be affected and not just *ptth* expression. (C and D) A comparison of Gt immuno-staining intensity between control and *gt*^{1} embryos indicates that Gt expression is reduced in the *gt*^{1} embryo (exposure time: C (1.693 sec) and D (1.754 sec). (E and F) At higher magnification, and upon increasing the exposure time for the *gt*^{1} embryo, the *gt*^{1} embryo in D show loss of Gt expression in some bilaterally symmetric Gt-expressing cells (yellow arrowheads). Loss of Gt is also seen in a cluster of three cells positioned anteriorly (blue arrows).

These results suggest that the fate of several neurons in the brain is likely affected in the *gt*^{1} mutant animals. Since we have no lineage tracers available to directly determine if the PG neurons are derived from earlier precursors that express Gt, we used an indirect assay to determine if PG neurons are mis-specified in *gt*^{1} hypomorphs. Previous axon tracing experiments have revealed that the PG neurons are the only neurons that innervate the prothoracic gland (Siegmund and Korge, 2001). To determine if *gt* affects the fating of PG neurons, we examined cysteine string protein (Csp) distribution on ring gland cells. As shown in Figure 13 (A-C) Csp co-localizes with PTTH in axon terminals and boutons on the surface of wildtype prothoracic gland cells as well as in *gt*^{1} mutant larvae that still show PTTH expression (Figure 13D-F). In contrast, developmentally delayed *gt*^{1} larvae in which PTTH expression is absent from all 4 PG neurons, no Csp-containing boutons are observed on prothoracic gland cells (Figure 13G-I). In these same larvae however, Csp-containing axons and boutons are still seen within the corpus cardiacum and corpus allatum, two regions of the ring gland that are innervated by different sets of neurons (Figure 13H, yellow arrowheads (Siegmund and Korge, 2001)). We conclude that loss of Gt affects the fate of the PG neurons since its absence leads to a loss of prothoracic gland innervation.

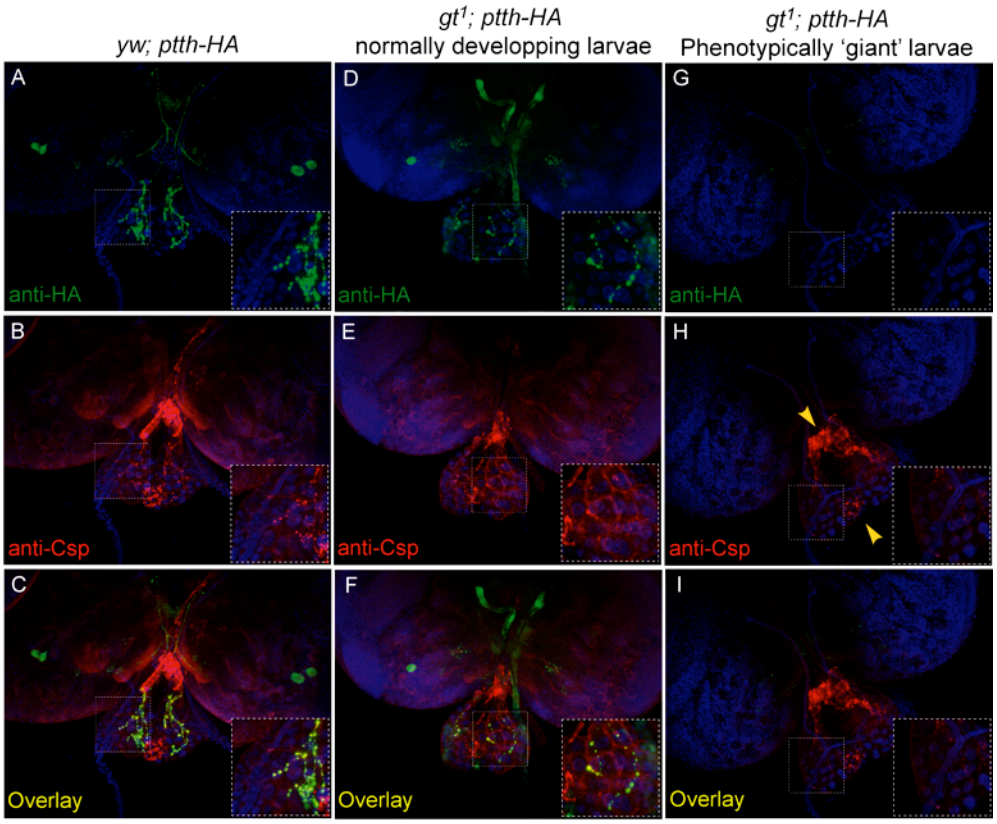

Figure 13: *gt*^{1} affects fate of the PTTH-producing PG neurons.

gt^{1} and *yw* control larvae expressing PTTH-HA under the endogenous *ptth* promoter were co-stained with anti-HA and anti-CSP (cysteine string protein) antibodies. (A and D) PTTH-HA staining is clearly seen in the PG neurons, and sites of innervation on the prothoracic gland in the *yw* control larvae and in *gt*^{1}*; ptth-HA* larvae that develop normally. (B, C, E and F) CSP co-localizes to the sites of innervation by the PG neurons on the prothoracic glands of these larvae. (G) *gt*^{1} larvae that manifest the 'giant' phenotype do not show any PTTH-HA staining either on the brain lobes where the PG neurons are located or on the prothoracic glands. (H and I) Csp staining is also absent on the prothoracic glands of these larvae indicating a loss of innervation by the PG neurons. However, Csp staining is still visible on the corpus cardiacum and the corpus allatum that are innervated by a different set of neurons than the PG neurons (H, yellow arrowheads).

2.2.4 PG neurons provide a tropic signal to the prothoracic gland.

While working with the *gt*^{1} mutants we observed that *gt*^{1} mutant larvae exhibiting unilateral innervation of the prothoracic glands consistently caused asymmetrical growth in which the innervated gland was significantly larger than the non-innervated lobe (Figure 14). DAPI staining revealed that the nuclei on the non-innervated side are much smaller compared to the innervated side (Figure 14B and C). This difference was consistently observed in all samples that failed to innervate one of the prothoracic glands indicating that cellular growth is likely reduced in absence of prothoracic gland innervation. Curiously, as previously reported (Mcbrayer et al., 2007) when both sides lacked innervation, the ring gland did not appear substantially smaller than wild type (compare Figure 13C and I). However these glands are from developmentally delayed larvae in which the extra growth time likely enables them to "catch up" to the wildtype in terms of prothoracic gland size. Ultimately we will need to examine PTTH null mutants to prove that PTTH, and not some other factor, is the tropic signal secreted from the PG neurons.

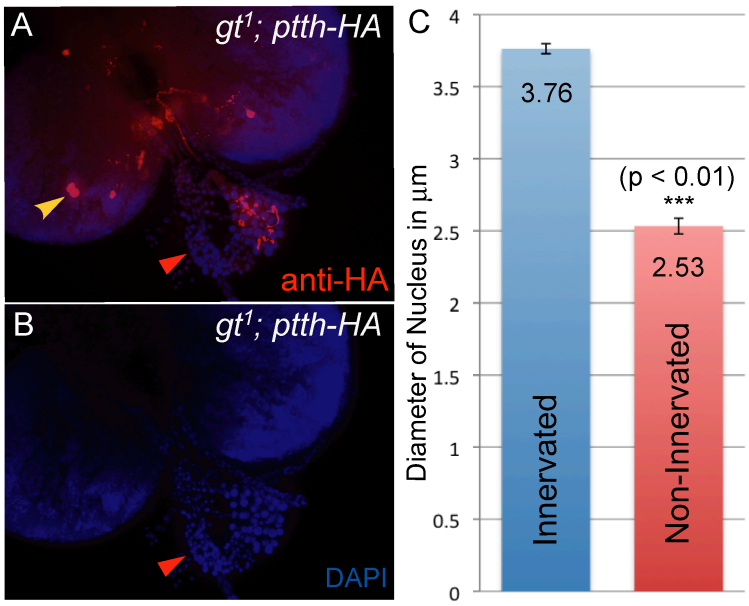

Figure 14: *gt*^{1} hypomorphs reveal that the PG neurons relay a tropic signal to the prothoracic glands that promotes growth

(A and B) *gt*^{1}; *ptth-HA* CNSs containing only one set of PG neurons (A, yellow arrowhead) mostly innervate only one of the prothoracic glands. The innervated prothoracic gland serves as an internal control to look for any growth promoting effect of the PG neurons. DAPI staining of these samples show that the prothoracic gland that is not innervated is consistently smaller than the control prothoracic gland indicating that the PG neurons provide a tropic signal to the prothoracic glands. The cells in the non-innervated prothoracic gland have much smaller nuclei (B red arrowhead) indicating impaired DNA synthesis. (C) To quantify the difference in size, we determined nuclei diameter for 12 nuclei from one PG and considered the average of these measurements as a single data point representing PG size. PG size was similarly calculated for innervated and non-innervated PGs from three independent brain ring glands complexes. The mean of these measurements is plotted and show that PGs that are not innervated are significantly smaller (p-value = 0.005). Significance was calculated using a paired student t-test to negate the effect of variations in PG size between the three samples.

2.2.5 Residual PG neurons show enhanced axon misrouting in *gt*^{1} mutant larvae

In addition to the absence of prothoracic gland innervation in many *gt*^{1} hypomorphic larvae, we noted that there is an enhanced frequency of axon misrouting in *gt* mutant larvae that still show *ptth-HA* expression in one or more of their PG neurons. In wild type larvae, the polarized PG neurons in the left lobe of the brain send out their axons from the cell body across the central axis of the CNS to the right brain lobe. There the axon forms a loop with a left hand twist and then projects anteriorly to innervate the prothoracic gland cells on the right half of the ring gland (Figure 15A and B, and Siegmund & Korge, 2001). Similarly the neurons in the right lobe extend their axons into the left lobe and innervate the left half of the ring gland. This innervation pattern is most clearly revealed in *gt*^{1} mutant larvae retaining one pair of the bilateral PG neurons. For example, in a *gt*^{1} mutant larva that retains the right PG neurons, there is innervation only within the left prothoracic gland (Figure 14A). In wild type larvae, the axon tracts from each pair of PG neurons are almost parallel to each other at the base of the ring gland and rarely exhibit cross (in a single experiment only 1 out of 23 CNSs showed branching). However, in the *gt*^{1} CNSs containing one or two PG neurons in only one brain lobe, we often see the axons branching at the base of the ring gland and innervating both prothoracic glands (Figure 15C, yellow arrowhead). Interestingly we observed similar branching events in

gt^{1} samples that have all the four PG neurons (Figure 15D and E, yellow arrowhead). This suggests that the cross innervations are not likely to be caused by a mechanism that tries to compensate for the lack of innervation on one side of the prothoracic gland. Consistent with this view, we find that in certain cases such branching events caused excessive innervation of one of the prothoracic glands at the cost of the other (Figure 15D, red arrowheads). Approximately 24% of *gt*^{1} CNSs that had at least one PG neuron showed cross innervation events with clear branching at the base of the ring gland. These results suggest that *gt* is required not only for correct fate determination of the PG neurons, but also influences the projection of PG neurites to their target tissue.

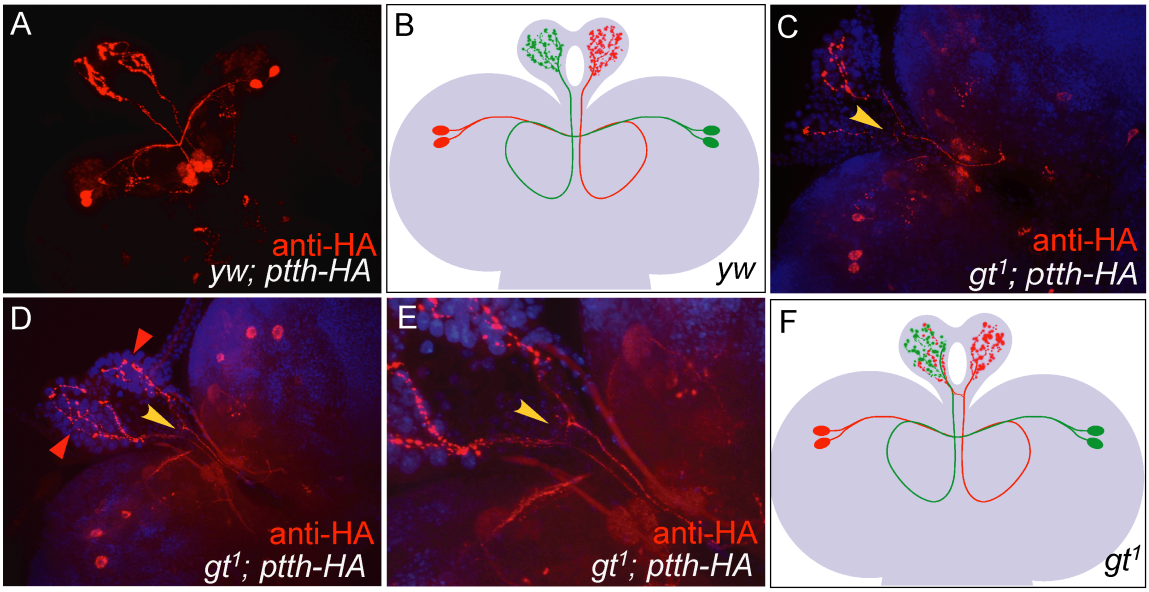

Figure 15: PG neurons in *gt*^{1} hypomorphs exhibit an increased frequency of axon misrouting.

(A) Anti-HA staining (red) of *yw; ptth-HA* CNS shows that axon projections from PG neurons follow a well defined path with the PG neurons in the left lobe of the brain innervating the right prothoracic gland and *vice versa* (modeled in B). (C) Similar staining of *gt*^{1}*; ptth-HA* CNSs show that *gt*^{1} mutants containing one or two PG neurons in one of the brain lobes often show branching of axons at the base of the ring gland (yellow arrowhead). (D) Such branching is also observed in *gt*^{1}*; ptth-HA* CNSs that retain all the four PG neurons and, in certain cases, leads to excessive innervation of one of the prothoracic glands at the cost of the other (red arrowheads). (E) An enlargement of the base of the ring gland in C clearly shows the branching (yellow arrowhead). (F) For a better understanding of the branching pattern a model of gt^{1} CNS showing axon branching is provided. While the model shows axons from only the red PG neurons cross innervating the PGs, it is possible for the green axon bundle or both the axon bundles to branch at the base of the PG.

2.3 DISCUSSION

Our work presented in this chapter shows that the hypomorphic *gt*^{1} mutation leads to developmental delay and ecdysone deficiency by affecting development of the PTTH-producing PG neurons. The gap gene *gt* has been shown to have a complex and dynamic expression pattern during late embryonic stages using *in situ* hybridization (Eldon and Pirrotta, 1991). Our immunohistochemistry (IHC) staining against Gt in late embryos confirm this expression pattern. We observe that the primary staining of Gt is in an anterior medial position that is anatomically close to or overlapping with the pars intercerebralis (PI) and pars lateralis (PL) region of the brain. This part of the developing brain gives rise to a number of neurosecretory cells including several neurons that innervate the corpus cardiacum and corpora allatum, two other portions of the ring gland (de Velasco et al., 2007). The PI placode derives from neuroepithilium that expresses *tailless* and *orthodenticle*, two anteriorly expressed gap genes (Sprecher et al., 2007). The exact origin of the PG neurons has not been established, but they may be derived from two other placodes that reside more posterior to the PI region (de Velasco et al., 2007). Interestingly, we did observe a prominent cluster of bilateral posterior midline neurons that expressed Gt in stage 13 embryos indicating that *gt* may be expressed in neuronal precursors of the PG neurons. While we could not show co-expression of Gt and PTTH-HA in the same neuron in the developing brain, our observation

that Gt can be seen in a couple of neurons sitting next to the PG neurons in the brain supports the possibility that Gt is located at the right place to be able to influence development of the PG neurons. Whether Gt does so in a cell-autonomous or cell-non-autonomous manner will require further fate mapping analysis of *gt* expressing cells. Nevertheless, these experiments add *gt* to the list of anteriorly expressed gap genes that affect the fate of the proto-cerebrum (Younossi-Hartenstein et al., 1997).

At a molecular level, gt^1 hypomorphic mutation is caused by two spontaneous insertions on either side of the giant coding region with one of the insertions located in the regulatory upstream region of *gt* (Mohler et al., 1989). gt^1 therefore is capable of affecting regulation of *gt* expression. A significant reduction in the level of Gt protein in late embryos, as seen with immunohistochemistry, confirms lower expression of *gt* in the gt^1 mutants. Based on the reduced abundance of Gt in gt^1 mutants and the expression pattern of *gt*, that includes precursory neurosecretory neurons, we conclude that gt^1 affects PG neuron specification by affecting development of neuronal precursor cells through an expression threshold effect. Such a developmental expression threshold effect also explains the random stochastic loss of the PG neurons leading to the incomplete penetrance of the ‘giant’ phenotype.

Prior to our study, it had been proposed that *gt* regulates developmental transitions and ecdysone production by affecting ecdysteroidogenesis genes

directly in the PGs. This conclusion was based on one study that showed presence of Gt in the embryonic PG using IHC, a conclusion drawn merely from the position of the Gt staining cells (Eldon and Pirrotta, 1991). The ring gland expression is intriguing since one possible way to restrict *ptth* expression to only the two neurons that innervate the prothoracic gland is by delivery of a required retrograde signal from the target tissue. Such a mechanism is involved in regulating the peptidergic phenotype of the FMRF producing Tv neurons (Allan et al., 2003; Marques, 2003), and perhaps *gt* expression in the ring gland could play an analogous role in regulating a retrograde signal that controls *ptth* expression. However, in our experiments involving IHC of embryos and larval brains did not show any staining of the PG. We suspect that the previously-reported expression of Gt in the embryonic ring gland (Eldon and Pirrotta, 1991) was a misidentified portion of the dorsal brain.

In *Manduca sexta* PTTH is believed to have a tropic effect on the larval prothoracic gland as it has been shown to induce general protein synthesis (Rybczynski and Gilbert, 1994). Similar to *Manduca sexta,* prothoracic gland cells in *Drosophila* are mitotically quiescent during larval stages. Nevertheless, the gland cells exhibit substantial growth during the three larval stages and this growth is characterized by the formation of polytene chromosomes and an increase in size of the gland cells (Aggarwal and King, 1969). Our observation that lack of PG innervation by the PG neurons lead to smaller PG cells indicates

that *Drosophila* PTTH also have a growth-promoting role in the PGs. Ultimately we will need to examine PTTH null mutants to prove that PTTH, and not some other factor, is the tropic signal secreted from the PG neurons in *Drosophila*. However, the recent finding that PTTH signals through the *Drosophila* receptor tyrosine kinase (RTK) *Torso* is certainly consistent with the idea that PTTH is the tropic factor since the Torso signal is transduced through the canonical Ras-Raf-ERK pathway (Rewitz et al., 2009) which is known to regulate cell proliferation in many systems (reviewed in (McCubrey et al., 2007)).

Lastly, we reported that PG neurons present in gt^1 mutants show an increased propensity of cross innervating the PGs. These results suggest that *gt* is required not only for correct fating of the PG neurons, but also influences the projection of PG neurites to their target tissue. At present, we cannot distinguish if these axon guidance defects represent reduction in the expression of intrinsic factors within the PG neurons that respond to guidance cues or whether Gt affects the fate of not only the PG neurons themselves, but also surrounding neurons that might provide guidance cues. Ultimately, lineage tracing experiments will be required to determine which neurons are descendent from Gt-expressing cells in order to address these issues.

In summary, our demonstration that gt^1 mutation affects the PPTH producing PG neurons resolves the long unanswered question as to how a hypomorphic mutation in a gap gene leads to developmental delay and ecdysone

deficiency. Our finding suggests that Giant may also play a crucial role in shaping the developing cortex. An extensive fate mapping study along with spatio-temporal deletion of *gt* expressing cells in the developing embryo will throw more light on this new role of Giant during development. Lastly, we present a direct evidence for the role of PTTH signaling in regulating cell growth in the PGs, which may also affect ecdysone production and developmental timing.

2.4 MATERIALS AND METHODS

2.4.1 *Drosophila* stocks and husbandry

The gt^{1} and gt^{E6} lines were obtained from the Bloomington *Drosophila* stock center. gt^{1}*; ptth-HA* stocks were generated by standard genetic methods. Genomic *ptth-HA* lines (*yw; ptth-HA*) and the *yw;Feb211-Gal4;UAS-GFP* (Feb211-GFP) line were described previously (Mcbrayer et al., 2007; Siegmund and Korge, 2001). gt^{1}*;UAS-GFP;Feb211-Gal4* larvae were obtained by crossing Feb211-GFP males to gt^{1} females and selecting male larvae. Flies were raised at 25^{O}C on standard food in vials.

2.4.2 Immunohistochemistry

The following antibodies were used at the indicated dilutions for immunohistochemistry: rat anti-HA 3F10 (Roche) 1/500, rat anti-Gt (generous gift from Dr. Vincenzo Pirrotta) 1/500 and mouse anti-CSP (Iowa Hybridoma Bank) 1/100. The Alexa series (Invitrogen) of secondary antibodies were used for

immunofluorescence at 1/500 dilution. CNSs from third instar wandering larvae were dissected out and fixed in 4% paraformaldehyde in PBS for 20 minutes at room temperature for anti-HA and anti-CSP staining. Antibody staining and washes of larval CNSs were conducted in 0.1% Triton-X100 in 1X PBS (PBST). Primary antibody treatments of CNSs were done at $4^{O}C$ for 24 hours. Embryos were dechorionated in 50% bleach, fixed in 4% paraformaldehyde in PBS for 15 minutes and all subsequent antibody reactions were in PBS + 0.1% Tween-20. Samples were mounted in 80% glycerol in PBS and visualized on a Zeiss Axioplan 2 with a CARV unit for confocal microscopy.

CHAPTER 3

The *Drosophila* TGF-β/Activin ligand Dawdle independently regulates insulin signaling and mitochondrial metabolism in the larvae

3.1 INTRODUCTION

Systemic homeostasis is a defining feature of multicellular organisms and is crucial for survival in diverse conditions such as starvation and fluctuations in temperature, pH and nutrient availability. Consequently, robust regulatory networks involving multiple sensors, feedback mechanisms and signalling pathways have evolved in most organisms to maintain homeostasis (Baker and Thummel, 2007; Léopold and Perrimon, 2007). Deciphering how components of these networks function to achieve homeostasis is essential for understanding biology and the underlying mechanisms behind multifaceted diseases like metabolic syndrome and diabetes.

Insulin signaling is a key pathway that regulates nutrient homeostasis in higher organisms. Released from specialized insulin producing cells (β cells in vertebrates) in response to nutrient availability, insulin induces cellular nutrient uptake and storage/utilization. Insulin also interacts with other regulatory pathways including glucagon signaling, nutrient sensing in the brain and TOR signaling (Avruch et al., 2005; Fernandez and Torres-Alemán, 2012; Potter et al., 2001). Apart from interactions mediating nutrient homeostasis, insulin levels can also indirectly affect pH homeostasis by up-regulating ketogenesis. Such cross-regulations is essential for maintaining a robust homeostatic state and involvement of classical developmental pathways in regulating homeostasis has gained much attention recently. One such developmental pathway that has been

shown to affect multiple aspects of metabolism including nutrient and energy homeostasis is TGF-β signaling (Ballard et al., 2010; Zamani and Brown, 2011).

A role for TGF-β signaling in regulating insulin signaling has been proposed based on a number of *in vitro* and *in vivo* studies. Several *in vitro* studies have shown that TGF-β ligand Activin-A can stimulate Ca^{2+} influx and insulin release from both rat and human β-cells in the presence of glucose (Florio et al., 2000; Totsuka et al., 1988). Yet prolonged exposure of cultured human islets cells to Activin-A antagonizes rather than stimulates insulin secretion and expression (Szabat et al., 2010). Activin-A also up-regulates *pax-4* gene expression in cultured cells indicating a potential role of activin-A in regulating β-cell replication and maturation (Brun, 2004; Ueda, 2000). Consistently, blocking activin signaling by either receptor deletion or by over-expression of a dominant negative receptor or inhibitory R-smad in the β-cells leads to hypoplastic islets and impaired glucose tolerance (Shiozaki et al., 1999; Smart et al., 2006; Yamaoka et al., 1998). Conversely, increasing activity of TGF-β superfamily ligands such as activins, myostatin and GDF11 by deleting their antagonist follistatin-like-3 (FSTL3) also affects β-cell differentiation and function, further confirming the role of TGF-β signaling in regulating insulin signaling (Mukherjee et al., 2007). Unlike Activin-A, Activin-B has been proposed to negatively regulate insulin release based on the phenotype of *ALK7* (type I receptor that recognizes Activin-B and not Activin-A) mutants (Bertolino et al., 2008). While most of the

above-mentioned results involve either ligand gain-of-function or receptor deletion, loss-of-function studies using the ligands in question are either lacking or have failed to complement the corresponding gain-of-function studies (Bonomi et al., 2012; Li et al., 2009).

In their study, Li et al. generated an Activin-A mutant by knocking in the Activin-B mature domain into the Activin-A locus. These mutants however did not develop any glucose intolerance or insulin resistance thereby questioning the in vivo role of Activin-A in insulin release in vertebrates. However, these mutants were much smaller and leaner than controls and these phenotypes could be rescued by growing the animals on a high-calorie diet. Further physiological and biochemical analysis of these mutants revealed characteristics that are associated with higher mitochondrial activity. Tissues from these mutants showed significantly higher expression of several mitochondrial genes and higher oxygen consumption. This effect of losing Activin-A on mitochondrial activity has significant pathophysiological implications, as mitochondrial dysfunction has been associated with many human diseases and disorders (Bayeva et al., 2013; Dromparis and Michelakis, 2013; Maléth et al., 2012; Mitchell et al., 2013; Watson et al., 2012; Zsurka and Kunz, 2013). Given the large number of TGF-β signaling components and redundancies in activity, parsing out the exact mechanisms by which TGF-β affects insulin signaling, metabolism and nutrient

and energy homeostasis using the vertebrate model system can be a challenging and time consuming.

In comparison, *Drosophila melanogaster* is an attractive alternative containing a conserved and more concise repertoire of both TGF-β and insulin signaling components (Schmierer and Hill, 2007). In *Drosophila*, TGF-β/Activin signaling is mediated by three ligands, Activin-β (Actβ), Dawdle (Daw) and Myoglianin (Myo), that signal through a single type I receptor Baboon (Babo) and a single intracellular transducer dSmad2 or Smox. Insulin signaling in *Drosophila* is mediated by Insulin-like growth factors that have been shown to be functionally similar to insulin in vertebrates (Baker and Thummel, 2007; Géminard et al., 2009; Rulifson et al., 2002; Teleman, 2010). *Drosophila* insulin-like peptides (DILPs) are produced primarily in a cluster of neurosecretory cells in the fly brain called the insulin producing cells (IPCs). These cells are functionally analogous to β-cells and produce 4 of the 7 *Drosophila* insulin-like peptides (DILP 1, 2, 3 and 5). The IPCs regulate both growth and nutrient homeostasis by releasing these DILPs in response to food and conducive growth conditions (Géminard et al., 2009; Musselman et al., 2011). Availability of these conserved pathways, along with the amenability of the fly to genetic and experimental approaches, allowed us to investigate in detail the role of TGF-β signaling in regulating insulin signaling and metabolism in the fly.

In this study we show that TGF-β signaling mediated by the TGF-β/Activin ligand Daw regulates sugar homeostasis, pH balance and mitochondrial metabolism in *Drosophila* larvae. We show that canonical signaling by Daw regulates sugar homeostasis primarily by affecting release of DILPs from the IPCs. The effect of Daw on pH is mediated independent of IIS by Daw's action on mitochondrial metabolism and production of metabolic acids in the larval fatbody. Interestingly, Daw affects both phenotypes in a dose-dependent manner, as demonstrated by both loss-of-function and over-expression/gain-of-function experiments, thereby providing evidence for a hormonal role of Daw in regulating systemic homeostasis.

3.2 RESULTS

3.2.1 Loss of *dawdle* (*daw*) leads to conditional lethality depending on growth conditions

We and others have previously shown that mutations in the locus coding for the *Drosophila* Activin-like ligand, Daw, lead to larval lethality and retardation in the outgrowth of motoneuron axons during embryogenesis (Parker et al., 2006; Serpe and O'Connor, 2006). Since the mutant motoneurons do eventually reach their muscle targets and form essentially functional synapses, the reasons for larval lethality remained unexplained. An opportunity to uncover the cause of *daw* mutant lethality arose when we noticed that the viability of null *daw* mutants depends on the food source (Figure 16). Growth on standard corn meal food

(CMF) resulted in developmental delay and larval lethality. On this food *daw*^{11} homozygotes showed multiphasic larval lethality with more than 90% of larvae dying before the third instar wandering stage. Moreover, mutant larvae that did reach the pupal stages (less than 10%) showed significant developmental delay compared to *yw* control larvae (Figure 16A), and the mutant pupae never reached the pharate stage (data not shown). Interestingly, both larval lethality and developmental delay were significantly/completely rescued when *daw*^{11} homozygous larvae were grown on 60% yeast paste food (YPF) (Figure 16A and B). Moreover, when grown on YPF, a significant number of *daw* mutants eclosed as adults that were similar in size to control animals (Figure 17). Severe lethality on CMF was also observed for *daw*$^{1/11}$ trans-heterozygotic larvae (Figure 16B). Since the *daw*^{1} and *daw*^{11} alleles were generated by imprecise excision of independent P element insertions we conclude that the food-dependent conditional lethality is specific to loss of *daw* and not caused by a genetic background effect. Both alleles are likely null since they delete most of the coding region of the gene including the translational start site (Gesualdi and Haerry, 2007; Serpe and O'Connor, 2006).

Interestingly, the *daw* lethal phenotype is dose-sensitive since *daw*$^{1/+}$ and *daw*$^{11/+}$ heterozygotes also showed significant larval lethality on CMF, although to a lesser extent than trans-heterozygotes (Figure 16C). Similar to *daw* mutants, loss of *babo* or *smox,* genes encoding the Daw receptor and R-Smad signal

transducer, respectively, also showed a food-dependent larval lethal phenotype (data not shown). The majority of either *babo* or *smox* mutant larva also failed to reach the pupal stage on CMF, but formed pre-pupae on YPF. Notably, unlike *daw*, null mutations in either *myo* or *actβ,* two other *Drosophila* Activin-like ligands, do not significantly affect pupariation rates on CMF food (data not shown). Thus the loss of larval viability on CMF for *babo* and *smox* mutants is primarily attributable to loss of *daw* signaling.

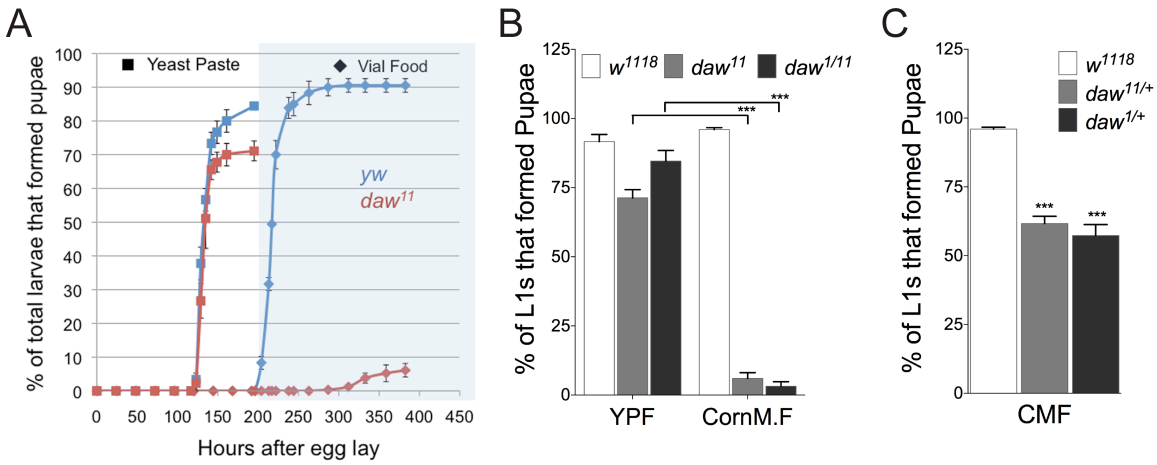

Figure 16: *daw* mutants exhibit food dependent growth and viability

(A) Developmental curves showing percentage of larvae that formed pupae and the time required to reach pupariation on cornmeal food (CMF) and yeast paste food (YPF). *daw* mutants (daw^{11}) show significant developmental delay and larval lethality on CMF compared to *yw* controls. Growing the mutants on YPF completely/significantly rescues the phenotypes. (B) Lethality on CMF is observed for both homozygous and trans-heterozygous *daw* mutants (daw^{11} and $daw^{1/11}$). (C) *daw* heterozygotes also show significantly higher ($p<0.001$) lethality on CMF compared to w^{1118} wildtype controls.

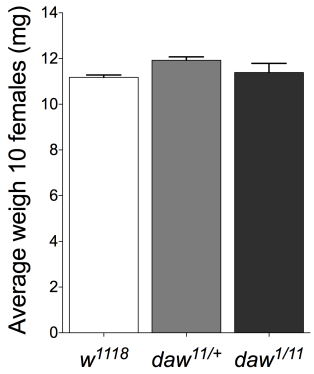

Figure 17: *daw* mutants can eclose as healthy looking adults on YPF

daw mutants when grown on YPF can reach adult stages and eclosed adults are similar in size to both w^{1118} wild-type and $daw^{11/+}$ heterozygous controls.

3.2.2 Daw is a key metabolic determinant that regulates both sugar homeostasis and pH balance

In an effort to explain the food-dependent lethality, we examined the steady-state levels of various key metabolites in *daw* mutant larvae grown on YPF and compared them to controls. We measured total triacylglycerol (TAG), glucose and glycogen stores of stage matched feeding *daw* mutant larvae and wildtype controls and found a significant increase in all three metabolites in the *daw* mutants (Figure 18 A-C). Elevated TAG and glycogen has previously been shown to be associated with loss of insulin-IGF signaling (IIS) in *Drosophila*. A significant increase in total TAG and glycogen content was observed in IPC-ablated flies (Broughton et al., 2005; Teleman, 2010), and similar results were reported for flies that lacked *dilp-2,3-5* or lacked the *Drosophila Inr* or the IRS homologue *chico* (Böhni et al., 1999; Grönke et al., 2010; Tatar, 2001). Our

observations suggested a role for Daw in regulating IIS in the *Drosophila* larva. Since IIS is also known to regulate circulating sugar concentration in larvae (Rulifson et al., 2002), we measured circulating sugar concentration of both feeding and 12 hour starved *daw* mutant and control larvae. We found a significant increase in circulating sugar levels in the *daw* mutants compared to both heterozygous and w^{1118} controls, consistent with a strong loss of IIS in *daw* mutants (Figure 18D). Interestingly, this "diabetic" phenotype was seen only in feeding animals and not in starved animals (Figure 19). A similar increase in circulating sugar concentration (about 40%) was also observed in *smox* null larva indicating that *daw* acts through the canonical Smad pathway to regulate IIS (Figure 19).

To further evaluate whether *daw* might regulate other metabolic processes, we performed a small-molecule gas chromatography/mass spectrometry (GC/MS) analysis comparing the metabolite content of *daw* mutant larvae to controls. This analysis revealed a significant increase in multiple intracellular sugar metabolism and TCA cycle intermediates including pyruvate, citrate, 2-ketoglutarare, succinate, fumarate and malate, strongly implicating *daw* in the regulation of intracellular sugar/mitochondrial metabolism (Figure 18F). Interestingly, these metabolites are known to be present in high concentrations in Lepidopterans (Harrison, 2001; Wyatt, 1961), and a further increase in the concentration of these organic acids could lead to pH imbalance. We therefore

assayed for changes in internal pH of the *daw* mutants. Consistent with the increase in various metabolic acids, we find significant acidification of *daw* larval hemolymph compared to controls (Figure 18G). Overall, our data suggest that the Activin-like ligand Daw positively regulates IIS in larvae and protects against acidosis most likely by regulating the production of several metabolic acids that are intermediates in sugar metabolism.

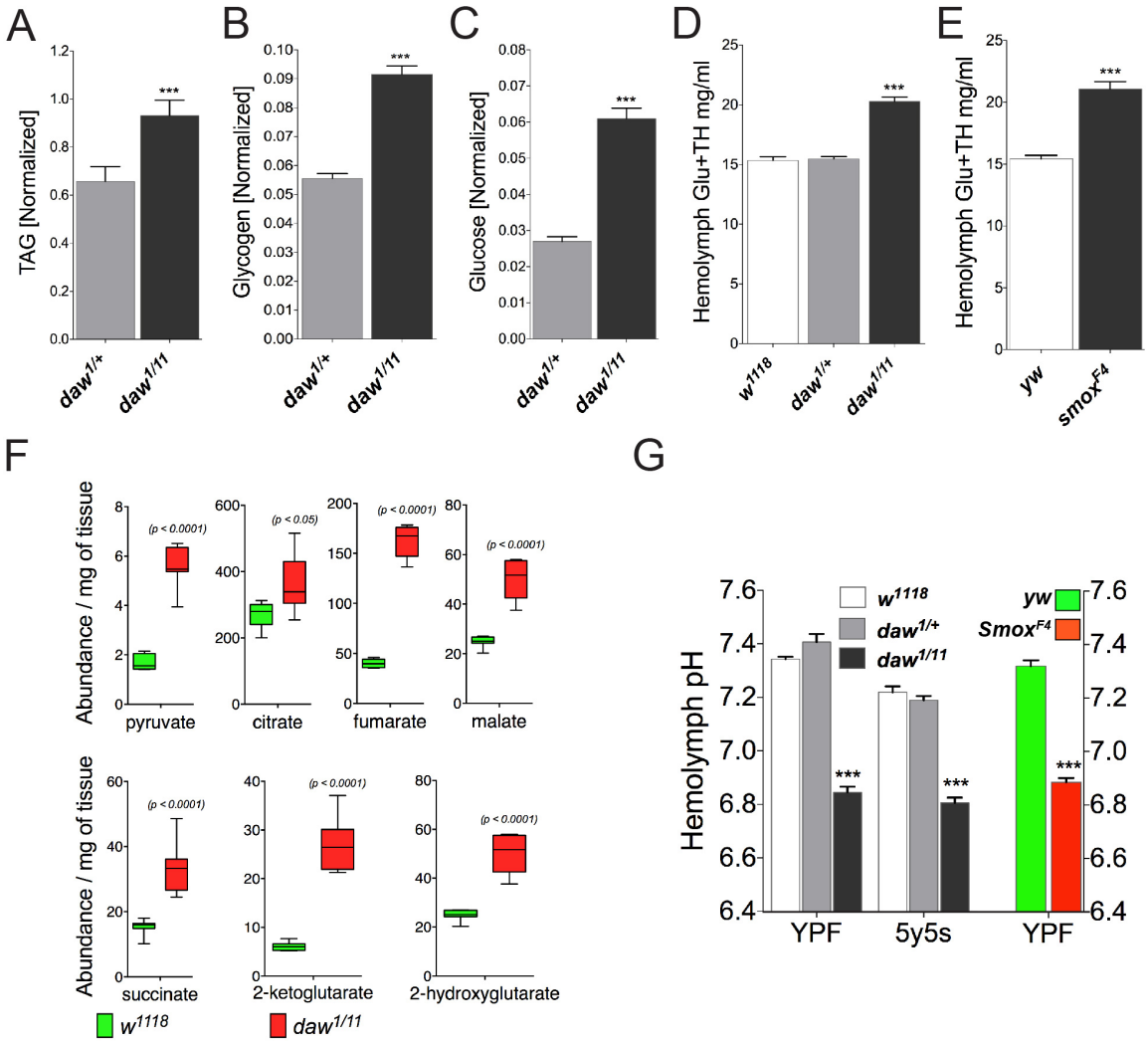

Figure 18: *daw* regulates both sugar homeostasis and pH balance.

(A-C) *daw* mutants show significantly higher TAG (A), glycogen (B) and glucose (C) content compared to controls. Metabolite contents were normalized to total soluble protein to account for differences in size of the animals. (D-E) Glucose + trehalose (Glu+TH) concentration of the hemolymph was measured for mutant and control feeding mid-third instar larvae. (D) *daw* mutants show a significant increase (~ 40 %) in circulating sugar concentration compared to both w^{1118} and $daw^{1/+}$ controls. (I) Feeding *smox* mutants ($smox^{F4}$) also show a significant increase in circulating sugar concentration (~ 40 %) compared to *yw* controls. (F) A high-throughput GC/MS based

metabolomic analysis of *daw*$^{1/11}$ and *w*^{1118} larvae show up-regulation of multiple sugar metabolism intermediates in the mutants. (G) Hemolymph pH of *daw* and *smox* mutants is significantly acidic (~pH 6.85) under conditions when *w*^{1118} and *daw*$^{1/+}$ controls maintain a pH ranging between pH 7.2 and pH 7.4.

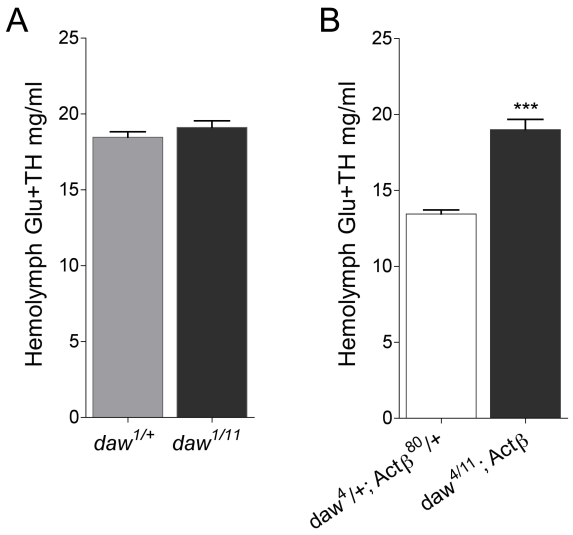

Figure 19: *daw* is the primary TGF-β ligand that affects hemolymph sugar and does so only in feeding animals

(A) *daw* mutant larvae when starved for 12 hours did not show any significant difference in circulating sugar concentration compared to heterozygous controls. (B) Feeding *daw*/*Actβ* double mutants showed an approximately 40% increase in circulating sugar concentration compared to matched controls.

3.2.3 High sugar content and acidity of CMF leads to lethality of *daw* mutants

Apart from YPF, a semi-defined food consisting of 5% yeast and 5% dextrose (5y5s) is also capable of completely rescuing viability of *daw* mutant larvae (Figure 20). We compared the major nutritional content of CMF, YPF and 5y5s food to determine if nutritional differences could explain lethality on CMF (Figure 20A). We note that both YPF and 5y5s food are lower in total carbohydrate content. This difference, along with our observation that loss of *daw* affects sugar metabolism and IIS, led us to hypothesize that *daw* mutants may be sensitive to the high sugar content of CMF. Consistent with this notion, we found that when challenged with a high sugar diet (HSD), *daw* mutants showed a statistically significant increase in larval lethality (Figure 20B).

Additionally, we examined the effect of acid in the food on the viability of *daw* mutants both because *daw* mutant larvae show internal acidosis and because CMF is more acidic (pH 4.3 compared to ~ pH 6.8 of 5y5s food) owing to the addition of propionic acid (PA) as a mold inhibitor. Acidic food (pH 4.3) indeed caused a significant decrease in the viability of *daw* mutants. Organic acids such as PA and acetic acid (AA) had a more profound effect on larval viability than inorganic acid (HCl) (Figure 20C). Interestingly, combining a high sugar diet with PA resulted in the most severe larval lethality, phenocopying the extent of lethality seen on CMF (less than 10% viability, Figure 20D). Acidic food

also led to significant developmental delay, with PA producing the strongest effect, followed by AA and HCl (Figure 20E).

We hypothesized that the acidic food conditions led to larval lethality and developmental delay by aggravating the already acidic internal pH of the *daw* mutant larvae. Consistent with this view, we find that transferring *daw* and control mid L3s to acidic food conditions further lowers the hemolymph pH of mutants compared to non-acidic food (Figure 20F, dotted line shows pH of mutants on YPF). Interestingly, heterozygous mutants also showed a significant but intermediate drop in hemolymph pH compared to wildtype controls signifying a dose-dependent role of *daw* in regulating the acidosis phenotype, analogous to the CMF-induced larval lethality phenotype. Apart from high sugar and acidic conditions we tried a number of food conditions that mimicked CMF in nutritional content, or represented extremes of nutritional conditions, for any effect on viability of *daw* mutants. None of these conditions significantly increased *daw* lethality compared to wild-type controls (Figure 21).

A

Nutrient	% in CMF	% in YPF	% in 5y/5s
Lipid	0.1	2.57	0.21
Carbohydrate	18.4	14.1	6.18
Protein	1.76	21.43	1.78
Free Sugar	5.43	0	5

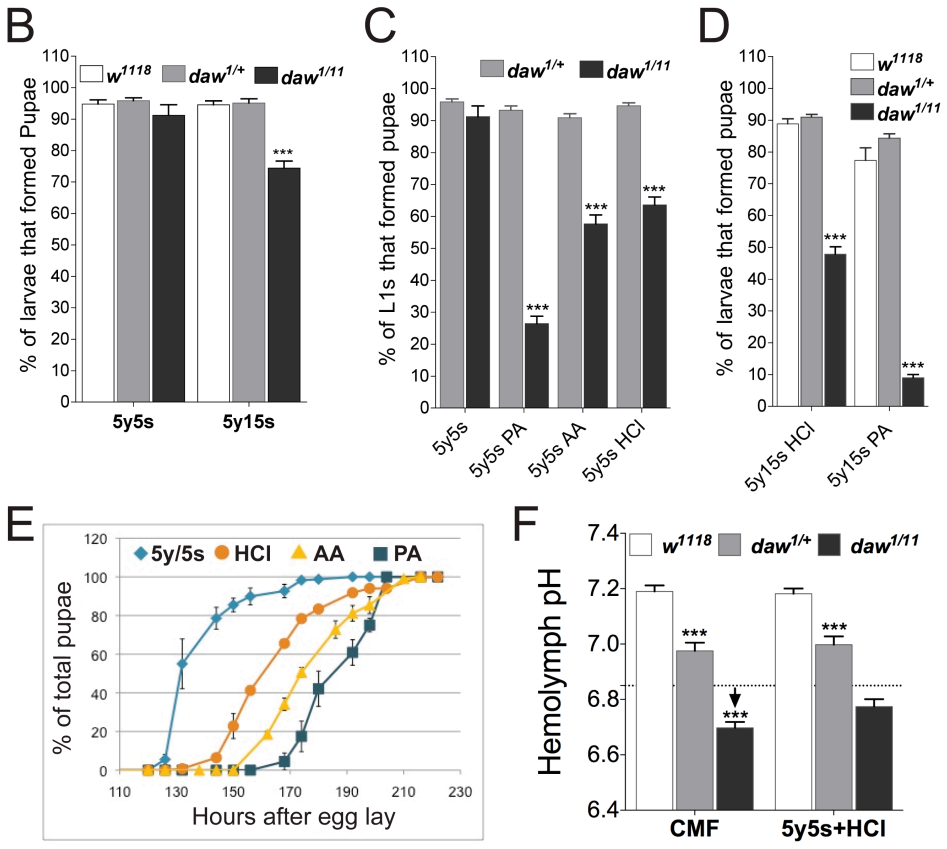

Figure 20: High sugar content and Propionic acid (PA) in CMF kills daw mutants

(A) A comparison of major nutritional content of CMF, YPF and 5% yeast+ 5% Dextrose (5y5s) food show a significantly higher carbohydrate content of CMF. (B) Viability of *daw* mutants is not significantly different from controls on 5y5s food. However, *daw* mutants show significantly higher lethality on food containing 15% sugar (5y15s). (C) Titrating the

pH of 5y5s food to pH 4.3 (same as CMF) leads to significant decrease in viability of *daw* mutants but not controls. Choice of acid to lower pH differentially affects larval viability with PA most severely reducing viability (~ 30 %). (D) Combining HSD with PA (pH 4.3) most severely decreases viability of *daw* mutants mimicking CMF (<10 % viability). (E) Acidic food condition also replicates delayed development of *daw* mutants as observed on CMF. PA once again most severely affects developmental timing. (F) 12 hour exposure to acidic environment is capable of impacting the internal pH of both *daw* heterozygotes and *daw* mutants (mutant pH on YPF or 5y5s food is shown with a dotted line) but not wild-type controls. PA induced acidity is more potent in reducing internal pH of *daw* mutants.

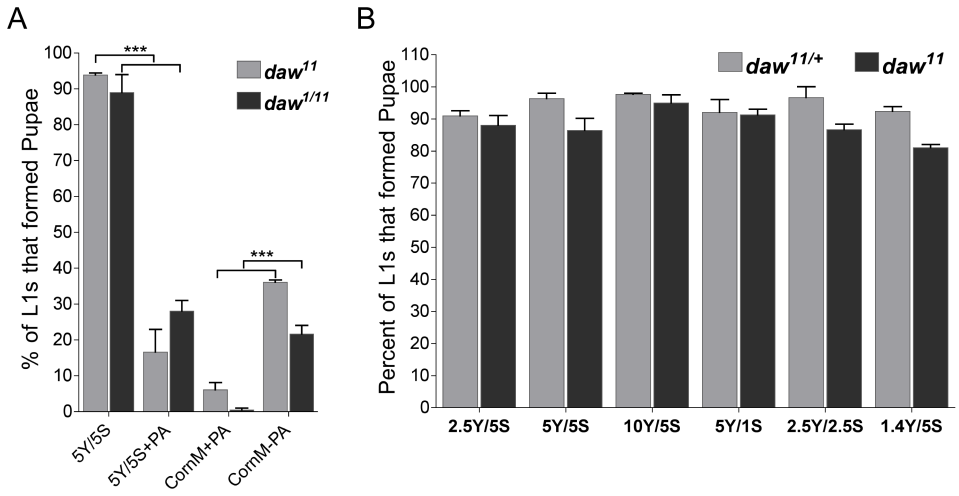

C

Food	Lipid	Carbohydrate	Protein	Free Sugar
1.4Y/5S	0.06	1.73	0.5	5
2.5Y/5S	0.1	3.09	0.89	5
5Y/5S	0.21	6.18	1.78	5
10Y/5S	0.42	12.36	3.5	5
5Y/1S	0.21	6.18	1.78	1
2.5Y/2.5S	0.1	3.09	0.89	2.5

Figure 21: Viability of *daw* mutant larvae on various food conditions

(A) Addition of PA to 5y5s food significantly increases lethality of both *daw* homozygous and trans-heterozygous mutants. Consistently, removing PA from CMF can significantly rescue lethality of *daw* mutants. (B) daw mutants did not show any significant change in viability on a range of food conditions mimicking either nutrient content of CMF or representing extremes of nutrient conditions. (C) Nutrient content of the various food conditions tested for *daw* viability. In green are the content in CMF for the corresponding class of nutrient. Red and dark-blue boxes show very low sugar and condition representing nutritionally poor food respectively.

3.2.4 *daw* dose-dependently regulates hemolymph sugar concentration and pH

We tested if ectopic over-expression of *daw* can rescue the novel loss-of-function phenotypes of *daw* described above. We found that over-expression of *daw* in the larval fat body using either the *cg-Gal4* or *fb-Gal4* driver completely rescues lethality of the mutants on CMF, enabling them to eclose as adults (Figure 22A, data not shown). Fat body over-expression of *daw* also causes a significant drop in circulating sugar concentration of *daw* mutants compared to controls (Figure 22B). Interestingly, excess *daw* causes circulating sugar concentration to drop below the normal range (~10 mg/ml compared to ~15mg/ml in feeding mid third instar larvae, Figure 18D,E and Figure 24E). A similar effect was observed for the hemolymph pH phenotype where over-expression of *daw* caused hemolymph pH of *daw* mutants to become significantly more basic than even the wildtype range (Figure 22C). These observations clearly show that Daw dose dependently regulates both circulating sugar concentration and hemolymph pH in *Drosophila* larvae. Consistent with dose-dependency, over-expressing *daw* in a much smaller number of cells, such as the ~ 14 larval IPCs (7 per brain hemisphere), rescues both diabetic and acidosis phenotypes but does not show an over-rescue effect (Figure 23). This result also highlights the ability of Daw to act as a systemic hormone in regulating both sugar balance and hemolymph pH.

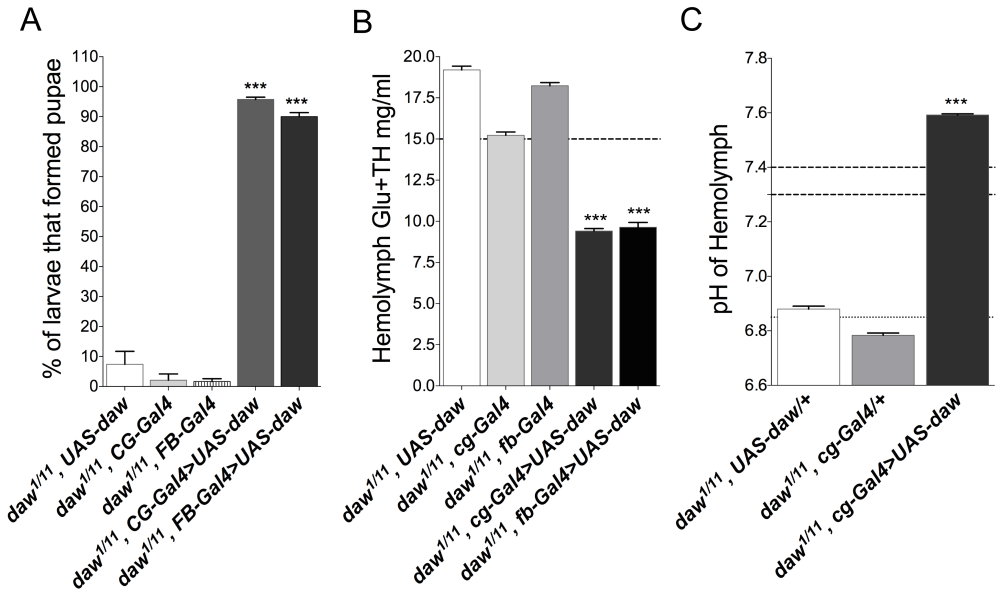

Figure 22: Ectopic expression of *daw* can rescue metabolic phenotypes of *daw* nulls

A *UAS-daw* construct was over-expressed in the *daw* mutant background using fatbody specific *cg-Gal4* or *fb-Gal4* drivers, and its ability to rescue lethality on CMF, circulating sugar concentration and hemolymph pH was assessed. Appropriate controls were *daw* mutants containing either the *UAS-daw* or *Gal4* construct alone. (A) Over-expression of *daw* using either driver was able to completely rescue viability of *daw* mutants on CMF. (B) Ectopic over-expression of *daw* using either driver significantly rescues circulating sugar concentration. Notably, *daw* over-expression lowered circulation sugar concentration to about 9mg/ml compared to ~ 15 mg/ml observed in wild-type controls (refer Figure. 2D,E) (C) Ectopic over-expression of *daw* was also able to significantly rescue hemolymph pH. Similar to its effect on sugar, *daw* over-expression increased hemolymph pH to ~ 7.6, much higher compared to the wild-type range of pH 7.3 to 7.4 (refer Figure 2G).

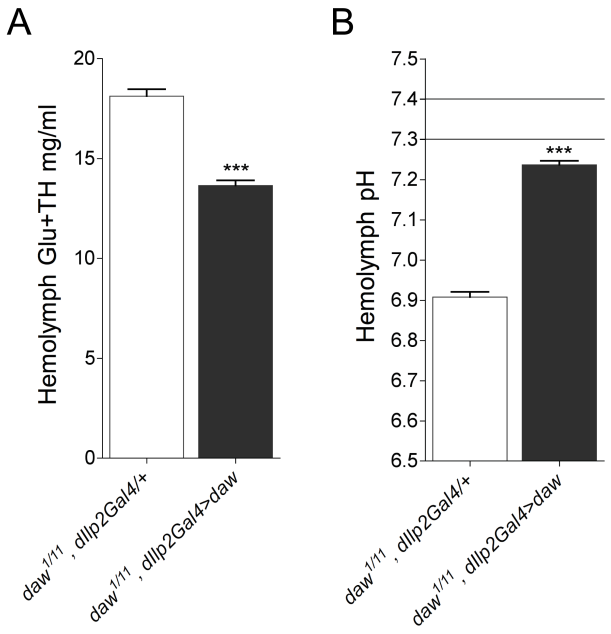

Figure 23: Over-expressing *daw* in the larval IPCs can rescue metabolic phenotypes of *daw* mutants

(A) Over-expressing daw in the IPCs using a dilp2-Gal4 driver can rescue the diabetic phenotype of daw mutants. (B) daw over-expression in the IPCs of daw mutants can also rescue the pH phenotype significantly.

3.2.5 Daw positively regulates DILP release from the larval Insulin Producing Cells (IPCs)

Metabolic phenotypes like elevated TAG, glucose, glycogen and elevated circulating sugar concentration, observed in the *daw* mutants, suggests a reduction of insulin signalling. To elucidate the mechanism by which *daw* may affect IIS, we examined various aspects of IIS such as *dilp* expression, Dilp release and signal reception in the *daw* mutants. We find that loss of *daw* does not affect expression levels of *dilps 1, 2, 3* or *5* in the IPCs of feeding mid third instar larvae (Figure 24A). However, immuno-staining of feeding larval CNSs using anti-Dilp2 antibody shows significant accumulation of Dilp2 in the IPCs of mutant animals (Figure 24B and B'). In the absence of any change in expression levels, this result indicates a deficiency in Dilp release from the IPCs. To examine this issue further, we checked for the efficiency of Dilp5 release from IPCs using a starvation/re-feeding experiment. Starving mid third instar larvae showed a strong accumulation of Dilp5 in both test and control CNSs (Figure 24C). Re-feeding for 4 hours on a nutritious media (2.5% yeast, 2.5% dextrose, 1% sucrose, 0.5% peptone and 0.5% yeast extract) induced control larvae to release nearly all Dilp5 peptide into circulation. However, *daw* mutants showed substantial retention of Dilp5 within the cell body upon refeeding, indicating a deficiency of Dilp release in mutant larvae in response to nutrients (Figure 24C).

If *daw* indeed regulates IIS upstream of the insulin receptor (Inr) by regulating Dilp release, increasing circulating Dilp titers in *daw* mutants should rescue the *daw* diabetic phenotype. Over-expressing *dilp2* in a group of non-insulin producing neuro-secretory cells using *Kurs6-Gal4* has been shown previously to hasten developmental timing and produce smaller adults as expected for Dilp overproduction (Géminard et al., 2009). Using the same *Kurs6-Gal4* driver line we found that overexpression of *dilp2* significantly reduces circulating sugar concentration in wildtype larvae (Figure 24D) and also significantly rescued the diabetic phenotype of *daw* null mutants (Figure 24E). These results show that the peripheral tissues in *daw* mutants are capable of responding to Dilps, and that loss of IIS in *daw* mutants is indeed largely caused by reduction in Dilp release into the hemolymph.

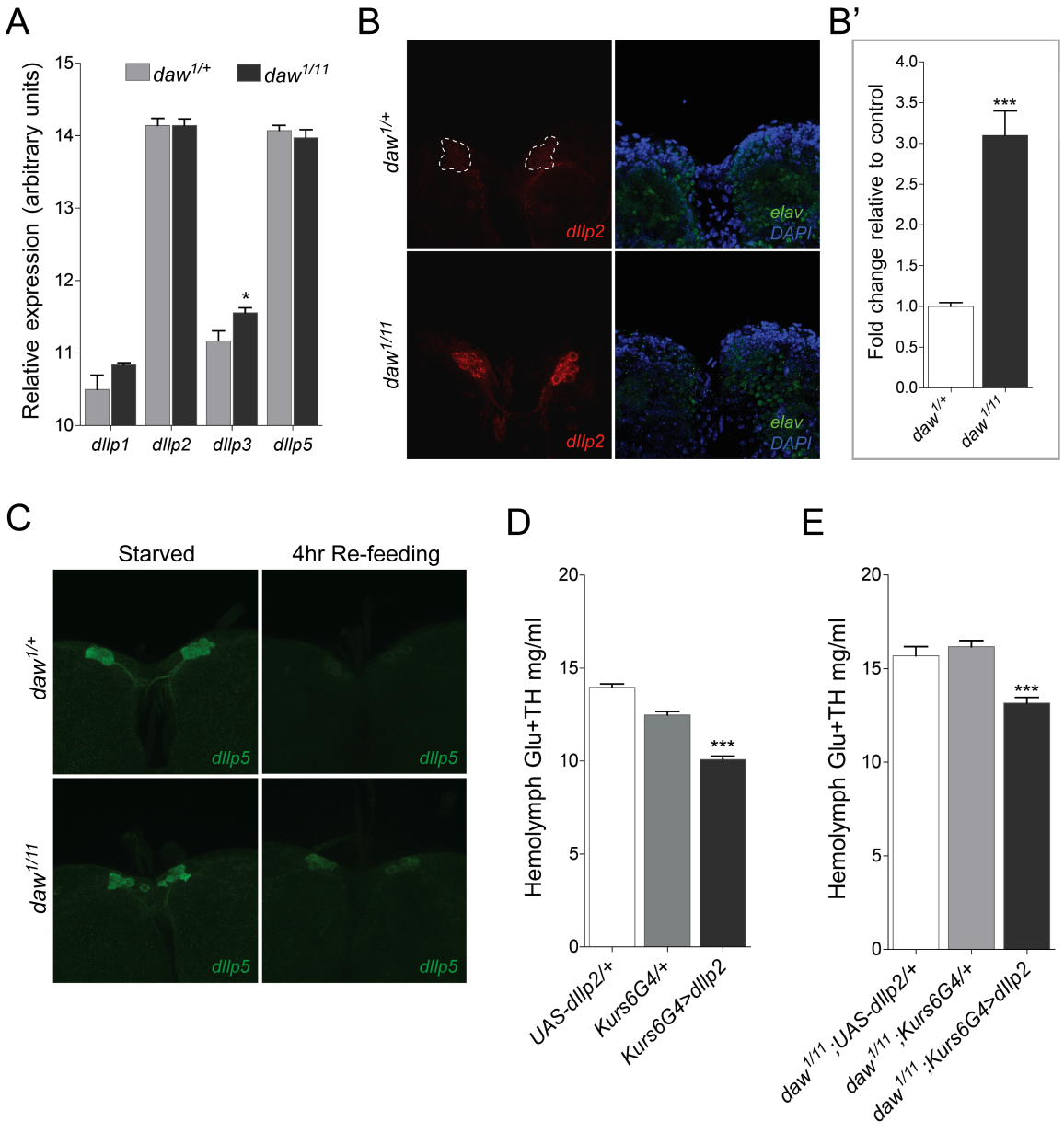

Figure 24: Daw positively regulates DILP release from the IPCs

(A) Expression level of *dilp 1,2, 3* and *5* in dissected *daw*$^{1/11}$ and control larval CNSs was measured using quantitative PCR and is reported as abundance relative to RPL23. (B) CNSs dissected from feeding control and mutant larvae was stained with anti-DILP2 antibody (red). Samples were imaged by confocal microscopy with laser and scan

settings adjusted to the accumulation state of *daw* CNS so as to avoid saturation. Under identical staining and imaging conditions control CNSs do not show any staining for DILP2 indicating significant accumulation of DILP2 in the mutants. Elav staining (green) of the same samples serve as staining controls showing that staining intensity of the test and control samples are comparable. (B') Quantified fluorescence intensity of DILP2 in the CNSs of *daw* mutant and control feeding larvae (n = 9 CNSs from 3 independent experiments for each plot) (C) CNSs dissected from 16 hour starved and 4 hour re-fed control and mutant larvae were stained with anti-DILP5 antibody (green). Under identical staining and imaging conditions DILP5 staining was much stronger in mutant re-fed CNSs than control animals. DILP5 staining in starved mutant and control animals was identical. (D) Increasing DILP2 titers in circulation of wild-type animals by over-expressing *dilp2* in non-insulin producing neuro-secretory cells (*Kurs6-Gal4>dilp2*) causes a significant decrease in circulating sugar concentration compared to matched controls. (E) *Kurs6-Gal4>dilp2* had a similar effect on circulating sugar concentration in *daw* mutant larvae.

3.2.6 Daw regulates acidosis by acting on large metabolic tissues like the larval fatbody

daw mutants show significant accumulation of several organic acids that are intermediates of normal sugar metabolism. Therefore, we predicted that the acidosis observed in *daw* mutants is likely caused by a metabolic imbalance. Consistent with this notion, we find that expression of an activated type-I receptor, $babo^{CA}$, in any large tissue like the gut, muscle or fat body, was able to significantly rescue the acidosis phenotype (Figure 25A). Interestingly, expressing $babo^{CA}$ in the fat body made the hemolymph pH of *daw* mutants significantly more basic than normal, as was observed for *daw* over-expression

(Figure 25A and Figure 25C). These results indicate that *daw* signaling likely regulates metabolic function in several large tissues which together contribute to overall pH balance in larval hemolymph. To determine if alterations in the organic acid levels are responsible for the acidosis observed in *daw* mutants, we compared *daw*^{11}*; fb-Gal4/+* controls and *daw*^{11}*; fb-Gal4>babo*^{CA} rescued animals for metabolite content using GC/MS analysis. The rescued animals had a significantly lower content of major organic acids compared to controls, indicating a direct correlation between acidosis and the level of these acids (Figure 25B). We therefore argue that *daw* signaling affects internal pH by altering metabolic accumulation of various organic acids including pyruvate, citrate, fumarate and malate.

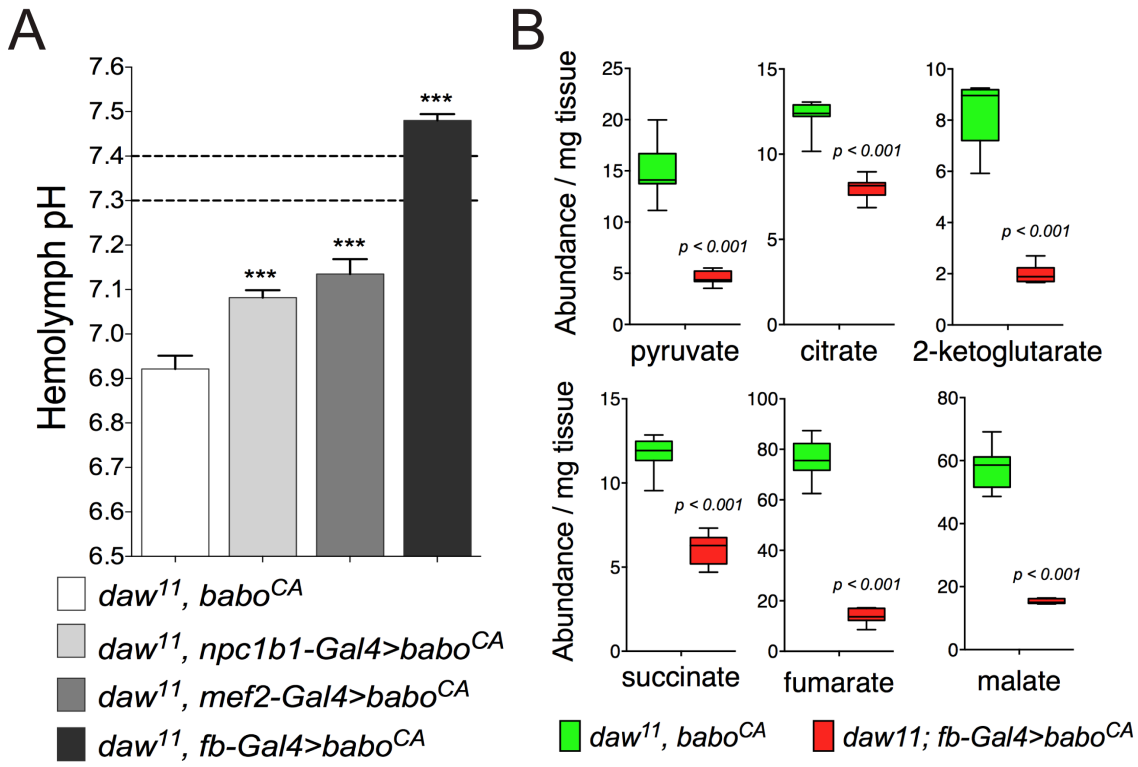

Figure 25: Daw regulates pH balance by acting on the larval fatbody

(A) Over-expression of a constitutively active type-I receptor, *babo*^{CA}, in major metabolic tissues of *daw* mutants can significantly rescue acidosis observed in mutant controls. Notably, expressing *babo*^{CA} in the fatbody mimics daw over-expression (Figure. 4C). (B) A GC/MS metabolomics analysis of mutant control and rescued larvae show significant down-regulation of multiple organic acids that are products of normal sugar metabolism.

3.2.7 Loss of Daw affects mitochondrial gene expression and physiology in the fatbody

We showed that loss of Daw leads to metabolic acidosis by causing accumulation of TCA cycle intermediates in major metabolic tissues like the FB. Since the acidosis phenotype is mediated by canonical TGF-β signaling we

decided to identify the transcriptional targets of Daw signaling to better understand how Daw regulates TCA cycle or mitochondrial metabolism. We focused on identifying targets of Daw in the FB as activating TGF-β signaling in the FB could rescue the acidosis phenotype of daw mutants. Gene expression changes in *daw* mutant FB compared to wildtype control were identified using Illumina next generation RNA sequencing. The sequencing results show that Daw primarily regulates genes that are involved in cellular metabolic processes (Figure 26A). A Gene Ontology (GO) class enrichment analysis of genes that were significantly deregulated in *daw* mutants (≥1.3 fold) showed that 37 out of 38 GO classes for down-regulated genes and 66 out of 68 classes for up-regulated genes belonged to cellular metabolic processes. This result shows that Daw is a major metabolic regulator and that effects of Daw loss-of-function on cellular metabolism cannot be attributed to any single metabolic gene or pathway. Notably, consistent with the role of Daw in accumulation of metabolic acids, GO classes involved in carboxylic acid and organic acid metabolic processes showed some of the most significant enrichments among deregulated genes in *daw* mutants (Figure 26A).

Of the genes that were deregulated in *daw* mutants we found many that encodes for enzymes of the glycolysis and TCA cycle pathway (Figure 26B). While the effect of Daw on glycolytic genes was incoherent, with some enzymes (Hex-A, Eno) being up-regulated and others very strongly down-regulated

(Gapdh1, Ald and Pdk), loss of Daw was consistent in causing up-regulation of a number of TCA cycle enzymes (Figure 26B). Loss of Daw also led to significant up-regulation of a large number of genes that encode mitochondrial proteins of the oxidative phosphorylation apparatus (Table1). Since loss of Activin-A in mammals has been proposed to cause increased mitochondrial biogenesis we checked if up-regulation of mitochondrial genes in the *daw* mutants is caused by increased mitochondrial mass. We visualized mitochondria of *daw* mutant and control larval FBs using mitotracker staining (Figure 26C). While we did not see any increase in the amount of mitochondria in the mutant cells, we did observe obvious differences in mitochondrial morphology. In w^{1118} FB cells mitochondria are visible as a network of fine tubular structures that are most dense near the surface of the cell (Figure 26C). In comparison *daw* mutant cells had mitochondria that were highly clustered leading to a less dense but clumpy and fragmented mitochondrial network (Figure 26C). Over all these results show that Daw negatively regulates a large number mitochondrial metabolic genes and is a major regulator of mitochondrial activity and morphology.

A

GO Category	Number of Genes (Total)	P Value
Genes Up-regulated in *daw*$^{1/11}$ mutants (≥1.3 fold)		
Oxidation-reduction process	84 (474)	4.18e-24
Carboxylic acid metabolic process	55 (286)	1.26e-17
Organic acid metabolic process	55 (299)	1.00e-16
Generation of metabolites & energy	31 (111)	4.61e-15
Respiratory electron transport chain	21 (65)	5.69e-12
cellular aminoacid metabolic process	36 (202)	6.35e-11
Lipid particle	47 (205)	2.17e-18
Mitochondrial part	56 (376)	6.50e-13
Genes Down-regulated in *daw*$^{1/11}$ mutants (≥1.3 fold)		
Small molecule metabolic process	61 (602)	5.86e-11
Organic acid metabolic process	35 (299)	2.73e-8
Nucleotide metabolic process	20 (170)	2.56e-5
Microtubule associated complex	32 (352)	2.64e-5
Amino acid metabolic process	22 (202)	3.43e-5
Gluconeogenesis	3 (4)	2.78e-4

B

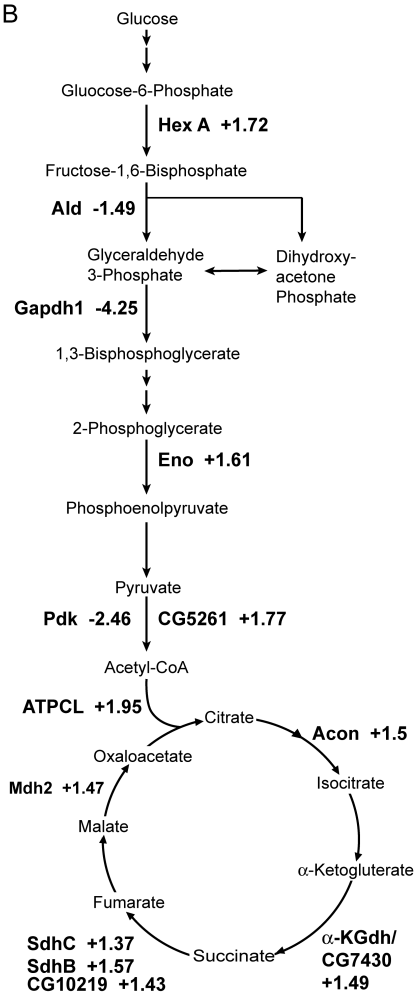

C

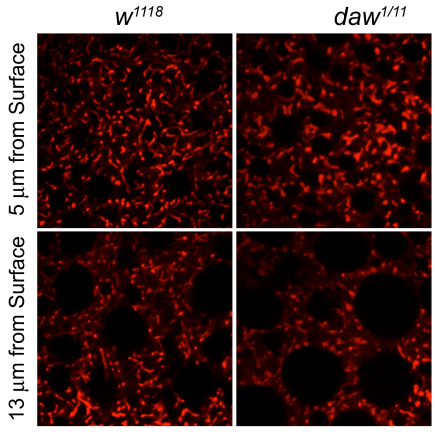

Figure 26: Daw is a major regulator of metabolic genes and mitochondrial metabolism.

(A) GO classes that were most significantly enriched in genes that were de-regulated in *daw* mutants. Up-regulated genes in *daw* mutants primarily affected oxidation-reduction, carboxylic acid metabolism and respiratory electron transport chain genes. (B) Glycolytic and TCA cycle enzymes that were significantly affected in the *daw* mutants. (C) Mitotracker staining of w^{1118} and $daw^{1/11}$ FB cells. Loss of Daw causes significant morphological changes in the mitochondrial network marked by fragmented larger mitochondrion.

Table 1: Electron transport chain genes that are up-regulated in *daw* mutants.

Gene ID	Gene Name	Function (electron transport chain)	Fold change
CG6030	ATPsyn-d	ATP synthase, subunit d	1.3
CG4412	ATPsyn-Cf6	ATP synthase coupling factor 6	1.5
CG11154	ATPsyn-β	ATP synthase, subunit β	1.4
CG10664	CoIV	Cytochrome c oxidase subunit IV	1.3
CG11015	CoVb	Cytochrome c oxidase subunit Vb	1.5
CG7181	CoVIII	Cytochrome c oxidase subunit VIII	1.3
CG17903	Cyt-c-p	Cytochrome c proximal	2.3
CG2968	l(1)G0230	Hydrogen-exporting ATPase activity	1.4
CG13240	l(2)35Di	NADH dehydrogenase (ubiquinone) activity	1.5
CG9762	l(3)neo18	NADH dehydrogenase (ubiquinone) activity	1.4
CG3683	NDUFA8	NADH dehydrogenase (ubiquinone) 1 alpha subcomplex, 8	1.5
CG8844	Pdsw	NADH dehydrogenase (ubiquinone) activity	1.5
CG7361	RFeSP	Rieske iron-sulfur protein	1.5
CG3321	**Predicted**	Hydrogen-exporting ATPase activity	1.3
CG8680	**Predicted**	NADH dehydrogenase (ubiquinone) activity	1.5
CG9306	**Predicted**	NADH dehydrogenase (ubiquinone) activity	1.4
CG10320	**Predicted**	NADH dehydrogenase (ubiquinone) activity	1.4
CG18624	**Predicted**	NADH dehydrogenase (ubiquinone) activity	1.6
CG32230	**Predicted**	NADH dehydrogenase (ubiquinone) activity	1.3
CG3621	**Predicted**	NADH dehydrogenase (ubiquinone) activity	1.5
CG4769	**Predicted**	Transferring electrons within CoQH2-cytochrome c reductase complex	1.4
CG3560	**Predicted**	Ubiquinol-cytochrome-c reductase activity	1.4
CG3731	**Predicted**	Ubiquinol-cytochrome-c reductase activity	1.4

3.2.8 Daw regulates IIS and acidosis via independent mechanisms

In vertebrates chronic loss of insulin signaling results in metabolic keto-acidosis. In contrast, metabolic acidosis has also been proposed to cause insulin resistance (Cuthbert and Alberti, 1978; Mak, 2008). To define the cause and effect relationship in *daw* mutants between reduced insulin signaling and acidosis, we first asked if loss of IIS contributes to acidosis (Figure 27A). We found that over-expressing the potassium channel *Ork1ΔC*, to block insulin release in the larval IPCs, leads to a significant diabetic phenotype (Figure 27B), but it does not affect hemolymph pH (Figure 27C). Additionally, *Kurs6-Gal4* driven over-expression of *dilp2*, which significantly rescues the diabetic phenotype in *daw* mutants, did not affect hemolymph pH of the mutants (Figure 27D). These results show that loss of IIS does not cause or contribute to the acidosis phenotype observed in the *daw* mutants. Next, we examined if expressing $babo^{CA}$ in the fat body of *daw* mutants, which is able to rescue the acidosis phenotype (Figure 25), is also able to rescue the diabetic phenotype of *daw* mutants. As shown in Figure 27E, fatbody specific expression of $babo^{CA}$ does not reduce the excess sugar levels in the hemolymph of *daw* mutants (Figure 27E). Taken together, these data indicate that acidosis does not contribute to loss of IIS, nor does impairment of IIS contribute to acidosis. Thus, we conclude that *daw* regulates accumulation of metabolic acids and IIS through separate mechanisms.

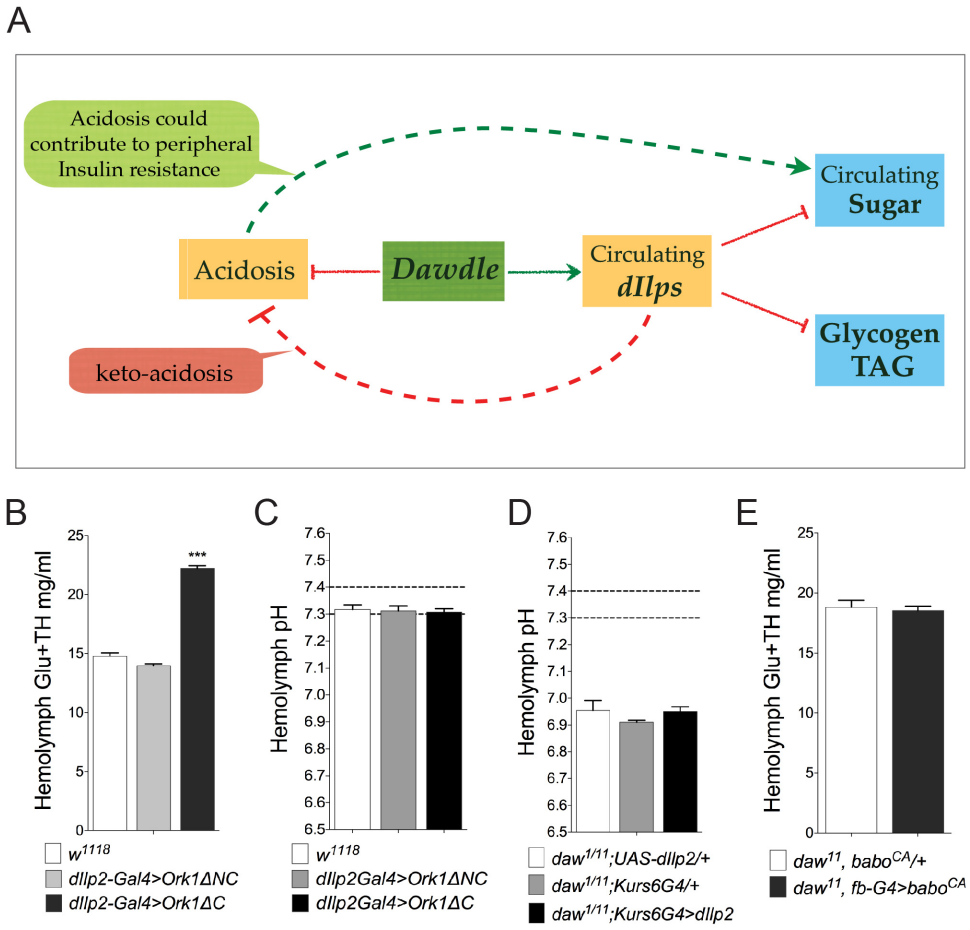

Figure 27: Daw regulates sugar and pH homeostasis independently

(A) Schematic showing the role of *daw* in regulating nutrient and pH homeostasis. Dotted lines represent possible interactions between the two prime phenotypes of loss of *daw*. (B) Over-expression of a potassium channel *Ork1ΔC* in the IPCs suppresses IIS and significantly up-regulates circulating sugar concentration in test animals compared to both wild-type and a genetically matched control. (C) *Ork1ΔC* over-expression in the IPCs did not affect the hemolymph pH of the diabetic animals. (D) Increasing DILP2 titer in circulation by over-expressing *dilp2* with *Kurs6-Gal4* did not affect hemolymph pH of *daw* mutant larvae. (E) Fatbody specific over-expression of $babo^{CA}$ failed to rescue hemolymph sugar concentration of the *daw* mutants.

3.3 DISCUSSION

Drosophila larvae spend much of their lives buried in food and therefore are constantly challenged by an environment that likely varies in hydration levels, pH, ionic strength, nutritional content and perhaps other factors, depending on the food type. Adapting to these challenges demands robust homeostatic mechanisms to cope with the potential variability. *Drosophila* larvae therefore serve an apt model system to study regulatory networks that maintain systemic homeostasis. In this study, we demonstrate a central role of *Drosophila* TGF-β/Activin signaling in regulating insulin signaling, metabolism, and pH balance, all of which are important for organismal homeostasis.

3.3.1 Daw affects IIS by regulating insulin release through a non-cell-autonomous process

Similar to vertebrate insulin, *Drosophila* insulin-like peptides are produced and stored in dense granules in the larval IPCs and are released into the hemolymph in response to nutrient availability (Géminard et al., 2009; Rutter, 2001). Apart from regulating Dilp release, nutrient availability also regulates transcription of certain *dilps,* since starvation has been shown to down-regulate *dilp3* and *dilp5* expression (Ikeya et al., 2002; Mukherjee et al., 2007). We did not observe any decrease in the steady state mRNA levels of *dilp 1, 2, 3* or *5* in the *daw* mutants indicating that these mutants are neither starved nor are they defective in production of Dilps. However, *daw* mutants showed a significant

accumulation of Dilp2 in the IPCs even when food is abundant indicating a deficiency in food-induced Dilp release. Similarly, we show that the efficiency of Dilp5 release in response to nutrient availability is also compromised in *daw* mutants. These observations, coupled with the finding that ectopic expression of *dilp2* in other neurosecretory cells is able to rescue the *daw* diabetic phenotype, indicate that in *daw* mutants, peripheral tissue is still responsive to Dilps, and that defective release of Dilps is the primary cause of the IIS defect.

Our observation that TGF-β/Activin signaling impacts IIS in *Drosophila* reinforces a growing body of evidence suggesting that this regulatory interaction is a general function of TGF-β/Activin signaling across a diversity of species. For example, recent work in *C. elegans* has documented a role for TGF-β signaling in mediating insulin release through transcriptional regulation of a potassium channel (*exp-2*) in the insulin producing cells (Park et al., 2012). However, such a cell-autonomous mechanism does not appear to be the case in *Drosophila* as neither *smoxRNAi* nor $babo^{CA}$ over-expression in the IPCs affected circulating sugar concentration in the wild-type or *daw* mutants, respectively (Figure 28A and B). Additionally, the *Drosophila exp-2* homologue, *shab*, did not show any expression change in the *daw* mutant larval CNSs (Figure 28C). Previous studies have demonstrated that non-cell-autonomous regulation of Dilp release is operative in *Drosophila* and in some cases involves nutrient-induced signals from the fat body (Géminard et al., 2009; Rajan and Perrimon, 2012). Once again,

however, expressing *babo*^{CA} in the fat body of *daw* mutants did not rescue the *daw* diabetic phenotype, suggesting that this tissue is not the source of the indirect Daw regulated signal that enhances Dilp release. Additional experiments are in progress to identify the relevant tissue or cell type involved in this relay.

Activin/TGF-β family members have also been implicated in the regulation of insulin signaling in vertebrates. However, in these cases the molecular details are ill defined, in part due to the complexity and redundancy of the components of the signaling pathway, as well as the involvement of non-canonical signaling mechanisms. Numerous mouse knockouts as well as gain-of-function studies using various Activin signaling components reveal clear effects on pancreas development and β-cell number, in many cases leading to generation of adult animals with reduced glucose tolerance (Wiater and Vale, 2012). In addition, Smad3, a homolog of *Drosophila* Smox, has been shown to bind to the insulin promoter, and loss or knockdown of Smad3 leads to an increase in insulin transcription (Lin et al., 2009; Tan et al., 2011; Yadav et al., 2011). In contrast, we find that loss of *daw* in *Drosophila* does not alter the specification or numbers of IPCs in the brain, nor does it affect transcription of the IPC-expressed *dilps*.

Intriguingly, there is evidence in mice that Activin family members can also modulate adult β-cell function at the level of insulin release. Both Activin A and B subunits are expressed in mature β-cells consistent with either autocrine or juxtacrine roles, but some data suggest that they affect insulin secretion in

opposite ways with Activin A promoting Ca^{2+} influx and insulin release but Activin B suppressing both (Bertolino et al., 2008; Florio et al., 2000; Totsuka et al., 1988). While this notion has been challenged by another more recent study (Bonomi et al., 2012), it is intriguing to note in this regard that mutations in *actβ*, a second *Drosophila* Activin-like ligand that is strongly expressed in the IPCs, result in precocious development and smaller pupae and adults perhaps indicative of a gain in IIS (L. Moss-Taylor and M.B. O'Connor unpublished). Another relevant issue to note with respect to any role of Activin A or B in insulin release in vertebrates is the likely involvement of non-canonical signaling. Stimulation of isolated rodent β-cells with Activin A or B can influence Ca^{2+} influx and insulin release very rapidly (~1 to 5 minutes, respectively) and this short reaction time suggests involvement of a non-Smad signaling pathway in the process (Bertolino et al., 2008; Furukawa et al., 1995). In contrast, in *Drosophila* we show that the release of Dilps appears to be Smad dependent. Taken together, these examples illustrate that although the ability of TGF-β/Activin signaling to regulate IIS appears to be conserved across species, the exact mechanisms employed may vary.

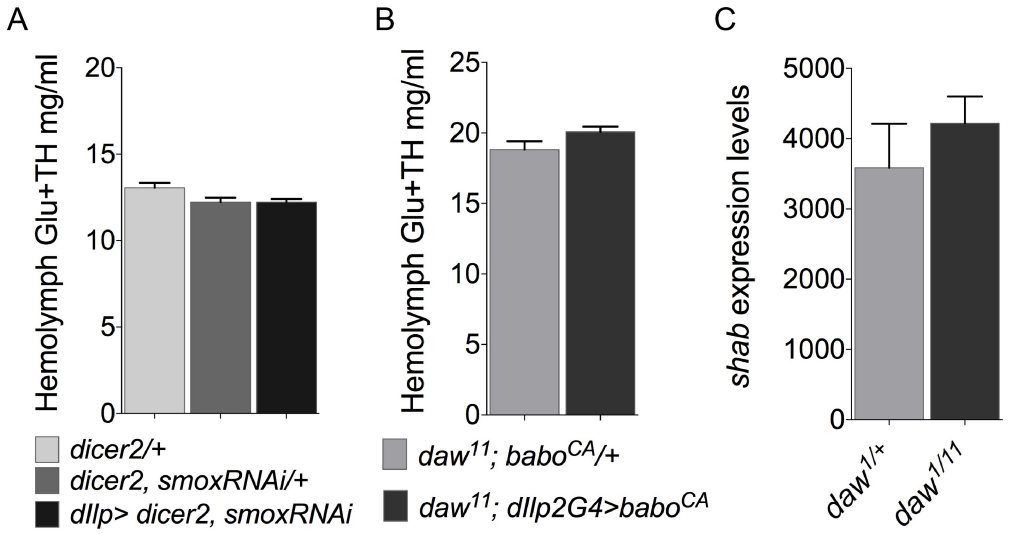

Figure 28: Daw regulates DILP release cell non-autonomously

(A) SmoxRNAi along with dicer2 over-expression in the IPCs was not able to induce a diabetic phenotype in w1118 larvae. (B) baboCA over-expression in the IPCs of daw mutants was not able to rescue the diabetic phenotype of daw mutants. (C) Expression level of shab larval CNSs of daw mutants and controls was measured using quantitative PCR. daw mutants did not show any significant difference in shab expression compared to controls.

3.3.3 Acidosis: does Daw regulate systemic pH or is it metabolic acidosis?

We showed that loss of *daw* causes significant acidification of the larval hemolymph, which if exacerbated by growth on low pH food leads to considerable larval lethality. The mechanisms influencing acid-base balance of the insect hemolymph involve a wide range of variables including CO_2 exchange, metabolism, ion transport and buffering molecules (Harrison, 2001; Wyatt, 1961). While alterations in any of these processes can result in pH imbalance, we

believe that acidosis in *daw* mutants is likely caused by metabolic dysfunction based on the observation that activating TGF-β signaling in metabolic tissues can rescue the acidosis phenotype of the *daw* mutants.

Much like in vertebrates, the insect renal system, comprising of the malpighian tubules, gut and anal pads, is a major regulator of hemolymph acid-base balance. These tissues regulate pH primarily by mediating ion and acid-base transport, and can effectively clear out inorganic acids like HCl from the hemolymph as demonstrated by acid injection and recovery experiments carried out in locusts (Harrison and Phillips, 1992; Phillips, 1981; Phillips et al., 1994; Thomson et al., 1988). However, expressing *smox* RNAi in the malpighian tubules did not induce acid sensitive lethality in wild-type animals indicating that the larval renal system is likely not impaired in the *daw* mutants (data not shown). More importantly, a role of *daw* in regulating acid-base balance solely through the renal system is refuted by the fact that expressing $babo^{CA}$ in the fat body or the muscle can significantly rescue the acidosis phenotype. This observation also makes it very unlikely that loss of *daw* is disrupting gas exchange through an affect on tracheal function. It is possible that alterations in buffering capacity might partially contribute to the *daw* acidosis since the fat body is the major source of hemolymph proteins (one of the major circulatory buffers (Harrison et al., 1990; Levenbook, 1950)) and we actually see a slight alkalinization of the hemolymph when we express $babo^{CA}$ in the fat body. However, the significant

changes in the amount of metabolic acids in the *daw* mutants makes it more likely that acidosis in *daw* mutants is caused by metabolic dysfunction.

In Lepidopterans, metabolites like succinate, citrate and organic phosphates are found in high concentrations in the hemolymph and are thought to play an important role in determining pH balance (Harrison, 2001; Wyatt, 1961). Most of these acids are produced by metabolic pathways, and loss of *daw* consistently leads to enhanced total body levels of major metabolic acids such as pyruvate, citrate, 2-ketoglutarate, succinate, fumarate and malate. This indicates that Daw likely globally regulates general cellular metabolism, and its loss leads to accumulation of these organic acids to excess levels such that they eventually overwhelm the various intrinsic buffering systems leading to acidosis. This also accounts for why expression of $babo^{CA}$ in any large tissue is able to partially rescue the acidosis phenotype.

3.3.4 Daw regulates expression of mitochondrial metabolism genes and mitochondrial fusion

Organic acids up-regulated in *daw* mutants are primarily TCA cycle intermediates. Since activating TGF-β signaling in the FB can rescue the concentration of these metabolites in the *daw* mutants, our data clearly indicates that Daw regulates peripheral cellular metabolism, particularly mitochondrial metabolism. Consistently, our deep sequencing result shows that Daw is a major regulator of cellular metabolic gene expression and expression level of multiple

TCA cycle and the electron transport chain enzymes go up in the *daw* mutants. Apart from TCA cycle enzymes multiple other genes that are involved in or are predicted to be involved in carboxylic acid and organic acid metabolic processes were also significantly up-regulated in the *daw* mutants. This up-regualtion of a whole suite of mitochondrial genes can predictably increase mitochondrial output, including output of TCA cycle intermediates, and explains why *daw* mutants accumulate a large amount of metabolic acids. Increased mitochondrial output would also require a steady supply of bio-fuels like free glucose or acetyl-CoA. However, we show that *daw* mutants are defective in IIS and therefore inefficient in cellular sugar uptake. Moreover, down-regulation of glycolytic enzymes like Hex-A, Gapdh-1 and Pdk makes it unlikely that glycolytic production of pyruvate and Acetyl-CoA fuels TCA cycle in the *daw* mutants. Rather, Acetyl-CoA is probably supplied by β-oxidation and ketogenesis pathways in the mutants, and consistent with this possibility we observed up-regulation of a number of β-oxidation and ketogenesis enzymes in the *daw* mutants.

Up-regulation of mitochondrial genes is also indicative of increased mitochondrial biogenesis as has been shown to be an outcome of losing Activin-A in vertebrate models (Li et al., 2009). While our mitotracker staining did show larger mitochondrion in *daw* mutant FB, we observed that the density of mitochondrial network was thinner and fragmented in the mutants indicating defects in mitochondrial fusion (Chen, 2005). Mitochondrial fusion is a regulated

event that, along with mitochondrial fission, allows remodeling of the architecture of the mitochondrial network within the cytoplasm. Loss of mitochondrial fusion leads to formation of less tubular and spherical/clumped mitochondria much like what we observed in *daw* mutants (Chen, 2005). While this change in mitochondrial physiology is the most obvious outcome of defects in mitochondrial fusion, physiological impact of this defect are also significant (reviewed in (Chen, 2005; Picard et al., 2013)). Two of the conserved and well-known regulators of mitochondrial fusion are Mitofusin 1 and 2 (Mfn1/2) and OPA1. Loss of these genes has been shown to cause a reduction in oxygen consumption caused by attenuation of electron transport rates in respiration complexes I, III and IV in mammalian cell cultures (Chen et al., 2005). Mfn-null and OPA1-RNAi cells also exhibit reversible inhibition of cell growth and loss of mitochondrial membrane potential (Chen et al., 2005). Consistently, despite an increase in expression of mitochondrial enzymes, *daw* mutants showed a significant reduction in ATP content indicating loss of mitochondrial activity (Figure 29). In line with the role of fusion in mitochondrial activity, artificially induced or naturally occurring mutations in Mfns and OPA1 has been implicated in developmental problems, neuropathies, obesity and vascular disease (Chen et al., 2003; Delettre et al., 2002; Züchner et al., 2004). The fact that a higher order transcriptional regulators like Daw regulates mitochondrial fusion and thereby mitochondrial activity opens up the possibility of further genetic dissection of the process in *Drosophila*.

Interestingly, expression level of the fly homologues of known regulator of mitochondrial fusion or fission like Mfns, OPA1 and DRP1 was not affected in the *daw* mutants. Therefore, it is likely that Daw regulates fusion by affecting expression of novel regulators of the process.

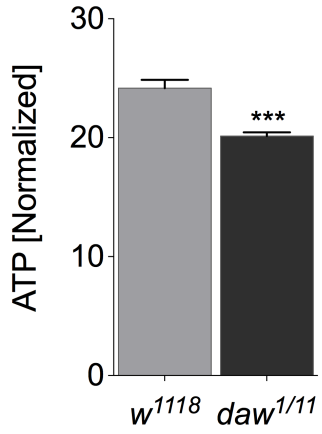

Figure 29: Total ATP content of *daw* mutant larvae

Total ATP content of *daw* mutant and control midthird instar larvae was measured and normalized to total protein content.

3.3.5 Daw regulates IIS and acidosis via independent mechanisms

Since IIS is an important metabolic regulator in both insects and vertebrates, and because chronic loss of insulin signaling in vertebrates often results in keto-acidosis, it was surprising to find that loss of IIS did not cause or contribute to the acidosis observed in *daw* mutants. Moreover, we found that chronic loss of IIS in wild-type *Drosophila* larvae also did not result in acidosis. We speculate that perhaps the differences in the manifestation of keto-acidosis

between vertebrates and *Drosophila* could be due to differences in how insulin signaling affects metabolic processes. In vertebrates loss of insulin eventually results in keto-acidosis because of increased fatty acid oxidation to meet energy demands. However in *Drosophila* and *Bombyx* larvae, loss of insulin actually leads to an increase in the storage of TAG suggesting that the modes of alternative energy production upon loss of IIS could be different in insect larvae and vertebrates (Böhni et al., 1999; Broughton et al., 2005; Satake et al., 1997; Tatar, 2001; Teleman, 2010).

While we showed that loss of IIS is not responsible for the acidosis phenotype, we also entertained the notion that acidosis might affect insulin signaling since in vertebrates several reports have proposed that acidosis can lead to insulin resistance, perhaps by affecting various ligand-receptor interactions (Cuthbert and Alberti, 1978; Mak, 2008). However, we could completely rescue acidosis in *daw* mutants without ameliorating the diabetic phenotype, indicating that acidosis does not contribute to the diabetic phenotype observed in *daw* mutants. It is important to note that acidosis always correlates with the relative amount of metabolic acids. Since we could reduce the output of metabolic acids without affecting the diabetic phenotype, we can also conclude that Daw regulates accumulation of metabolic acids independent of IIS.

3.3.6 Hormone-like function of Daw

We showed that expressing *daw* in any large, metabolically active, tissue is able to rescue the lethality of *daw* mutant larvae. In addition, we showed that Daw influences circulating sugar concentration and hemolymph pH in a dose-dependent manner. These observations indicate that Daw is likely released into the hemolymph from tissues of origin and exerts its effect in an endocrine manner much like a hormone. Curiously, unlike most hormones, *daw* expression is not limited to one tissue or gland. Rather *daw* is expressed in a wide array of tissues including muscle, FB, gut, imaginal discs and surface glia of the CNS (Parker et al., 2006; Serpe and O'Connor, 2006). One possible purpose for such a wide distribution of a hormone like peptide could be that, being a metabolic regulator, *daw* expression is regulated by nutritional cues and its distribution in multiple tissues ensures integration of systemic metabolic status.

3.3.7 Homeostasis and its significance in adapting to extreme conditions

The ability to maintain physiological homeostasis is crucial for survival under conditions of environmental variability and the phenotypes of *daw* mutants we present here reflect the consequences of impaired sugar homeostasis and pH balance. We show that *daw* mutants manifest significantly higher lethality on a high sugar diet (HSD). Interestingly, HSD has been shown to induce peripheral insulin resistance in *Drosophila* larvae (Musselman et al., 2011; Pasco and Léopold, 2012) and such HSD-induced peripheral resistance in combination with

impaired insulin release already present in the *daw* mutants can lead to larval lethality. Alternatively, HSD could further elevate circulating sugar concentrations and cause lethality by damaging tissues. However, since circulating sugar in the larvae is primarily non-reducing trehalose, and since insects do not contain a capillary system, which is often the target of damage by high sugar in vertebrates, it is unlikely that hyper-trehalosemia alone can cause tissue damage in the larvae.

Alterations in pH homeostasis however, can have wide spread physiological and behavioral consequences such as muscle degeneration, altered enzymatic activity and habitat and food choice (Harrison, 2001). Predictably, acidosis is expected to have a more severe impact on the viability of the *daw* mutants. Consistent with this prediction, aggravating the acidosis of *daw* mutants by exposing them to acidic food conditions leads to significantly higher lethality of the mutant larvae. Interestingly, in our feeding experiments, HCl acidified food was less detrimental to the growth of *daw* mutant larvae than food acidified with organic acids. This may indicate that the larval renal system is better able to cope with excess simple ions such as Cl^- and H^+ than larger organic acids like propionate and acetate. Consistently, food acidified with organic acids like PA and AA also had a significantly more severe effect on developmental timing and viability compared to HCl acidified food.

The mechanisms by which acidic food affects developmental timing remain an open question. However, one possible explanation for developmental delay might be alterations in hormonal signals involved in regulation of developmental timing, caused by low pH of the hemolymph. In support of this possibility, studies using honey bees and locusts have shown that changing partial pressure of CO_2 affects pH balance and alters juvenile hormone levels (Bühler et al., 1983; Fuzeau-Braesch et al., 1982). Additionally, acidosis has been shown in vertebrates to affect secretion and activation of several hormones including corticosteroids, thyroid hormone and parathyroid hormone (Mitch, 2006; Wiederkehr et al., 2004).

3.5 EXPERIMENTAL PROCEDURES

3.5.1 Fly Strains and Food

daw alleles daw^{11} and daw^{aact1} (referred in short as daw^{1}) has been described previously, as have the $smox^{F4}$, $babo^{Fd4}$ and $babo^{CA}$ alleles (Brummel et al., 1999; Peterson et al., 2012; Serpe and O'Connor, 2006; Zheng et al., 2003). Other fly lines used: *UAS-daw* (Serpe and O'Connor, 2006), *UAS-dilp2* (Brogiolo et al., 2001), *UAS-Ork1ΔC* and *UAS-Ork1ΔNC* (Bloomington stock center), *UAS-smoxRNAi3B3* (Peterson et al., 2012), *cg-Gal4* (Bloomington stock center, (Hennig et al., 2006)), *fb-Gal4* (Neufeld lab.), *mef2-Gal4* (Bloomington stock center), *NCP1B1-Gal4* and *Kurs6-Gal4* (Siegmund and Korge, 2001). A list

of recombinant fly lines generated during the course of this study is shown in Table 1.

Table 1. Recombinant fly lines generated during the course of this study

daw^{1}, UAS-dilp2/CyoYFP	*daw^{11}, UAS-babo^{CA}/CyoGFP*	*daw^{11}, fb-Gal4/CyoGFP*
daw^{11}, cg-Gal4/CyoGFP	*daw^{11}, mef2-Gal4/CyoGFP*	*daw^{11}, OK72-Gal4/CyoGFP*
daw^{11}, npc1b1-Gal4/CyoGFP	*daw^{11}, Kurs6-Gal4/CyoGFP*	*daw^{11}, dilp2-Gal4/CyoGFP*

For all over-expression experiments a single *Gal4* element was used to drive a single UAS construct. Controls contained either a single copy of the *Gal4* element (Gal4 control) or a single copy of the UAS element (UAS control). For example *daw$^{1/11}$, cg-Gal4>UAS-daw* is an abbreviation for *daw^{1},UAS-daw/ daw^{11},cg-Gal4*. Corresponding controls are *daw^{1},UAS-daw/+* and *daw^{11},cg-Gal4/+.*

Flies were raised on standard cornmeal food (CMF). Mutant and control larvae were grown on yeast paste food (YPF) or semi-defined food from the time of hatching onwards, unless mentioned otherwise.

L1 larvae were collected 24 hours after egg collection (collections made daily from 11am to 2pm) and reared at 30-40 animals per plate/tube in a 12 hour

light/dark cycle. Experiments were performed 24 hours prior to when 25% of the larvae formed pupae. Time required for reaching 25% pupariation was determined by generating a developmental timing curve using the first egg collection of every collection cage.

Analysis of nutrient content of CMF was done by Medallion labs (Minneapolis, MN). Contribution of yeast to nutrient content was calculated from nutrition facts per gram of yeast provided by the manufacturer (Saf-instant, Lesaffre Yeast Corporation).

3.5.2 Metabolite and pH assays

Triacylglycerol (TAG) assay: Samples were prepared by homogenizing 3 mid third instar larvae per sample in 250 µl of PBT (PBS + 0.1 % tritonX-100). Homogenization was performed in microcentrifuge tubes using a plastic pestle. Subsequently, samples were sonicated for 4 seconds with a 0.5 sec pulse at 20% amplitude setting. 10 µl of homogenate was mixed with 200 µl of triglyceride reagent and the mixture was incubated at room temperature for 15 minutes. Samples were then briefly centrifuged to get rid of any particulate material and supernatants were transferred to 1 ml disposable cuvettes. 800 µl of free glycerol reagent was added to each sample and incubated at room temperature for 15 minutes to allow development of color. Spectrophotometric measurements were performed at 540 nm. TAG content was calculated from TAG standard curves generated with each experiment as per manufacturer's instructions (Sigma TAG

standards). Protein estimation was performed using BCA kit using the sonicated samples and ratio of total TAG content to total protein content was reported as normalized TAG content.

Glycogen assay: Samples were prepared by homogenizing 3-4 mid third instar larvae per sample in 100 µl of cold PBS. Samples were subsequently centrifuged at 5000 rpm for 1 min and supernatant was transferred to 0.2 ml PCR tubes. 10-20 µl of each sample was preserved for protein assay. Remaining supernatants were heat treated at 70^0C for 5 minutes using a thermo-cycler. Subsequently, samples were immediately chilled on ice. Protein aggregates were separated by centrifugation (13,000 rpm for 10 minutes at 4^0C) and supernatants were used for glycogen estimation. For estimation of total glucose + glycogen content 30 µl of the prepared supernatant was incubated with 100 µl of glucose oxidase/peroxidase reagent (Sigma Glucose assay kit, GAGO 20) containing amyloglycosidase (1 µl per ml of glucose reagent, Sigma, A1602-25MG) for 30 minutes at 37^0C. In parallel 30 µl of supernatant was incubated with glucose oxidase/peroxydase reagent alone in identical conditions to estimate for total glucose content. At the end of the incubation period reactions were terminated by adding 100 µl of H_2SO_4 and left at room temperature for 5 minutes for color to develop. OD was measured at 555 nm and metabolite contents were calculated from glucose/glycogen standard curved generated along with every experiment. Total glycogen content was determined by subtracting total glucose content from

glucose+glycogen content. Measurements were normalized to total protein estimated with a BCA kit.

Hemolymph glucose + trehalose concentration: For each sample 5-6 mid third instar larvae were washed in PBS and dabbed on kim wipe^{TM}. Larvae were then quickly ripped open on a piece of parafilm under the dissecting microscope. 1.5 to 2 µl of hemolymph was carefully collected from this heap of dissected animals using a P2 pipette and placed on the parafilm to form a small drop. 1 µl of hemolymph was subsequently pipetted out of this drop to 19 µl of trehalase buffer in 0.5 ml tubes, mixed by tapping and stored on ice while more samples are being collected. This two step pipetting prevents inadvertent pipetting errors caused by larval tissues clogging the pipette tip. The samples were then centrifuged briefly (3 minutes at 13,000 rpm) ad supernatants were transferred to 0.2 ml PCR tubes. Samples were heat treated at 70^0C for 5 minutes in a thermocycler and immediately chilled on ice. Protein aggregates were separated by centrifugation at 13,000 rpm for 12 minutes at 4^0C. Supernatants were transferred to new tubes and used for sugar estimation. For sugar (glucose + trehalose) estimation 2 µl of sample was added to 28 µl of threhalase buffer containing x units/ml of porcine trehalase and the mixtures were incubated at 37^0C (water bath) for 16-18 hours to convert trehalose to glucose. Subsequently, total glucose concentration was measured using the sigma glucose oxidase kit as mentioned above. Standard curves were generated

with every experiment using 1 mg/ml of trehalose stock and were used to calculate sugar concentration in the hemolymph.

pH assay: For hemolymph pH measurement, 3 µl hemolymph was extracted from a collection of 10-12 mid third instar animals (refer to hemolymph collection for sugar assay for more details), mixed with 2 µl pyranine dye (Invitrogen, 1.2 mM final concentration). Mixture was briefly centrifuged and absorbance spectrum of the supernatant was measured using a multichannel nanodrop spectrophotometer (NanoDrop 8000). The ratio of absorbance at 450 nm and 405 nm was plotted against a standard curve to determine the pH. pH standards ranging between pH 6.6 and pH 7.6 by were prepared by titrating 50 mM Tris with HCl. Samples were maintained on ice or 4 degree centigrade until measurements were made on the nanodrop in order to avoid any oxidation of phenolic compounds.

3.5.3 Statistics

All graphs and statistical analyses were generated using Graphpad prism4. For two-sample experiments standard student t-test was used for calculating significances. For multiple sample analyses, one-way or two-way anova followed by a post-hoc Tukey's HSD test was used. p-values are designated using the following convention: single asterisk means p-value ≤ 0.05, two p-value ≤ 0.01 and three p-value ≤ 0.001.

3.5.4 Antibodies and immunostaining

Antibodies used: Rat anti-Dilp2 (1/500), mouse anti-Dilp5 (1/800) (Géminard et al., 2009), mouse anti-Elav (1/500) (9F8A9, DSHB), rat anti-dFOXO (1/500) (gift from O. Puig lab) (Hennig et al., 2006). Antibody straining was performed as described elsewhere (Géminard et al., 2009). Samples were imaged using a confocal laser-scanning microscope (Zeiss LSM710).

3.5.5 Fluorescence Quantification

To quantify Dilp2 levels, confocal Z series of the IPCs were obtained using a 1 µm step size and identical laser power and scan settings. Zeiss Zen software was used to generate multiple intensity projection images. Subsequently background signal was subtracted and fluorescence intensity was measured by drawing selections on the IPCs. Fluorescence intensity is presented as average of total selections made per sample.

3.5.6 Quantitative PCR

Tissues dissected from mid-third instar larvae were flash-frozen on dry-ice. Total RNA was extracted using QIAGEN RNeasy Tissue Mini Kit according to the manufacturer's protocol. RNA samples (5 µg per reaction) were reverse transcribed using SuperScript III (Invitrogen), and the generated cDNA was used for quantitative-PCR (Roche LightCycler 480 Real-Time PCR system). Rpl23 was used as a reference gene for normalization. Three to six separate samples

were collected for each condition and triplicate measurements were conducted for each sample. Primers were designed specifically for qPCR using a web-based software Primer3 (http://frodo.wi.mit.edu/).

3.5.7 Mitotracker staining

Larvae were dissected and inverted in Schneider's media at RT. Samples were subsequently incubated in Schneider's media containing mitotracker dye (MitoTracker Red CMXRos, Life Technologies) at a final concentration of 300 nM for 40 minutes with mild rocking. Samples were washed twice with 1X PBS for 10 minutes each and fixed in 4% paraformaldehyde for 30 minutes at RT. Subsequently, samples were washed twice with PBT (1X PBS+1% tween) for 30 minutes each with a 10 min incubation with DAPI in PBT in between. Samples were cleared in 40% glycerol before mounting in Vectashield mounting media. Final dissection was performed on microscope slides to mount fatbodies only. Imaging was done using confocal laser-scanning microscope (Zeiss LSM710) with a magnification of 100X.

3.5.8 RNA sequencing

RNA sequencing of FB RNA was performed by Genewiz, Inc. Data analysis was done using the Galaxy tool set made available by the Minnesota Supercomputing Institute.

CHAPTER 4:

Eukaryotic pyrimidine salvaging enzyme UPRT is active in *Drosophila* and limits specificity of tissue-specific RNA isolation by TU tagging.

4.1 INTRODUCTION

Biosynthesis of pyrimidine bases is a critical part of cellular metabolism and growth, as these bases provide pyrimidine nucleosides that are important components of various biomolecules including DNA and RNA. Most multicellular organisms contain two pathways to generate pyrimidine nucleotides, a *de-novo* pathway that synthesizes pyrimidine bases from non-pyrimidine precursors and a salvage pathway that allows reutilization of pyrimidine bases from preformed pyrimidine nucleotides. Pyrimidine salvage pathway enzymes are vital for many microbes and most bacteria (Kim et al., 2009). However, the repertoire of enzymes involved in pyrimidine salvage can vary considerably between different species (Beck and O'Donovan, 2007). For instance members of the genus *Pseudomonas* have been shown to contain different pyrimidine salvaging enzymes depending on the species type. While *Pseudomonas aeruginosa* possesses a nonspecific ribonucleoside hydrolase enzyme, *Pseudomonas mendocina* does not. Likewise *P. mendocina* possesses cytidine deaminase and uridine phosphorylase enzymes and *P. aeruginosa* has neither cytidine deaminase nor uridine phosphorylase (Beck and O'Donovan, 2007). This species specific presence of these enzymes along with the fact that many pyrimidine analogs can have cytotoxic effects make these enzymes lucrative targets for the treatment of infectious diseases (Carter et al., 1997; Koyama et al., 2000).

The salvage pathway enzymes have also been targeted for treatment of cancer cells as many of these enzymes have been shown to be inactive or not present in humans. Treatments targeting the salvage pathway enzymes use these enzymes as suicide genes, which are responsible for metabolizing an otherwise harmless pyrimidine analog to a cytotoxic derivative within the target cells. The target cell could be either a parasite that naturally expresses the suicide gene or cancer cells that have been primed with the suicide gene (or a combination of genes to increase specificity). While suicide gene therapy using pyrimidine analogs like 5-fluorouracil (5-FU) has been used successfully in cancer chemotherapy for decades, these analogs can cause much harm to the host as well if the target gene is expressed and active in the host (Kim et al., 2009). Therefore, an ideal suicide gene is one that is not active in the host, and the uracil salvage pathway enzyme uracil phosphoribosyltransferase (UPRT) has been proposed to be a good candidate (Carter et al., 1997; Villela et al., 2011).

UPRT catalyzes the conversion of uracil base and 5'-phosphoribosyl-α-1'-pyrophosphate (PRPP) to uridine monophosphate (UMP) and PP_i (Figure 30A) (Carter et al., 1997). The enzyme thus salvages free uracil bases and converts them to a form that can be incorporated back into newly synthesized RNA (Figure 30A). UPRT derived from certain microbes like *Toxoplasma gondii* has been shown to be efficient in recognizing derivatives of uracil, including 5-FU, and can convert it to its cytotoxic forms F-UTP or F-dUTP. Incorporation of such

a microbial enzyme in cancer cells via an adenoviral delivery system thus has been shown to remarkably improve the efficiency of 5-FU as a chemotherapy agent (Hartkopf et al., 2013; Hasegawa et al., 2013). Interestingly, a recent study has shown that the human UPRT homologue, although conserved and expressed in most cells, is not enzymatically active in its purified form *in vitro* hereby making UPRT an ideal candidate for suicide gene therapy (Li et al., 2007). However, it is not known if the enzyme would be active *in vivo*, especially under circumstances like embryonic growth or wound healing, when rapid cell proliferation demands rapid turnover of RNA synthesis and therefore a steady supply of UMP.

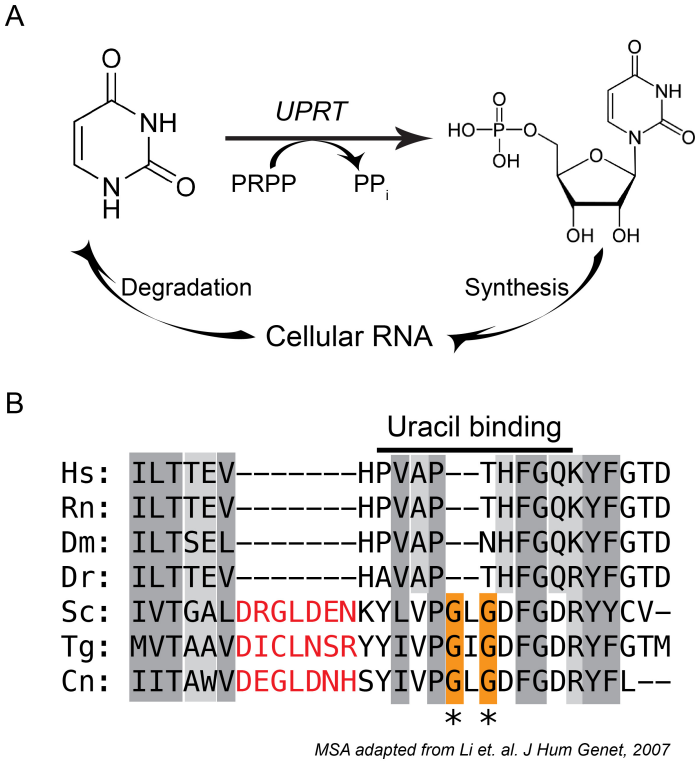

Figure 30: Role of UPRT as a salvage pathway and a comparison of protein sequence between higher and lower eukaryotes.

(A) UPRT catalyzes conversion of uracil base to uridine monophosphate (UMP) thereby allowing salvage of uracil produced by RNA degradation. UMP can subsequently be incorporated back into newly synthesized RNA by the cells RNA synthesis machinery. (B) Multiple sequence alignment of the uracil-binding region of UPRT derived from lower eukaryotes (*S. cerevisiar* (Sc), *T. gondii* (Tg) and *C. neoformans* (Cn)) and higher eukaryotes (Zebrafish (Dr), *Drosophila* (Dm), Rat (Rn) and human (Hs)) is shown. In red are 7 amino acids present in microbes that are essential for forming a beta sheet necessary for proper folding of the uracil-binding site. Two conserved glycines, shown with an asterisk, are directly involved in urail binding and are missing or replaced in UPRT from higher eukaryotes.

Inactivity of the human UPRT enzyme has been attributed to its inability to bind uracil, its substrate (Figure 30B). A multiple sequence alignment of 62 UPRT homologues from different organisms show that one proline and 2 glycines are critical for uracil binding in the uracil-binding site of UPRT. Human UPRT lacks the two glycines and in addition a Met conserved in the PRPP binding region of microbial UPRT is replaced with Ile or Thr (Li et al., 2007). Lastly, a stretch of seven amino acid residues present in prokaryotes (close to the uracil-binding site) that forms a beta-sheet essential for generating a suitable uracil-binding pocket is also missing in human UPRT (Figure 30B, Red). Interestingly, every change present in human UPRT were also present in enzymes from all higher eukaryotes, including *C. elegans* and *Drosophila*, indicating that the enzyme could be inactive in all higher eukaryotes (Li et al., 2007).

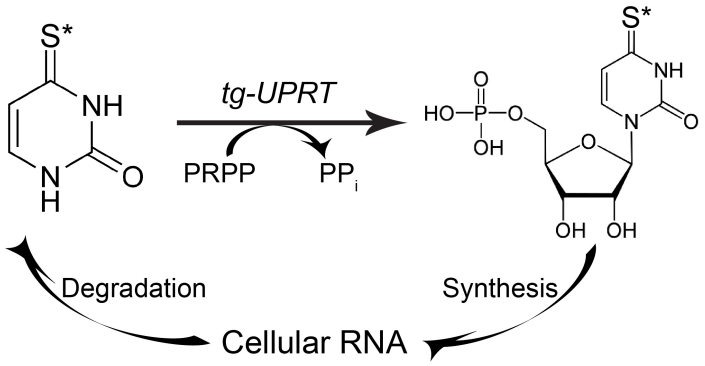

Figure 31: *T. gonddi* UPRT can incorporate uracil derivatives like 4-thio-uracil (4TU) into cellular RNA.

Based on this premise that UPRT is inactive in higher eukaryotes, a promising cell-type specific RNA labeling technique called thio-uracil-tagging (TU-tagging) has also been proposed (Cleary et al., 2005; Miller et al., 2009). Cell-type specific RNA tagging is of particular interest in order to understand cell-specific gene expressing changes that are critical for the functioning of multicellular organisms. The technique is even more important for research using small model organisms like *Drosophila*, *C. elegans* or zebrafish where dissection of small tissues for gene expression analysis can be challenging and in some cases impossible. TU-tagging utilizes the *Toxoplasma gondii* UPRT (Tg-UPRT) enzyme that is known to recognize uracil derivatives like 4-thio-uracil (4TU) and convert them to 4-thio-uridine monophosphate (4T-UMP) (Figure 31). In brief the technique involves expression of *Tg-uprt* in the cell type of interest followed by feeding of the experimental animal with 4TU. While 4TU is thereby delivered to all cells in the animal, conversion of 4TU to 4T-UMP takes place only in the cells that are expressing *Tg-uprt*. The 4T-UMP is subsequently incorporated in newly synthesized RNA in the target cells. Since naturally occurring RNA does not contain any thiol groups this technique results in labeling cell-type specific RNA with unique thiol groups. The thiolated RNA can subsequently be purified from total RNA extracted from the animals using chemical addition of biotin to the thiol groups and subsequent purification with streptavidin beads. The efficiency and specificity of the technique depends on the extent of background incorporation in

the tissues that are not expressing *Tg-uprt* and the understanding that the endogenous UPRT enzyme in higher eukaryotes is inactive. Thus 4TU-tagging is a promising cell-type specific RNA tagging and isolation technique.

However, given the fact that a UPRT homologue is present in all organisms and that the catalytic site of the enzyme is conserved from prokaryotes to humans indicate that the enzyme may still have some function in higher eukaryotes (Li et al., 2007). *In vivo* the enzyme could be capable of converting uracil to UMP if a cofactor brings the substrate to the enzymatic site. If this machinery also recognizes 4TU, then specificity of the 4TU-tagging technique would be hampered. An active UPRT in higher eukaryotes would also mean that use of the microbial UPRT as a suicide gene therapy target needs to be re-considered carefully and more cautiously to avoid host tissue damage. Apart from salvaging uracil, the enzyme could also have a secondary biological function in higher eukaryotes that does not require the uracil-binding site. Such functionality could explain the necessity to conserve the enzyme through evolution (Figure 32).

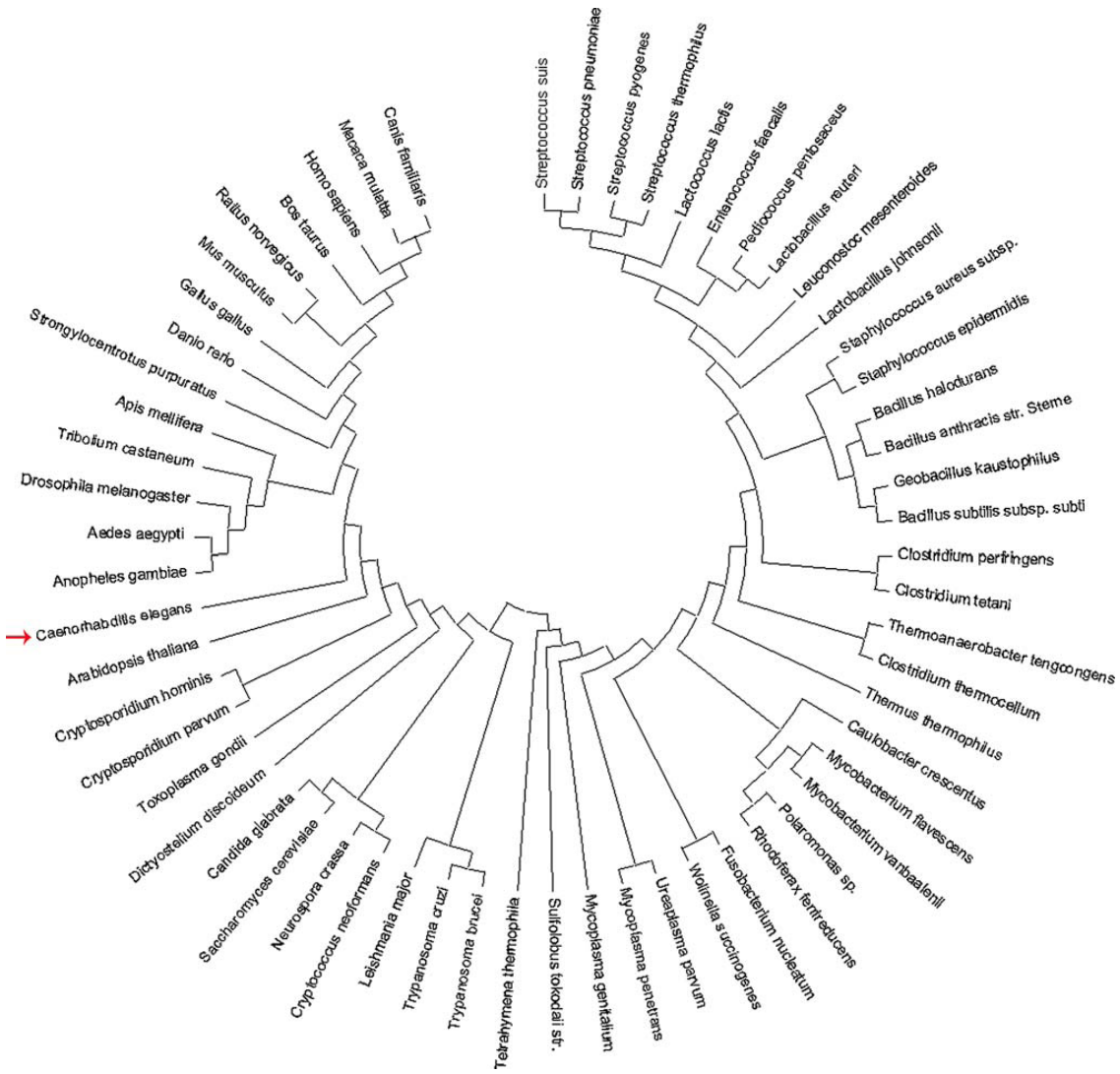

Figure 32: A UPRT family tree based on sequence homology of conserved UPRT domains.

Evolutionary tree of UPRT or UPRT-ase domain containing proteins from 62 organisms (Taken from (Li et al., 2007)). The red arrow shows UPRT of *C. elegans*.

In this chapter, I show that the *Drosophila* UPRT homologue (CG5537) can actively incorporate 4TU into RNA indicating that the enzyme is active *in vivo*. We also show that *Drosophila* UPRT is essential for larval growth as knocking out the gene leads to impaired larval growth and increased larval and pupal lethality. Lastly I show that partial knockdown of CG5537 using RNAi can be a viable option for improving the specificity of 4TU-tagging without affecting viability of the animals.

4.2 RESULTS

4.2.1 *Drosophila* Uracil phosphoribosyltransferase (Krishah) is enzymatically active *in vivo*.

Eukaryotic uracil salvage pathway enzyme uracil phosphoribosyltransferase (UPRT) is considered enzymatically inactive in higher eukaryotes including *Drosophila melanogaster*. To test this premise we fed *Drosophila* S2 cells or larvae with 4TU and checked for incorporation of thiol groups in RNA extracted from these samples. We find that S2 cells were cable of efficiently incorporating 4TU into RNA, and the extent of incorporation was directly proportional to the duration of 4TU feeding (Figure 33A). We could reduce this incorporation by about 60% by knocking down the *Drosophila* UPRT homologue *krishah* (*kri*) indicating that Kri is actively converting 4TU to 4TUMP in the S2 cells and leading to thiolation of cellular RNA (Figure 33A and B). The efficiency of *kri* knockdown was verified using qRT-PCR and *kri-RNAi* cells showed a 5-10 fold

reduction in *kri* mRNA levels (Figure 33C). Similar to S2 cells, knocking down *kri* in mid third instar larvae using a ubiquitous driver like *da-Gal4* led to a severe reduction in 4TU incorporation (Figure 33D and E). These observations show that the *Drosophila* UPRT homologue Kri is active in both S2 cells and in the larvae.

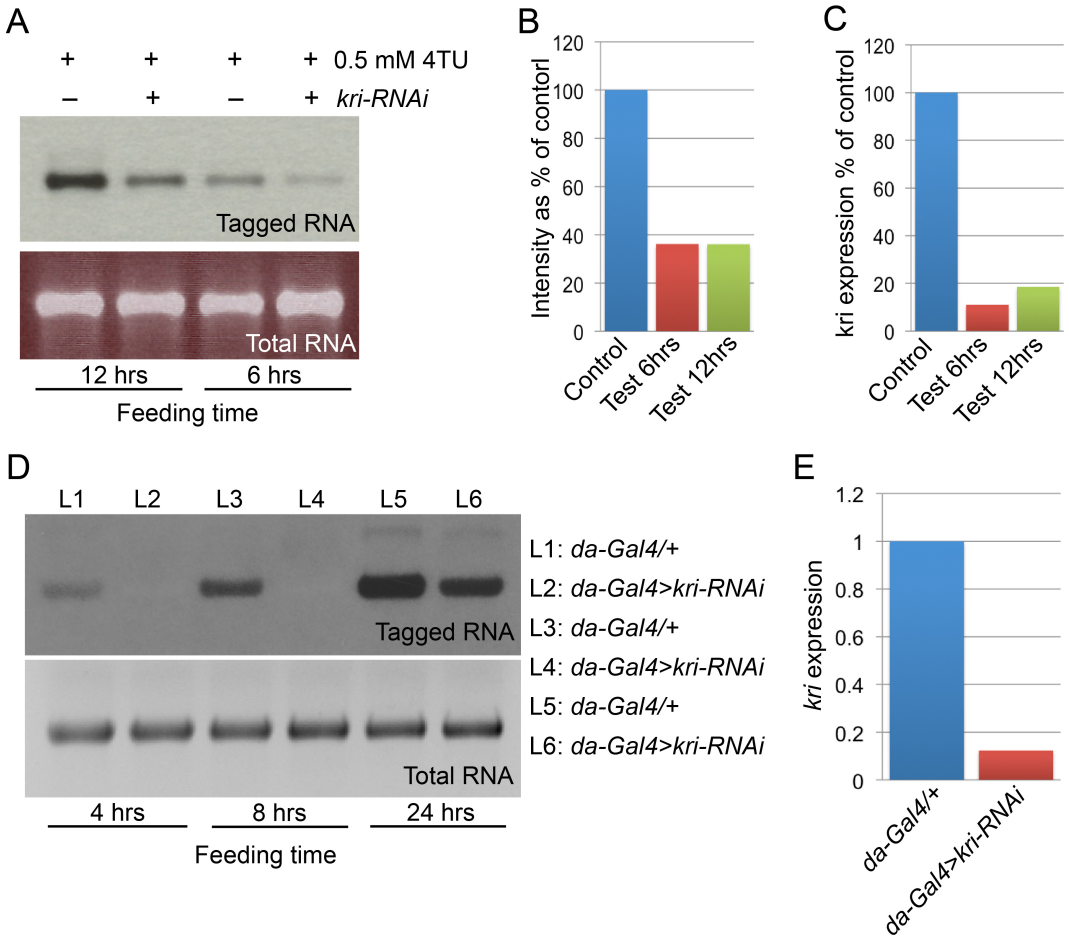

Figure 33: *Drosophila* UPRT homologue Kri can actively incorporate 4TU into cellular RNA.

(A-C) Drosophila S2 cells can actively incorporate 4TU into cellular RNA. Knocking down *kri* can significantly impair this incorporation. The efficiency of *kri* knockdown was

verified using quantitative PCR (C). (D) *Drosophila* larvae can also incorporate 4TU into cellular RNA. This incorporation could also be strongly impaired by knocking down *kri*. (E) Once again efficiency of *kri* knockdown was verified using quantitative PCR.

4.2.2 Generation of a *kri* mutant.

Drosophila larvae grow a remarkable 150-200 fold during the three larval instars. Such a rapid growth demands a huge amount of biosynthesis of cellular material including proteins and therefore mRNA. It is therefore likely that an active uracil salvage pathway is essential for larval growth. To test this possibility we decided to make a *kri* mutant. The most effective method to generate a loss of function mutation in *Drosophila* is to perform an imprecise excision of a P-element that is located in or near the target gene and in the process create a deletion that takes out the gene of interest. Such a technique, however, was not possible to use for generating a *kri* mutant as *kri* is located in the promoter region of *s6k* which is an essential gene (Figure 34A). *kri* also overlaps with a third gene, *mad2*, that sits at the other end of the gene. Therefore deleting *kri* would have affected the expression level of *s6k* and *mad2* and made characterization of loss of *kri* difficult. Hence, to generate a *kri* mutant we started with an available large deletion, *mad2Δ*, that deletes *kri* and portions of *s6k* and *mad2* (Figure 34A). *mad2*Δ thus is a *s6k*, *kri*, *mad2* triple mutant that has been shown to be larval lethal (Buffin et al., 2007). We first show that it is possible to rescue the triple mutant by inserting a large genomic DNA fragment, which supplements for all the three genes, on the second chromosome (*mad2Δ*^{Res}) (Figure 34A and see Figure

35). For generating the *kri* mutant, a stop codon was introduced in the same genomic DNA in the *kri* exon to give rise to a nonsense mutation (Figure 34B). This genomic DNA was then inserted in chromosome 2 of *mad2Δ* mutants thereby rescuing them for *s6k* and *mad2* only (Figure 34C). Insertion of the stop codon was achieved by modifying a novel recombineering technique developed for inserting small tags in genomic fragments and were performed by MaryJane O'Connor in the lab (Venken et al., 2008).

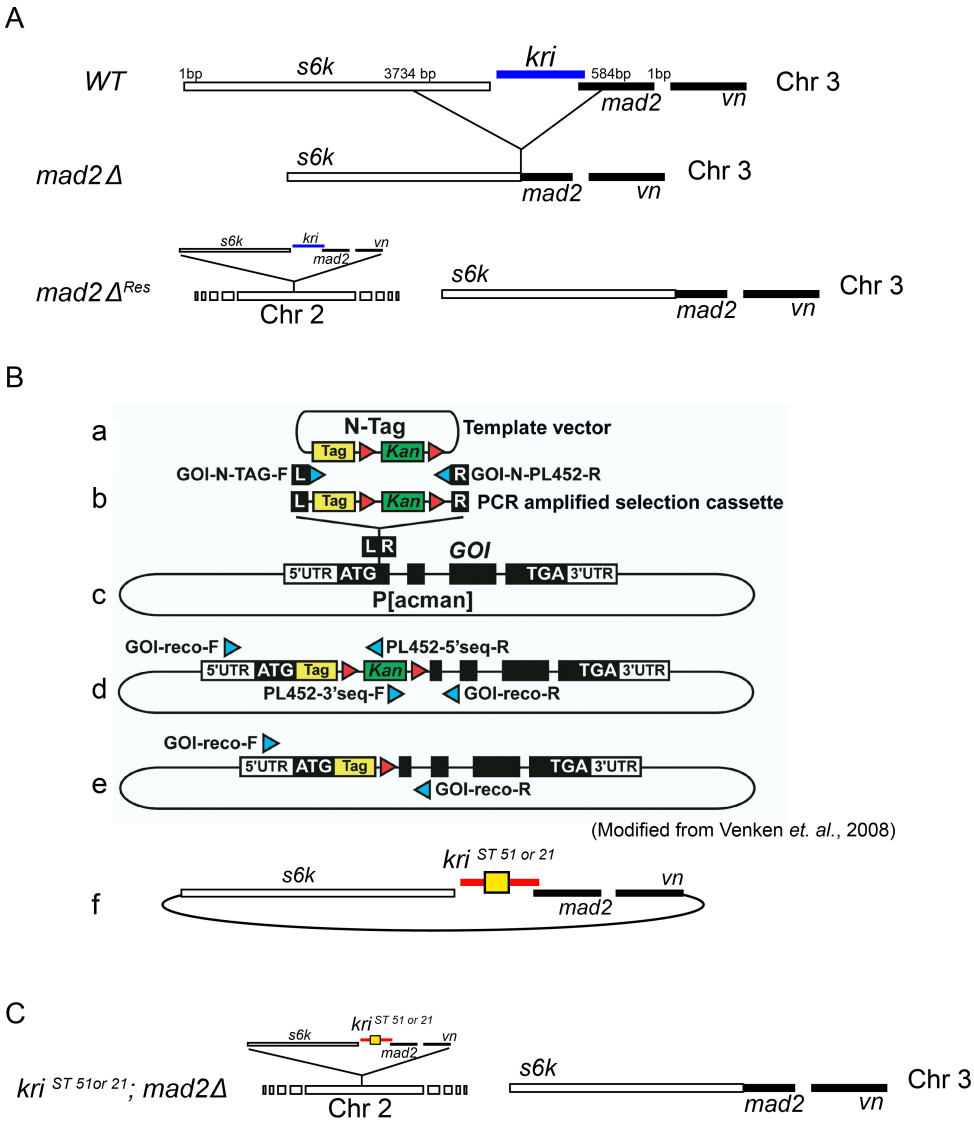

Figure 34: Methodology for generating a *kri* loss-of-function mutant.

(A) Schematic of the w^{1118}, *mad2*Δ and *mad2*Δ^{Res} animals is shown. *mad2*Δ contains a large deletion on chromosome 3 that deletes *kri* and portions of the flanking genes, *s6k* and *mad2*, giving rise to a *s6k*, *kri*, *mad2* triple mutant. *mad2*Δ^{Res} animals are rescued *mad2*Δ animals in which a large genomic DNA containing *s6k, kri* and *mad2* is inserted into the second chromosome. (B) A recombineering technique used to insert small tags into large genomic fragments. The same technique was used to introduce a small DNA fragment containing a stop codon into the *kri* locus of the same genomic DNA used in

*mad2*Δ^{Res} animals. (C) Schematic of a *kri* mutant which is essentially the same as the *mad2*Δ^{Res} animal but has a stop codon introduced in the *kri* locus of the rescue genomic DNA construct.

4.2.3 Loss of *kri* leads to impaired larval growth and pupal lethality.

The loss-of-function mutation in *kri* led to a larval/pupal lethality phenotype. Both *kri* mutants, one in which a stop codon was introduced at the 51st amino acid and the second at the 20th amino acid, failed to grow during larval stages and gave rise to wandering larvae that were thinner and smaller than both *w*^{1118} and *mad2*Δ^{Res} control animals (Figure 35A). These thin larvae formed thin pupae or pre-pupae that mostly failed to reach the pharate stage (Figure 35B). Propensity of the mutants and controls to form pupae, pharates and adults were also measured (Figure 35C). *w*^{1118} and *mad2*Δ^{Res} controls were not significantly different in their ability to form pupae. *kri* mutants, however, showed a significant reduction in the percentage of animals that reached the pupal stage (Figure 35C). Similarly, while *mad2*Δ^{Res} control pupae were able to reach the pharate stage as frequently as the *w*^{1118} controls, *kri* mutant pupae almost completely failed to reach the pharate stage (~ 3% of pupae reached pharate stage) (Figure 35C). We also looked at the ability of the control and mutant animals to survive untill adult stages. The *mad2*Δ^{Res} animals showed a significant decrease of about 30% in the ability to survive to adult stages with most of the deaths occurring at the pharate stage (Figure 35C). The *kri* mutants however, were rarely able to survive to adult stages. Lastly, I checked if supplementing the *kri* mutants with an

active UPRT enzyme could rescue the phenotypes we observed. For these experiments, I over-expressed a codon-optimized *Tg-uprt* construct (*uprt**, see next section) using a ubiquitous *da-Gal4* driver in the *kri* mutant background. UPRT* caused only a minor improvement in growth of the *kri* mutants as reflected by a significant increase in the ability of the rescued animals to form pupae from larvae and pharate from pupae (Figure 35C). However, UPRT* failed to cause any rescue of survivability to adult stages. Since UPRT* can actively convert uracil to UMP, the failure of the enzyme to rescue viability and growth of the *kri* mutants shows that Kri may have an additional physiological role in higher eukaryotes.

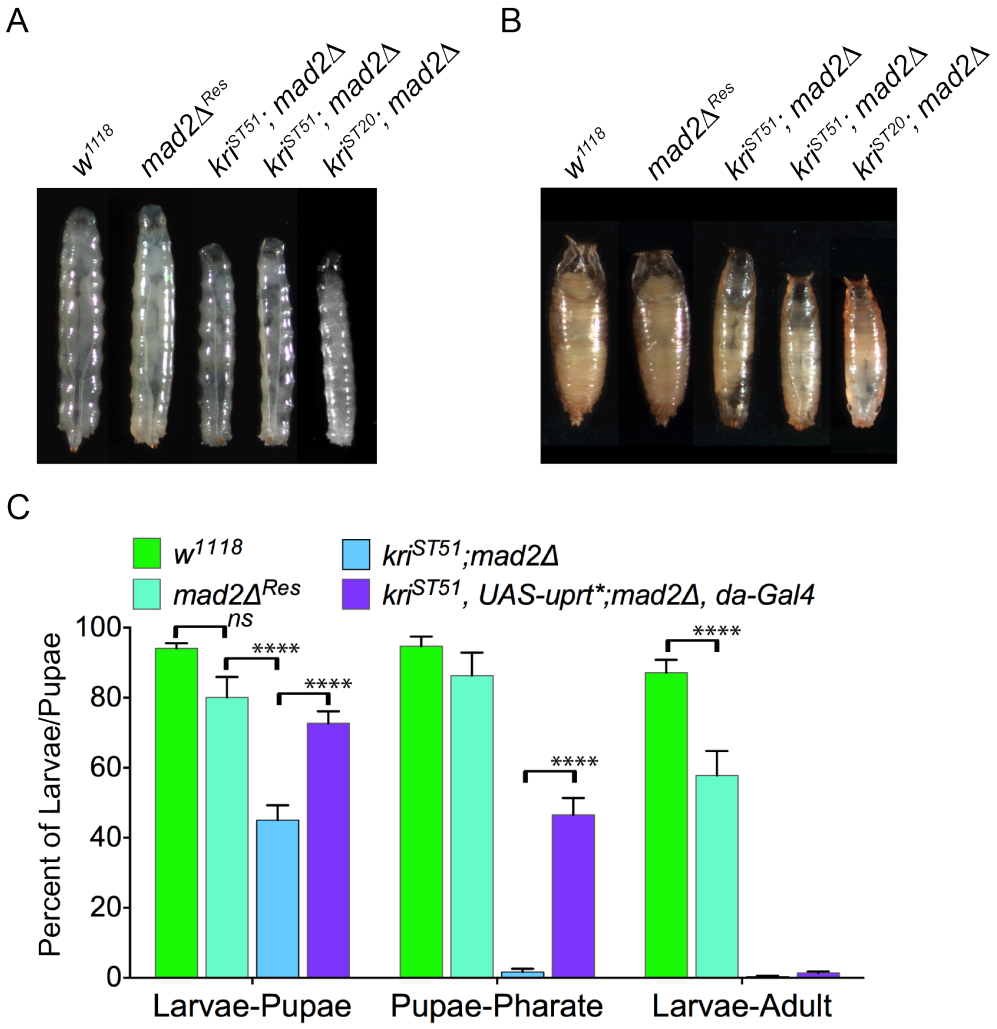

Figure 35: Loss of Kri leads to impaired larval growth and a larval/pupal lethality phenotype.

(A) Wandering third instar control and *kri* mutant larvae. *kri* mutants are much smaller and thinner than both wildtype and *mad2Δ*^{Res} controls. (B) Control and *kri* mutant pupae. *kri* mutants form small and thin pupae or pre-pupae that mostly die before reaching the pharate stage. (C) Quantification of the propensity of control, kri mutants and tg-UPRT rescued *kri* mutants to from pupae from larvae, pharate form pupae and adult from larvae. *n = 5-10* measurements per genotype with 40 animals per measurement. Significances were calculated using two-way ANOVA with a Tuky's post hock analysis to generate p values.

4.2.4 Potential improvement of specificity and efficiency of a cell-type specific RNA isolation technique using *kri-RNAi*.

A cell-type specific RNA labeling and isolation technique using Tg-UPRT mediated 4TU incorporation has recently been proposed based on the premise that *Drosophila* UPRT is enzymatically inactive. However, the technique has not gained much popularity because of lack of efficiency in labeling and lack of specificity. I find that the *Tg-uprt* (referred to as *uprt* in Figure 36) construct used in previous studies is not translated efficiently in *Drosophila* larvae (Figure 29 A-C). Since we do not have an antibody against Tg-UPRT, we over-expressed an N-terminally HA tagged Tg-UPRT construct, *HA-uprt*, in *Drosophila* motoneurons or whole animals and looked for HA-UPRT protein using immunohistochemistry (IHC) or Western blots. Quantitative PCR shows that *UAS-HA-uprt* was similar to *UAS-uprt* in terms of inducibility in the presence of a Gal4 driver (Figure 36A). However, when *HA-uprt* was expressed in motoneurons using a motoneuron-specific *OK371-Gal4* driver and the tissues were immunostained with anti-HA antibodies, we did not observe any staining (Figure 29B). This indicated that *HA-uprt* mRNA was probably not translated efficiently, and the amount of protein was below detection level of IHC. When over-expressed using a strong pan-larval *da-Gal4* driver and the whole animal extract used to perform a Western blot, we could observe HA-UPRT as a band of 26 kDa, as expected (Figure 36C). However, we also observed multiple smaller bands in the test lane indicating

truncated protein products that had the N-terminal HA tag. Once again this indicated that *HA-uprt* mRNA is not translated efficiently. A bioinformatics analysis of the *Tg-uprt* sequence indicated that the *Toxoplasma* construct had at least 6 codons that were not recognized or very poorly recognized by *Drosophila*. We therefore synthesized the gene with these codons optimized for *Drosophila* and injected this codon-optimized construct, *uprt**, to make *UAS-uprt** lines. We also generated N-terminally HA tagged *HA-uprt** constructs and injected them to generate *UAS-HA-uprt** flies. When the *HA-uprt** construct was expressed in S2 cells and cell extract was used for Western blot, we could see a more prominent HA-UPRT* band on the blot and much reduced truncated products (Figure 36C). This showed that the new codon optimized *uprt** construct can be translated more efficiently. I could also detect HA-UPRT* in S2 cells using IHC (Figure 36D). We next tested if the new *uprt** construct was translated into an enzymatically active product. For this, S2 cells were transfected with *uprt** or vector alone constructs. The cells were fed 4TU and incorporation of 4TU in total RNA was measured. UPRT* was able to cause significantly higher incorporation of 4TU compared to background incorporation indicating that the UPRT* construct is efficiently translated and is enzymatically active (Figure 36E).

A second concern with the Tg-UPRT mediated cell-type specific RNA labeling technique is lack of specificity. Our finding that the *Drosophila* UPRT homologue Kri is active *in vivo* and can efficiently incorporate 4TU may explain

why the technique has failed to achieve the level of specificity that is theoretically possible. Removing the endogenous UPRTase activity by knocking out *kri* would remedy this problem by eliminating background incorporation of 4TU. However, as we showed in the previous section, loss-of-function mutation in *kri* leads to larval growth defects and lethality making the $kri^{ST51orST20}$ mutants unusable for any functional study. Nevertheless, we observed that *da-Gal4* driven *kri-RNAi* can significantly reduce 4TU incorporation and does not cause lethality. Therefore, we explored the possibility of using *kri-RNAi* in combination with *uprt** over-expression to improve tissue specificity of RNA tagging. In order to be used together it is important that *kri-RNAi* does not target *uprt** mRNA. The sequence of *Tg-uprt* is quite different from *kri* (29.52% identity), and codon optimization of *Tg-uprt* (to *uprt**) caused the sequences to become further divergent (only 24.94% identity). We therefore predicted that *kri-RNAi* will not target *uprt** mRNA. We tested this in S2 treated with *kri-RNAi* by feeding 4TU for 6 hours either in the presence or absence of *uprt**. When fed for 6 hours, background incorporation of 4TU in S2 cells was similar to cells that were expressing *uprt** (Figure 36F). In the presence of *kri-RNAi*, cells expressing *uprt** showed a similar level of 4TU when compared to *uprt** expressing cells in the absence of *kri-RNAi*. However, background incorporation of 4TU was reduced significantly. These results show that *kri-RNAi* can indeed be used along with *uprt** over-expression to simultaneously reduce background incorporation of 4TU and cause UPRT*

mediated incorporation of 4TU. Notably, the fact that UPRT* can rescue the incorporation of 4TU in *kri-RNAi* treated cells validates the specificity of *kri-RNAi* and *kri-RNAi*-induced loss of 4TU incorporation.

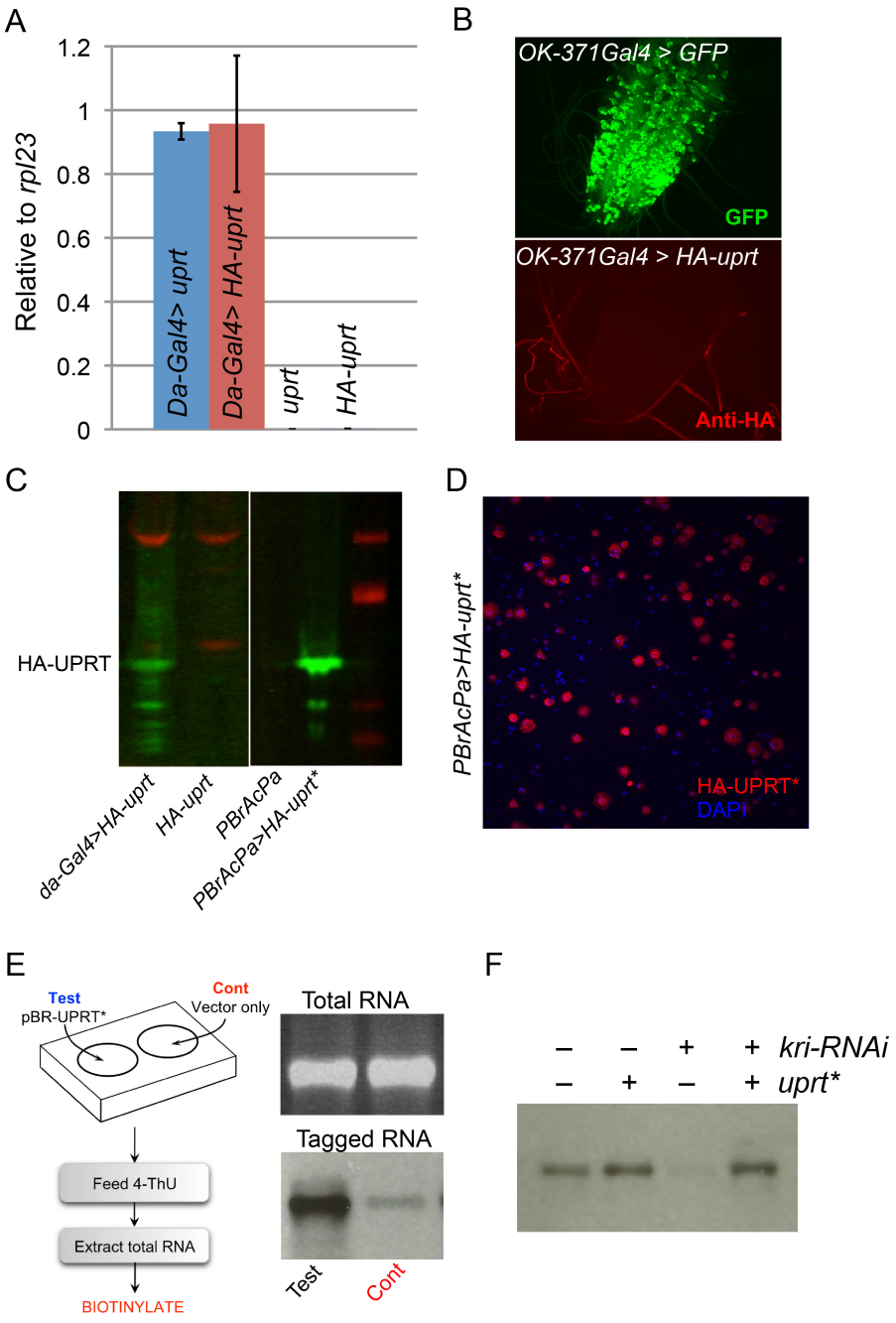

Figure 36: Enhancing the efficiency and specificity of 4TU tagging in *Drosophila*.

(A) UAS-HA-UPRT and UAS-UPRT constructs containing the tg-UPRT and an N-terminally HA-tagged version of the gene are highly inducible in the presence of a *da-Gal4* driver. (B) Expressing UAS-HA-UPRT in the motoneurons using an OK371-Gal4 driver (expected expression pattern shown with UAS-GFP in the same sample) did not show any HA-UPRT peptide detectable using IHC. (C) *tg-UPRT* mRNA is not translated efficiently in Drosophila larvae and HA-UPRT peptide is seen as a series of 26kd and smaller bands on Western blot. However, a codon-optimized construct *HA-UPRT**, when expressed in S2 cells was able to produce peptides that were primarily 26 kd in length. (D) HA-UPRT* peptide could also be detected in S2 cells using IHC. (E) UPRT* is enzymatically active and can efficiently incorporate 4TU in S2 cell RNA. (F) UPRT* can incorporate 4TU even in the presence of *kri-RNAi* and can significantly enhance the ratio of test to background incorporation of 4TU.

4.3 DISCUSSION

I studied the ability of the *Drosophila* UPRT homologue Krishah (CG5537) to convert 4TU into 4TUMP by assaying for incorporation of 4TU into cellular RNA in both S2 cells and *Drosophila* larvae. This work revealed that the endogenous enzyme is capable of incorporating 4TU into RNA in both S2 cells and larvae. Kri shares a high sequence similarity to human UPRT protein, which has been shown to be inactive *in vitro* and it has been proposed that this is most likely due to a non-functional uracil-binding site (Li et al., 2007). Since the sequence of the uracil-binding site of Kri is exactly same as humans (Li et al., 2007), and since Kri can recognize a uracil derivative *in vivo* and allow incorporation of the compound into RNA, it is possible that Kri is able to bring its substrate to the catalytic site *in vivo*. This finding has important implications for cancer chemotherapy as microbial UPRT is considered a good target for suicide

gene therapy in treating cancer with a cytotoxic uracil derivative 5FU. Microbial UPRT has also been proposed as a drug target for treatment of infectious diseases like tuberculosis based on the understanding that human UPRT is inactive and is not essential. However, similar to *Drosophila* Kri, human UPRT may also be functional *in vivo* and future investigation of this possibility will be critical for justifying the use of *uprt* as a suicide gene for cancer chemotherapy or microbial infection management. Interestingly, while the activity and function of UPRT has been extensively studied in various microbes, activity of the enzyme in any higher eukaryote has not been reported before. Therefore, our observation that *Drosophila* UPRT is active *in vivo* is the very first evidence of the activity of this salvage pathway enzyme in any higher eukaryote.

It has been proposed before, based on the fact that UPRT is conserved in higher eukaryotes despite being incapable of binding uracil, that UPRT in higher eukaryotes may have some unknown physiological function. My work with the *kri* mutant indicates a similar possibility. Loss of *kri* in *Drosophila* led to impaired larval growth and larval/pupal lethality. It is this lack of larval growth and formation of thinner larvae that prompted us to name this yet un-annotated gene *'krishah'* (kri), which in Sanskrit means 'thin'. One possible explanation for this lack of larval growth in the *kri* mutants would be that the uracil salvage pathway is essential for growth particularly in the larvae. *Drosophila* larvae show a phenomenal 150-200 fold increase in mass during the larval stages. The larvae

therefore may need a very rapid turnover of mRNA to sustain this growth, and the *de novo* UMP synthesis pathway may not be sufficient to maintain a steady supply of UMP. Under these circumstances the uracil salvage pathway mediated by Kri may become essential. If this hypothesis is true, it can be predicted that the activity of UPRT in mammals may be important during biological processes that require fast cell proliferation like embryogenesis and wound healing. Such a possibility is worth exploring. While necessity to salvage uracil could be one of the reasons for lack of larval growth in the *kri* mutants, the fact that over-expressing *Tg-uprt* in the *kri* mutants caused only a mild improvement in larval growth shows that *kri* most likely has other essential roles in larval growth. Tg-UPRT can substitute only for the uracil-salvaging role of Kri in the larvae. However, being derived from an evolutionarily divergent source, Tg-UPRT is likely not capable of substituting for Kri for any, yet unknown, physiological role. A rescue of the *kri* mutants with over-expression of *kri* itself will be the best future experiment to perform for confirming any physiological role of Kri in larval growth. Reagents for such a rescue experiment are already being prepared, and the experiments will be performed soon.

One of the reasons behind our interest in studying the enzymatic activity of Kri is the possibility of using an exogenously expressed UPRT to achieve cell-type specific RNA tagging and isolation. This technique is essential for studying cell-type specific gene expression profiles and transcriptional responses to

signaling pathways like TGF-β signaling which we study in the lab. A recent study has explored this possibility and has shown that expressing *Tg-uprt* in a cell-type specific manner can allow incorporation of 4TU into cell specific RNA, facilitating cell specific RNA isolation (Cleary et al., 2005; Miller et al., 2009). The technique however, has not gained much popularity and issues with efficiency of 4TU incorporation and specificity of 4TU have been reported (unpublished). We find that the wildtype *Tg-uprt* construct used in previous studies contains codons that are not efficiently translated in *Drosophila*. This could be one of the reasons behind lack of efficiency in 4TU incorporation. We have generated a codon optimized *Tg-uprt* construct called *uprt** and we have shown here that UPRT* can actively and efficiently incorporate 4TU. A comparative analysis of the ability of Tg-UPRT and UPRT* to incorporate 4TU in *Drosophila* cells has not be performed. However, Western blot and IHC experiments looking at the peptide product of N-terminally HA-tagged Tg-UPRT and UPRT* shows much more efficient translation of UPRT* in the *Drosophila* system.

Lack of specificity with 4TU tagging can be attributed to the activity of the *Drosophila* UPRT homologue Kri. Kri shows significant ability to recognize 4TU and cause incorporation of the uracil derivative into cellular RNA from non-target tissues. I show that this background incorporation can be strongly reduced by knocking down *kri*. Since loss-of-function mutations in *kri* lead to larval lethality, a controlled knockdown of *kri* that reduces background but does not cause lethality

will be our next best choice at improving the specificity of the technique. This improvement may not be necessary for tagging RNA in larger tissues that would require a shorter duration of 4TU feeding and thereby keep background incorporation to a minimum. However, when tagging a very small number of cells, especially in tissues like the brain that are separated by a blood brain barrier, prolonged feeding becomes necessary to increase incorporation. Such prolonged feeding increases non-specific incorporation of 4TU, and previous attempts have shown that dissection of the small tissue becomes necessary to isolate cell-type specific RNA (Miller et al., 2009). For such experiments knocking down *kri* could significantly improve specificity and yield of cell-type specific tagged RNA. Knocking down *kri* may also avoid dissection of small tissues thereby allowing easy scale-up for isolation of RNA from small populations of cells.

4.4 MATERIALS AND METHODS

4.4.1 *Drosophila* stocks and husbandry

w^{1118} and *UAS-kri-RNAi* (kk110071) line was obtained from VDRC. *UAS-UPRT* and *UAS-HA-UPRT* lines were generous gifts from Dr. Chris Doe's lab. *Mad*2Δ line was a generous gift from Dr. Roger Karess's lab. *da-Gal4* was obtained from Bloomington Stock Center. Flies were raised on standard cornmeal food at 25^{O}C and a 12 hour light dark cycle. For 4TU feeding experiments larvae were grown under axenic conditions. Embryos were sterilized using 50% bleach for 2 minutes

followed by a quick 70% ethanol wash and then transferred to autoclaved cornmeal food. Before feeding larvae were floated using filter sterilized 20% sucrose and transferred to autoclaved food containing 4TU.

4.4.2 Immunohistochemistry

Rat anti-HA 3F10 (Roche) antibodies were used at a 1/500 dilution. CNSs from third instar wandering larvae were dissected out and fixed in 4% paraformaldehyde in PBS for 20 minutes at room temperature for anti-HA and anti-CSP staining. Antibody staining and washes of larval CNSs were conducted in 0.1% Triton-X100 in 1X PBS (PBST). Primary antibody treatments of CNSs were done at 4ºC for 24 hours. S2 cells were fixed on glass culture slides as per standard protocol.

4.4.3 S2 cell culture and transfection

S2 cells were cultured in standard cell culture plates with M3 media supplemented with Insect Media Supplement (IMS), 2% Fetal Calf Serum and penicillin/ streptomycin (PS) (growth media). Cells were maintained at 25 ^{O}C and passaged every 6 days at a density of 2 million cells per ml. All cell transfections were done using CellfectinII (Invitrogen). Freshly passaged cells growing in confluence (24 hours after passaging) were harvested, 3.2 million cells were plated in each well of a 6 well plate in 1.6 ml of M3+IMS media, and then allowed to attach to the bottom of the plate for 2 hours. Before transfection 1.2 microgram of DNA was mixed with 120 µl of M3+IMS media in a microcentrifuge tube and 8

µl of cellfectinII reagent was mixed with 120 µl of M3+IMS media in a separate tube. The tubes were incubated at RT for 15 minutes. Post incubation the solutions were mixed together and incubated at RT for another 5 minutes. At the end of this incubation the solution was added drop wise to the S2 cells. 8-16 hours post transfection the medium was exchanged for M3+IMS+PS media, and cells grown for another 4 days before performing any experiment. For 4TU feeding post transfection, M3+IMS+PS media was exchanged with growth media containing 0.5 mM or 0.2 mM 4TU.

4.4.4 Quantitative PCR

Total RNA was extracted from S2 cells or whole larvae using QIAGEN RNeasy Tissue Mini Kit according to the manufacturer's protocol. RNA samples (5 µg per reaction) were reverse-transcribed using SuperScript III (Invitrogen), and the generated cDNA was used for quantitative-PCR (Roche LightCycler 480 Real-Time PCR system). Rpl23 was used as a reference gene for normalization. Three separate samples were collected for each condition and triplicate measurements were conducted for each sample. Primers were designed specifically for qPCR using Primer3 (http://frodo.wi.mit.edu/).

4.4.4 4TU incorporation assay

Incorporation of 4TU in RNA upon feeding with 4TU was assayed by chemically biotinylating thiol groups on RNA and probing for biotinylated RNA on a Northern blot using streptavidin HRP. Briefly, 20 µg of total RNA was incubated in 1X

biotinylation buffer (20mM tris and 1mM EDTA, pH 7.4) in a total volume of 166 µl that included 40µl of Biotin-HPDP in DMF (1mg/ml stock). The reaction mixture was incubated in a 55 ^{O}C water bath for 20 minutes and then for 2 hour and 40 minutes at RT, protected from light. Biotinylated RNA was extracted with acidic phenol (Ambion) to remove any free biotin reagent. Total RNA was precipitated from the aqueous phase by adding 1/10 th volume of 5 M NaCl and precipitating with 1:1 parts of isopropanol. The precipitate was centrifuged (maximum speed) for 10 minutes and the resultant pellet was washed once with 70% ethanol, dried, and re-suspended in 15 µl of RNAse free water. 1 µg of this RNA was run on a formaldehyde-agarose gel. RNA was transferred to a nylon membrane overnight using standard Northern blot technique. The RNA was then crosslinked to the nylon membrane using UV irradiation (auto setting, repeat once after flipping the blot) and blocked using 10X blocking solution (125mM NaCl, 17mM Na_2HPO_4, 7.3mM NaH_2PO_4, and 1% SDS) by rocking at RT for 20 minutes. Subsequently the blot was incubated with streptavidin-HRP at 1/1500 dilution (1mg/ml stock) in 10X blocking solution. The blot was washed twice with 1X blocking solution and twice with 1X assay buffer (10mM Tris, 10mM NaCl, 1m $MgCl_2$, pH 9.5) before detecting with a standard ECL kit (Pierce) and photo-reactive film. Band intensities were measured using Image-J analysis software whenever applicable.

References

Aggarwal, S.K., and King, R.C. (1969). Comparative study of the ring glands from wild type and 1(2)gl mutant *Drosophila melanogaster*. J Morphol *129*, 171–199.

Allan, D.W., St Pierre, S.E., Miguel-Aliaga, I., and Thor, S. (2003). Specification of neuropeptide cell identity by the integration of retrograde BMP signaling and a combinatorial transcription factor code. Cell *113*, 73–86.

Avruch, J., Lin, Y., Long, X., Murthy, S., and Ortiz-Vega, S. (2005). Recent advances in the regulation of the TOR pathway by insulin and nutrients. Curr Opin Clin Nutr Metab Care *8*, 67–72.

Baker, K.D., and Thummel, C.S. (2007). Diabetic larvae and obese flies-emerging studies of metabolism in *Drosophila*. Cell Metab *6*, 257–266.

Balemans, W., and Van Hul, W. (2002). Extracellular regulation of BMP signaling in vertebrates: a cocktail of modulators. Developmental Biology *250*, 231–250.

Ballard, S.L., Jarolimova, J., and Wharton, K.A. (2010). Gbb/BMP signaling is required to maintain energy homeostasis in *Drosophila*. Developmental Biology *337*, 375–385.

Bayeva, M., Gheorghiade, M., and Ardehali, H. (2013). Mitochondria as aTherapeutic Target in Heart Failure. Jac *61*, 599–610.

Beck, D.A., and O'Donovan, G.A. (2007). Pathways of Pyrimidine Salvage in Pseudomonas and Former Pseudomonas: Detection of recycling enzymes using high-performance liquid chromatography. Curr Microbiol *56*, 162–167.

Bertolino, P., Holmberg, R., Reissmann, E., Andersson, O., Berggren, P.-O., and Ibáñez, C.F. (2008). Activin B receptor ALK7 is a negative regulator of pancreatic β-cell function. Proc Natl Acad Sci USA *105*, 7246–7251.

Bonomi, L., Brown, M., Ungerleider, N., Muse, M., Matzuk, M.M., and Schneyer, A. (2012). Activin B regulates islet composition and islet mass but not whole body glucose homeostasis or insulin sensitivity. AJP: Endocrinology and Metabolism *303*, E587–E596.

Böhni, R., Riesgo-Escovar, J., Oldham, S., Brogiolo, W., Stocker, H., Andruss, B.F., Beckingham, K., and Hafen, E. (1999). Autonomous control of cell and

organ size by CHICO, a *Drosophila* homolog of vertebrate IRS1-4. Cell *97*, 865–875.

Bridges, C.B. (1935). Salivary chromosome maps with a key to the banding of the chromosomes of *Drosophila melanogaster.* Journal of Heredity *26*, 60–64.

Bridges, C.B.G.E. (1928). The giant mutation in *Drosophila melanogaster*. Part I. The heredity of giant. Z. Indukt. Abstamm. Vererbungsl. *46*, 231–247.

Brogiolo, W., Stocker, H., Ikeya, T., Rintelen, F., Fernandez, R., and Hafen, E. (2001). An evolutionarily conserved function of the *Drosophila* insulin receptor and insulin-like peptides in growth control. Curr Biol *11*, 213–221.

Broughton, S.J., Piper, M.D.W., Ikeya, T., Bass, T.M., Jacobson, J., Driege, Y., Martinez, P., Hafen, E., Withers, D.J., Leevers, S.J., et al. (2005). Longer lifespan, altered metabolism, and stress resistance in *Drosophila* from ablation of cells making insulin-like ligands. Proc Natl Acad Sci USA *102*, 3105–3110.

Broughton, S., Alic, N., Slack, C., Bass, T., Ikeya, T., Vinti, G., Tommasi, A.M., Driege, Y., Hafen, E., and Partridge, L. (2008). Reduction of DILP2 in *Drosophila* triages a metabolic phenotype from lifespan revealing redundancy and compensation among DILPs. PLoS ONE *3*, e3721.

Bruce, K.D., and Hanson, M.A. The developmental origins, mechanisms, and implications of metabolic syndrome. J Nutr *140*, 648–652.

Brummel, T.J., Twombly, V., Marques, G., Wrana, J.L., Newfeld, S.J., Attisano, L., Massague, J., O'connor, M.B., and Gelbart, W.M. (1994). Characterization and relationship of Dpp receptors encoded by the saxophone and thick veins genes in *Drosophila*. Cell *78*, 251–261.

Brummel, T., Abdollah, S., Haerry, T.E., Shimell, M.J., Merriam, J., Raftery, L., Wrana, J.L., and O'connor, M.B. (1999). The *Drosophila* activin receptor baboon signals through dSmad2 and controls cell proliferation but not patterning during larval development. Genes Dev *13*, 98–111.

Brun, T. (2004). The diabetes-linked transcription factor PAX4 promotes -cell proliferation and survival in rat and human islets. J Cell Biol *167*, 1123–1135.

Buffin, E., Emre, D., and Karess, R.E. (2007). Flies without a spindle checkpoint. Nature *9*, 565–572.

Bühler, A., Lanzrein, B., and Wille, H. (1983). Influence of temperature and carbon dioxide concentration on juvenile hormone titre and dependent

parameters of adult worker honey bees (*Apis mellifera* L.). Journal of Insect Physiology *29*, 885–893.

Caldwell, P.E., Walkiewicz, M., and Stern, M. (2005). Ras Activity in the *Drosophila* prothoracic gland regulates body size and developmental rate via ecdysone release. Current Biology *15*, 1785–1795.

Capovilla, M., Eldon, E.D., and Pirrotta, V. (1992). The giant gene of *Drosophila* encodes a b-ZIP DNA-binding protein that regulates the expression of other segmentation gap genes. Development *114*, 99–112.

Carter, D., Donald, R.G., Roos, D., and Ullman, B. (1997). Expression, purification, and characterization of uracil phosphoribosyltransferase from Toxoplasma gondii. Mol Biochem Parasitol *87*, 137–144.

Cáceres, L., Necakov, A.S., Schwartz, C., Kimber, S., Roberts, I.J.H., and Krause, H.M. (2011). Nitric oxide coordinates metabolism, growth, and development via the nuclear receptor E75. Genes Dev *25*, 1476–1485.

Chen, H. (2005). Emerging functions of mammalian mitochondrial fusion and fission. Human Molecular Genetics *14*, R283–R289.

Chen, H., Chomyn, A., and Chan, D.C. (2005). Disruption of fusion results in mitochondrial heterogeneity and dysfunction. J Biol Chem *280*, 26185–26192.

Chen, H., Detmer, S.A., Ewald, A.J., Griffin, E.E., Fraser, S.E., and Chan, D.C. (2003). Mitofusins Mfn1 and Mfn2 coordinately regulate mitochondrial fusion and are essential for embryonic development. J Cell Biol *160*, 189–200.

Cleary, M.D., Meiering, C.D., Jan, E., Guymon, R., and Boothroyd, J.C. (2005). Biosynthetic labeling of RNA with uracil phosphoribosyltransferase allows cell-specific microarray analysis of mRNA synthesis and decay. Nat Biotechnol *23*, 232–237.

Colombani, J., Bianchini, L., Layalle, S., Pondeville, E., Dauphin-Villemant, C., Antoniewski, C., Carré, C., Noselli, S., and Léopold, P. (2005). Antagonistic actions of ecdysone and insulins determine final size in *Drosophila*. Science *310*, 667–670.

Colombani, J., Raisin, S., Pantalacci, S., Radimerski, T., Montagne, J., and Léopold, P. (2003). A nutrient sensor mechanism controls *Drosophila* growth. Cell *114*, 739–749.

Cuthbert, C., and Alberti, K.G. (1978). Acidemia and insulin resistance in the

diabetic ketoacidotic rat. Metab. Clin. Exp. *27*, 1903–1916.

Das, P., Inoue, H., Baker, J.C., Beppu, H., Kawabata, M., Harland, R.M., Miyazono, K., and Padgett, R.W. (1999). *Drosophila* dSmad2 and Atr-I transmit activin/TGF-β signals. Genes Cells *4*, 123–134.

de Velasco, B., Erclik, T., Shy, D., Sclafani, J., Lipshitz, H., McInnes, R., and Hartenstein, V. (2007). Specification and development of the pars intercerebralis and pars lateralis, neuroendocrine command centers in the *Drosophila* brain. Developmental Biology *302*, 309–323.

Delettre, C., Lenaers, G., Pelloquin, L., Belenguer, P., and Hamel, C.P. (2002). OPA1 (Kjer type) dominant optic atrophy: a novel mitochondrial disease. Mol. Genet. Metab. *75*, 97–107.

Dromparis, P., and Michelakis, E.D. (2013). Mitochondria in vascular health and disease. Annu. Rev. Physiol. *75*, 95–126.

Ebling, F.J., and Cronin, A.S. (2000). The neurobiology of reproductive development. Neuroreport *11*, R23–R33.

Edgar, B.A. (2006). How flies get their size: genetics meets physiology. Nat Rev Genet *7*, 907–916.

Eldon, E.D., and Pirrotta, V. (1991). Interactions of the *Drosophila* gap gene giant with maternal and zygotic pattern-forming genes. Development *111*, 367–378.

Feng, X.H., and Derynck, R. (2005). Specificity and versatility in TGF-β signaling through Smads. Annu. Rev. Cell. Dev. Biol. *21*, 659–693.

Fernandez, A.M., and Torres-Alemán, I. (2012). The many faces of insulin-like peptide signalling in the brain. Nat Rev Neurosci *13*, 225–239.

Florio, P., Luisi, S., Marchetti, P., Lupi, R., Cobellis, L., Falaschi, C., Sugino, H., Navalesi, R., Genazzani, A.R., and Petraglia, F. (2000). Activin A stimulates insulin secretion in cultured human pancreatic islets. J. Endocrinol. Invest. *23*, 231–234.

Furukawa, M., Nobusawa, R., Shibata, H., Eto, Y., and Kojima, I. (1995). Initiation of insulin secretion in glucose-free medium by Activin A. Mol. Cell. Endocrinol. *113*, 83–87.

Fuzeau-Braesch, S., Nicolas, G., and Baehr, J.C. (1982). A study of hormonal levels of the locust *Locusta migratoria* cinerascens artificially changed to the

solitary state by a chronic CO_2 treatment of one minute per day. Comp. Biochem. Physiol. A *71*, 53–58.

Gergen, J.P., and Wieschaus, E.F. (1985). The localized requirements for a gene affecting segmentation in *Drosophila*: analysis of larvae mosaic for runt. Developmental Biology *109*, 321–335.

Gesualdi, S.C., and Haerry, T.E. (2007). Distinct signaling of *Drosophila* Activin/TGF-beta family members. Fly (Austin) *1*, 212–221.

Géminard, C., Rulifson, E.J., and Léopold, P. (2009). Remote control of Insulin secretion by fat cells in *Drosophila*. Cell Metab *10*, 199–207.

Gibbens, Y.Y., Warren, J.T., Gilbert, L.I., and O'connor, M.B. (2011). Neuroendocrine regulation of *Drosophila* metamorphosis requires TGF-β/Activin signaling. Development *138*, 2693–2703.

Gilbert, L.I., Rybczynski, R., and Warren, J.T. (2002). Control and biochemical nature of the ecdysteroidogenic pathway. Annu. Rev. Entomol. *47*, 883–916.

Grönke, S., Clarke, D.-F., Broughton, S., Andrews, T.D., and Partridge, L. (2010). Molecular evolution and functional characterization of *Drosophila* insulin-like peptides. PLoS Genet *6*, e1000857.

Gutierrez, E., Wiggins, D., Fielding, B., and Gould, A.P. (2007). Specialized hepatocyte-like cells regulate *Drosophila* lipid metabolism. Nature *445*, 275–280.

Harrison, J.F. (2001). Insect acid-base physiology. Annu. Rev. Entomol. *46*, 221–250.

Harrison, J.F., and Phillips, J.E. (1992). Recovery from acute haemolymph acidosis in unfed locusts: II. Role of ammonium and titratable acid excretion. J Exp Biol *165*, 97–110.

Harrison, J.F., Wong, C.J.H., and Phillips, J.E. (1990). Haemolymph buffering in the locust *Schistocerca gregaria*. J Exp Biol *154*, 573–579.

Hartkopf, A.D., Bossow, S., Lampe, J., Zimmermann, M., Taran, F.A., Wallwiener, D., Fehm, T., Bitzer, M., and Lauer, U.M. (2013). Enhanced killing of ovarian carcinoma using oncolytic measles vaccine virus armed with a yeast cytosine deaminase and uracil phosphoribosyltransferase. Gynecologic Oncology *130*, 362–368.

Hasegawa, N., Abei, M., Yokoyama, K.K., Fukuda, K., Seo, E., Kawashima, R.,

Nakano, Y., Yamada, T., Nakade, K., Hamada, H., et al. (2013). Cyclophosphamide enhances antitumor efficacy of oncolytic adenovirus expressing uracil phosphoribosyltransferase (UPRT) in immunocompetent Syrian hamsters. Int. J. Cancer *133*, 1479–1488.

Hennig, K.M., Colombani, J., and Neufeld, T.P. (2006). TOR coordinates bulk and targeted endocytosis in the *Drosophila melanogaster* fat body to regulate cell growth. J Cell Biol *173*, 963–974.

Huang, X., Warren, J.T., and Gilbert, L.I. (2008). New players in the regulation of ecdysone biosynthesis. J Genet Genomics *35*, 1–10.

Ikeya, T., Galic, M., Belawat, P., Nairz, K., and Hafen, E. (2002). Nutrient-dependent expression of insulin-like peptides from neuroendocrine cells in the CNS contributes to growth regulation in *Drosophila*. Curr Biol *12*, 1293–1300.

Ishizaki, H., and Suzuki, A. (1994). The brain secretory peptides that control moulting and metamorphosis of the silkmoth, *Bombyx mori*. Int. J. Dev. Biol. *38*, 301–310.

Itoh, S., and Dijke, ten, P. (2007). Negative regulation of TGF-β receptor/Smad signal transduction. Curr Opin Cell Biol *19*, 176–184.

Jensen, P.A., Zheng, X., Lee, T., and O'Connor, M.B. (2009). The *Drosophila* Activin-like ligand Dawdle signals preferentially through one isoform of the Type-I receptor Baboon. Mech. Dev. *126*, 950–957.

Kaplowitz, P.B., and Oberfield, S.E. (1999). Reexamination of the age limit for defining when puberty is precocious in girls in the United States: implications for evaluation and treatment. Drug and Therapeutics and Executive Committees of the Lawson Wilkins Pediatric Endocrine Society. Pediatrics *104*, 936–941.

Kim, E., Goraksha-Hicks, P., Li, L., Neufeld, T.P., and Guan, K.-L. (2008). Regulation of TORC1 by Rag GTPases in nutrient response. Nature *10*, 935–945.

Kim, S., Park, D.-H., Kim, T.H., Hwang, M., and Shim, J. (2009). Functional analysis of pyrimidine biosynthesis enzymes using the anticancer drug 5-fluorouracil in *Caenorhabditis elegans*. Febs J. *276*, 4715–4726.

Kim, S.K., and Rulifson, E.J. (2004). Conserved mechanisms of glucose sensing and regulation by *Drosophila* corpora cardiaca cells. Nature *431*, 316.

Kirk, E.P., and Klein, S. (2009). Pathogenesis and pathophysiology of the

cardiometabolic syndrome. J Clin Hypertens (Greenwich) *11*, 761–765.

Koyama, F., Sawada, H., Fuji, H., Hamada, H., Hirao, T., Ueno, M., and Nakano, H. (2000). Adenoviral-mediated transfer of Escherichia coli uracil phosphoribosyltransferase (UPRT) gene to modulate the sensitivity of the human colon cancer cells to 5-fluorouracil. Eur. J. Cancer *36*, 2403–2410.

Lazar, L., and Phillip, M. (2012). Pubertal disorders and bone maturation. Endocrinol. Metab. Clin. North Am. *41*, 805–825.

Lee, G., and Park, J.H. (2004). Hemolymph sugar homeostasis and starvation-induced hyperactivity affected by genetic manipulations of the adipokinetic hormone-encoding gene in *Drosophila melanogaster*. Genetics *167*, 311–323.

LeMaire, W.J. (1989). Mechanism of mammalian ovulation. Steroids *54*, 455–469.

Letsou, A., Arora, K., Wrana, J.L., Simin, K., Twombly, V., Jamal, J., Staehling-Hampton, K., Hoffmann, F.M., Gelbart, W.M., Massague, J., et al. (1995). *Drosophila* Dpp signaling is mediated by the punt gene product: a dual ligand-binding type II receptor of the TGF beta receptor family. Cell *80*, 899–908.

Levenbook, L. (1950). The physiology of carbon dioxide transport in insect blood. Part III. The buffer capacity of Gastrophilus blood. J Exp Biol *27*, 184–191.

Léopold, P., and Perrimon, N. (2007). *Drosophila* and the genetics of the internal milieu. Nature *450*, 186–188.

Li, J., Huang, S., Chen, J., Yang, Z., Fei, X., Zheng, M., Ji, C., Xie, Y., and Mao, Y. (2007). Identification and characterization of human uracil phosphoribosyltransferase (UPRTase). J Hum Genet *52*, 415–422.

Li, L., Shen, J.J., Bournat, J.C., Huang, L., Chattopadhyay, A., Li, Z., Shaw, C., Graham, B.H., and Brown, C.W. (2009). Activin Signaling: Effects on body composition and mitochondrial energy metabolism. Endocrinology *150*, 3521–3529.

Lin, H.M., Lee, J.H., Yadav, H., Kamaraju, A.K., Liu, E., Zhigang, D., Vieira, A., Kim, S.J., Collins, H., Matschinsky, F., et al. (2009). TGF-β/Smad3 signaling regulates Insulin gene transcription and pancreatic islet β-cell function. Journal of Biological Chemistry *284*, 12246–12257.

Long, Y.C. (2006). AMP-activated protein kinase signaling in metabolic regulation. J. Clin. Invest. *116*, 1776–1783.

Mak, R.H. (2008). Insulin and its role in chronic kidney disease. Pediatr. Nephrol. *23*, 355–362.

Maléth, J., Rakonczay, Z., Jr, Venglovecz, V., Dolman, N.J., and Hegyi, P. (2012). Central role of mitochondrial injury in the pathogenesis of acute pancreatitis. Acta Physiol *207*, 226–235.

Marques, G. (2003). Retrograde Gbb signaling through the Bmp type 2 receptor Wishful Thinking regulates systemic FMRFa expression in *Drosophila*. Development *130*, 5457–5470.

Martin, J.F., Hersperger, E., Simcox, A., and Shearn, A. (2000). Minidiscs encodes a putative amino acid transporter subunit required non-autonomously for imaginal cell proliferation. Mech. Dev. *92*, 155–167.

Mcbrayer, Z., Ono, H., Shimell, M., Parvy, J.-P., Beckstead, R.B., Warren, J.T., Thummel, C.S., Dauphin-Villemant, C., Gilbert, L.I., and O'Connor, M.B. (2007). Prothoracicotropic hormone regulates developmental timing and body size in *Drosophila*. Dev Cell *13*, 857–871.

McCubrey, J.A., Steelman, L.S., Chappell, W.H., Abrams, S.L., Wong, E.W., Chang, F., Lehmann, B., Terrian, D.M., Milella, M., Tafuri, A., et al. (2007). Roles of the Raf/MEK/ERK pathway in cell growth, malignant transformation and drug resistance. Biochim. Biophys. Acta *1773*, 1263–1284.

Menut, L., Vaccari, T., Dionne, H., Hill, J., Wu, G., and Bilder, D. (2007). A mosaic genetic screen for *Drosophila* neoplastic tumor suppressor genes based on defective pupation. Genetics *177*, 1667–1677.

Miller, M.R., Robinson, K.J., Cleary, M.D., and Doe, C.Q. (2009). TU-tagging: cell type-specific RNA isolation from intact complex tissues. Nature Methods *6*, 439.

Mirth, C.K., and Riddiford, L.M. (2007). Size assessment and growth control: how adult size is determined in insects. Bioessays *29*, 344–355.

Mirth, C., Truman, J.W., and Riddiford, L.M. (2005). The role of the prothoracic gland in determining critical weight for metamorphosis in *Drosophila melanogaster.* Current Biology *15*, 1796–1807.

Mitch, W.E. (2006). Metabolic and clinical consequences of metabolic acidosis. J. Nephrol. *19 Suppl 9*, S70–S75.

Mitchell, T., Chacko, B., Ballinger, S.W., Bailey, S.M., Zhang, J., and Darley Usmar, V. (2013). Convergent mechanisms for dysregulation of mitochondrial

quality control in metabolic disease: implications for mitochondrial therapeutics. Biochem Soc Trans *41*, 127–133.

Mohler, J., Eldon, E.D., and Pirrotta, V. (1989). A novel spatial transcription pattern associated with the segmentation gene, giant, of *Drosophila*. Embo J *8*, 1539–1548.

Mukherjee, A., Sidis, Y., Mahan, A., Raher, M.J., Xia, Y., Rosen, E.D., Bloch, K.D., Thomas, M.K., and Schneyer, A.L. (2007). FSTL3 deletion reveals roles for TGF-β family ligands in glucose and fat homeostasis in adults. Proc Natl Acad Sci USA *104*, 1348–1353.

Musselman, L.P., Fink, J.L., Narzinski, K., Ramachandran, P.V., Hathiramani, S.S., Cagan, R.L., and Baranski, T.J. (2011). A high-sugar diet produces obesity and insulin resistance in wild-type *Drosophila*. Dis Model Mech *4*, 842–849.

Nijhout, H.F. (2003). The control of body size in insects. Developmental Biology *261*, 1–9.

Oakley, A.E., Clifton, D.K., and Steiner, R.A. Kisspeptin Signaling in the Brain.

Pan, D.A., and Hardie, D.G. (2002). A homologue of AMP-activated protein kinase in Drosophila melanogaster is sensitive to AMP and is activated by ATP depletion. Biochem J *367*, 179–186.

Park, D., Jones, K.L., Lee, H., Snutch, T.P., Taubert, S., and Riddle, D.L. (2012). Repression of a potassium channel by nuclear hormone receptor and TGF-β signaling modulates Insulin signaling in *Caenorhabditis elegans*. PLoS Genet *8*, e1002519.

Parker, L., Stathakis, D.G., and Arora, K. (2004). Regulation of BMP and activin signaling in *Drosophila*. Prog Mol Subcell Biol *34*, 73–101.

Parker, L., Ellis, J.E., Nguyen, M.Q., and Arora, K. (2006). The divergent TGF-β ligand Dawdle utilizes an activin pathway to influence axon guidance in *Drosophila*. Development *133*, 4981–4991.

Pasco, M.Y., and Léopold, P. (2012). High sugar-induced insulin resistance in *Drosophila* relies on the lipocalin Neural Lazarillo. PLoS ONE *7*, e36583.

Peterson, A.J., Jensen, P.A., Shimell, M., Stefancsik, R., Wijayatonge, R., Herder, R., Raftery, L.A., and O'Connor, M.B. (2012). R-Smad competition controls Activin receptor output in *Drosophila*. PLoS ONE *7*, e36548.

Petryk, A., Warren, J.T., Marqués, G., Jarcho, M.P., Gilbert, L.I., Kahler, J., Parvy, J.-P., Li, Y., Dauphin-Villemant, C., and O'Connor, M.B. (2003). Shade is the *Drosophila* P450 enzyme that mediates the hydroxylation of ecdysone to the steroid insect molting hormone 20-hydroxyecdysone. Proc Natl Acad Sci USA *100*, 13773–13778.

Petschek, J.P., Perrimon, N., and Mahowald, A.P. (1987). Region-specific defects in l(1)giant embryos of *Drosophila melanogaster*. Dev Biol *119*, 175–189.

Phillips, J. (1981). Comparative physiology of insect renal function. Am. J. Physiol. Regul. Integr. Comp. Physiol. *241*, R241–R257.

Phillips, J.E., Thomson, R.B., Audsley, N., and Peach, J.L. (1994). Mechanisms of acid-base transport and control in locust excretory system. Physiol. Zool. *67*, 95–119.

Picard, M., Shirihai, O.S., Gentil, B.J., and Burelle, Y. (2013). Mitochondrial morphology transitions and functions: implications for retrograde signaling? AJP: Regulatory, Integrative and Comparative Physiology *304*, R393–R406.

Potter, C.J., Huang, H., and Xu, T. (2001). *Drosophila* Tsc1 functions with Tsc2 to antagonize insulin signaling in regulating cell growth, cell proliferation, and organ size. Cell *105*, 357–368.

Rajan, A., and Perrimon, N. (2012). *Drosophila* cytokine unpaired 2 regulates physiological homeostasis by remotely controlling insulin secretion. Cell *151*, 123–137.

Reinitz, J., and Levine, M. (1990). Control of the initiation of homeotic gene expression by the gap genes giant and tailless in *Drosophila*. Dev Biol *140*, 57–72.

Rewitz, K.F., Yamanaka, N., Gilbert, L.I., and O'Connor, M.B. (2009). The insect neuropeptide PTTH activates receptor tyrosine kinase torso to initiate metamorphosis. Science *326*, 1403–1405.

Ruberte, E., Marty, T., Nellen, D., Affolter, M., and Basler, K. (1995). An absolute requirement for both the type II and type I receptors, punt and thick veins, for dpp signaling in vivo. Cell *80*, 889–897.

Rulifson, E.J., Kim, S.K., and Nusse, R. (2002). Ablation of insulin-producing neurons in flies: growth and diabetic phenotypes. Science *296*, 1118–1120.

Rutter, G.A. (2001). Nutrient–secretion coupling in the pancreatic islet β-cell:

recent advances. Molecular Aspects of Medicine *22*, 247–284.

Rybczynski, R., and Gilbert, L.I. (1994). Changes in general and specific protein synthesis that accompany ecdysteroid synthesis in stimulated prothoracic glands of Manduca sexta. Insect Biochem Mol Biol *24*, 175–189.

Sancak, Y., Peterson, T.R., Shaul, Y.D., Lindquist, R.A., Thoreen, C.C., Bar-Peled, L., and Sabatini, D.M. (2008). The Rag GTPases bind raptor and mediate amino acid signaling to mTORC1. Science *320*, 1496–1501.

Satake, S., Masumura, M., Ishizaki, H., Nagata, K., Kataoka, H., Suzuki, A., and Mizoguchi, A. (1997). Bombyxin, an insulin-related peptide of insects, reduces the major storage carbohydrates in the silkworm *Bombyx mori*. Comp. Biochem. Physiol. B, Biochem. Mol. Biol. *118*, 349–357.

Schmierer, B., and Hill, C.S. (2007). TGF-β-SMAD signal transduction: molecular specificity and functional flexibility. Nat Rev Mol Cell Biol *8*, 970–982.

Schwartz, M.B., Imberski, R.B., and Kelly, T.J. (1984). Analysis of metamorphosis in *Drosophila melanogaster*: characterization of giant, an ecdysteroid-deficient mutant. Developmental Biology *103*, 85–95.

Serpe, M., and O'Connor, M.B. (2006). The metalloprotease tolloid-related and its TGF-β-like substrate Dawdle regulate *Drosophila* motoneuron axon guidance. Development *133*, 4969–4979.

Shimmi, O., Ralston, A., Blair, S.S., and O'connor, M.B. (2005). The crossveinless gene encodes a new member of the Twisted gastrulation family of BMP-binding proteins which, with Short gastrulation, promotes BMP signaling in the crossveins of the *Drosophila* wing. Developmental Biology *282*, 70–83.

Shin, S.C., Kim, S.H., You, H., Kim, B., Kim, A.C., Lee, K.A., Yoon, J.H., Ryu, J.H., and Lee, W.J. (2011). *Drosophila* microbiome modulates host developmental and metabolic homeostasis via insulin signaling. Science *334*, 670–674.

Shiozaki, S., Tajima, T., Zhang, Y.Q., Furukawa, M., Nakazato, Y., and Kojima, I. (1999). Impaired differentiation of endocrine and exocrine cells of the pancreas in transgenic mouse expressing the truncated type II activin receptor. Biochim. Biophys. Acta *1450*, 1–11.

Siegmund, T., and Korge, G. (2001). Innervation of the ring gland of *Drosophila melanogaster*. J Comp Neurol *431*, 481–491.

Smart, N.G., Apelqvist, A.A., Gu, X., Harmon, E.B., Topper, J.N., MacDonald, R.J., and Kim, S.K. (2006). Conditional expression of Smad7 in pancreatic β-cells disrupts TGF-β signaling and induces reversible diabetes mellitus. PLoS Biol *4*, e39.

Sonis, W.A., Comite, F., Blue, J., Pescovitz, O.H., Rahn, C.W., Hench, K.D., Cutler, G.B., Loriaux, D.L., and Klein, R.P. (1985). Behavior problems and social competence in girls with true precocious puberty. J. Pediatr. *106*, 156–160.

Sousa-Nunes, R., Yee, L.L., and Gould, A.P. (2011). Fat cells reactivate quiescent neuroblasts via TOR and glial insulin relays in *Drosophila*. Nature *471*, 508–512.

Sprecher, S., Reichert, H., and Hartenstein, V. (2007). Gene expression patterns in primary neuronal clusters of the *Drosophila* embryonic brain. Gene Expression Patterns *7*, 584–595.

Stanojevic, D., Small, S., and Levine, M. (1991). Regulation of a segmentation stripe by overlapping activators and repressors in the *Drosophila* embryo. Science *254*, 1385–1387.

Szabat, M., Johnson, J.D., and Piret, J.M. (2010). Reciprocal modulation of adult beta cell maturity by Activin A and follistatin. Diabetologia *53*, 1680–1689.

Tan, C.K., Leuenberger, N., Tan, M.J., Yan, Y.W., Chen, Y., Kambadur, R., Wahli, W., and Tan, N.S. (2011). Smad3 Deficiency in Mice Protects Against Insulin Resistance and Obesity Induced by a High-Fat Diet. Diabetes *60*, 464–476.

Tatar, M. (2001). A mutant *Drosophila* Insulin Receptor homolog that extends life-span and impairs neuroendocrine function. Science *292*, 107–110.

Teleman, A.A. (2010). Molecular mechanisms of metabolic regulation by insulin in *Drosophila*. Biochem J *425*, 13–26.

Tennessen, J.M., and Thummel, C.S. (2011). Coordinating Growth andMaturation — Insights from *Drosophila*. Curr Biol *21*, R750–R757.

Tennessen, J.M., Baker, K.D., Lam, G., Evans, J., and Thummel, C.S. (2011). The *Drosophila* estrogen-related receptor directs a metabolic switch that supports developmental growth. Cell Metab *13*, 139–148.

Thompson, T.B., Lerch, T.F., Cook, R.W., Woodruff, T.K., and Jardetzky, T.S. (2005). The structure of the follistatin: activin complex reveals antagonism of both

type I and type II receptor binding. Dev Cell *9*, 535–543.

Thomson, R.B., Speight, J.D., and Phillips, J.E. (1988). Rectal acid secretion in the desert locust, *Schistocerca gregaria*. Journal of Insect Physiology *34*, 829–837.

Thummel, C.S. (2001). Molecular mechanisms of developmental timing in *C. elegans* and *Drosophila*. Dev Cell *1*, 453–465.

Totsuka, Y., Tabuchi, M., Kojima, I., Shibai, H., and Ogata, E. (1988). A novel action of activin A: stimulation of insulin secretion in rat pancreatic islets. Biochem Biophys Res Commun *156*, 335–339.

Truman, J.W., and Riddiford, L.M. (1974). Physiology of insect rhythms. 3. The temporal organization of the endocrine events underlying pupation of the tobacco hornworm. J Exp Biol *60*, 371–382.

Tseng, Y.-H., Cypess, A.M., and Kahn, C.R. (2010). Cellular bioenergetics as a target for obesity therapy. Nature Reviews Drug Discovery *9*, 465.

Ueda, Y. (2000). Activin A increases Pax4 gene expression in pancreatic β-cell lines. FEBS Letters *480*, 101–105.

Venken, K.J.T., Kasprowicz, J., Kuenen, S., Yan, J., Hassan, B.A., and Verstreken, P. (2008). Recombineering-mediated tagging of *Drosophila* genomic constructs for in vivo localization and acute protein inactivation. Nucleic Acids Research *36*, e114–e114.

Villela, A.D., Sánchez-Quitian, Z.A., Ducati, R.G., Santos, D.S., and Basso, L.A. (2011). Pyrimidine salvage pathway in Mycobacterium tuberculosis. Curr. Med. Chem. *18*, 1286–1298.

Walvoord, E.C. (2010). The timing of puberty: is it changing? Does it matter? J Adolesc Health *47*, 433–439.

Watson, R.O., Manzanillo, P.S., and Cox, J.S. (2012). Extracellular *M. tuberculosis* DNA targets bacteria for autophagy by activating the host DNA-sensing pathway. Cell *150*, 803–815.

Wiater, E., and Vale, W. (2012). Roles of activin family in pancreatic development and homeostasis. Mol. Cell. Endocrinol. *359*, 23–29.

Wiederkehr, M.R., Kalogiros, J., and Krapf, R. (2004). Correction of metabolic acidosis improves thyroid and growth hormone axes in haemodialysis patients.

Nephrol. Dial. Transplant. *19*, 1190–1197.

Wyatt, G.R. (1961). The biochemistry of insect hemolymph. Annu. Rev. Entomol. *6*, 75–102.

Yadav, H., Quijano, C., Kamaraju, A.K., Gavrilova, O., Malek, R., Chen, W., Zerfas, P., Zhigang, D., Wright, E.C., Stuelten, C., et al. (2011). Protection from Obesity and Diabetes by Blockade of TGF-β/Smad3 Signaling. Cell Metab *14*, 67–79.

Yamanaka, N., Rewitz, K.F., and O'Connor, M.B. (2013). Ecdysone Control of Developmental Transitions: Lessons from *Drosophila*. Annu. Rev. Entomol. *58*, 497–516.

Yamaoka, T., Idehara, C., Yano, M., Matsushita, T., Yamada, T., Ii, S., Moritani, M., Hata, J., Sugino, H., Noji, S., et al. (1998). Hypoplasia of pancreatic islets in transgenic mice expressing activin receptor mutants. J. Clin. Invest. *102*, 294–301.

Younossi-Hartenstein, A., Green, P., Liaw, G.J., Rudolph, K., Lengyel, J., and Hartenstein, V. (1997). Control of early neurogenesis of the *Drosophila* brain by the head gap genes tll, otd, ems, and btd. Developmental Biology *182*, 270–283.

Zamani, N., and Brown, C.W. (2011). Emerging roles for the TGF-β superfamily in regulating adiposity and energy expenditure. Endocrine Reviews *32*, 387–403.

Zheng, X., Wang, J., Haerry, T.E., Wu, A.Y.-H., Martin, J., O'Connor, M.B., Lee, C.-H.J., and Lee, T. (2003). TGF-β signaling activates steroid hormone receptor expression during neuronal remodeling in the *Drosophila* brain. Cell *112*, 303–315.

Zsurka, G., and Kunz, W.S. (2013). Mitochondrial involvement in neurodegenerative diseases. IUBMB Life *65*, 263–272.

Züchner, S., Mersiyanova, I.V., Muglia, M., Bissar-Tadmouri, N., Rochelle, J., Dadali, E.L., Zappia, M., Nelis, E., Patitucci, A., Senderek, J., et al. (2004). Mutations in the mitochondrial GTPase mitofusin 2 cause Charcot-Marie-Tooth neuropathy type 2A. Nat. Genet. *36*, 449–451.

Appendix I

Transcriptional targets of TGF-β signaling in larval tissues

Daw specifically signals through a novel isoform of *babo*, $babo_c$, which is expressed tissue specifically. Limited analysis of major tissues indicates that $babo_c$ is expressed strongly in tissues such as midgut and fatbody. Therefore, it is likely that *daw* regulates gene expression in a tissue specific manner and may be more active in regulating gene expression in tissues that are metabolically active and are involved in nutrient absorption. Identifying the transcriptional targets of TGF-β signaling in these tissues is vital for understanding the role of Daw in regulating metabolism. We decided to direct our endeavor towards finding the targets of Daw signaling in the larval fatbody primarily because we could rescue the acidosis and cellular metabolism phenotypes of *daw* mutants by activating TGF-β signaling in the fatbody only. To identify the transcriptional targets of Daw signaling in the fatbody I performed illumina RNA sequencing with total RNA extracted from fatbody dissected from w^{1118}, $daw^{1/+}$ and $daw^{1/11}$ stage matched feeding mid third instar larvae. The table below shows genes that showed significant change in the mutants compared to either w^{1118} or $daw^{1/+}$ controls. Apart from the deep sequencing experiment I performed a S2 cells based Daw stimulation assay to look for potential targets of TGF-β signaling. In these experiments S2 cells were stimulated with Daw and total RNA was extracted from the cells. This RNA was used to perform quantitative PCR to look

changes in expression of some 100 genes that were selected from a microarray dataset that I had performed previously. S2 cells that were not stimulated with Daw served as controls. This secondary screen showed strong upregulation of one gene, Dh31-R1, which is a diuretic hormone receptor, up on Daw stimulation. The screen also showed down-regulation of 5 genes up on Daw stimulation. Consistent with these genes being targets of TGF-β signaling, in my deep sequencing experiment Dh31-R1 showed a strong down-regulation in the *daw* mutants (Table X, shaded in pink). Additionally, two of the 5 genes (tobi and Dab) which were down-regulated on Daw stimulation showed strong up-regulation in the *daw* mutants. These genes could therefore be strong candidates for being direct transcriptional targets of TGF-β signaling in *Drosophila* and could serve to identify the Smox-binding site in *Drosophila* that is still unknown.

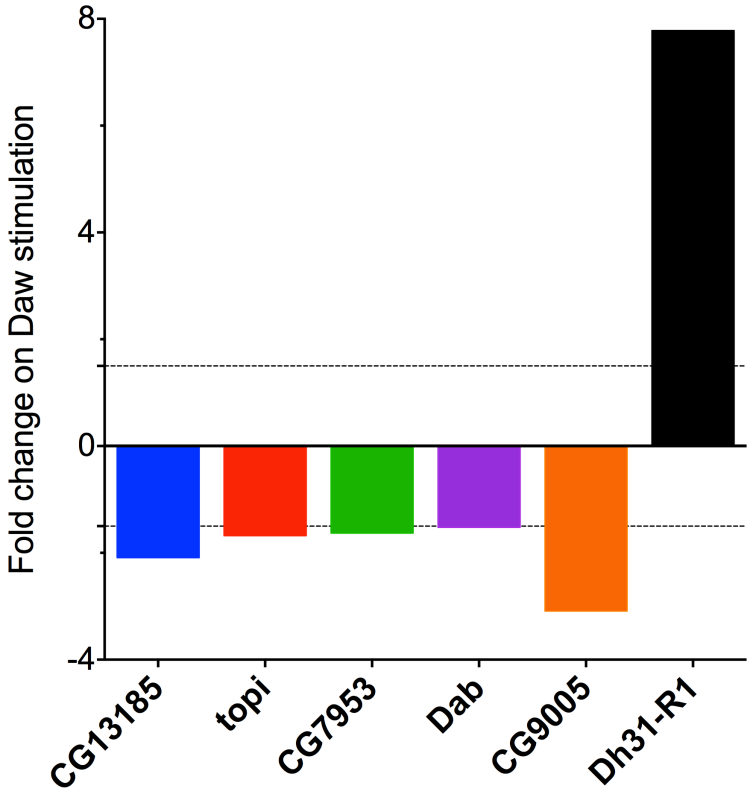

Figure 37: Genes whose expression changed significantly in S2 cells up on stimulation with Daw.

Fold change in the expression level of genes that responded to stimulation with Daw in S2 cells. Expression level relative to *rpl23* was assayed using quantitative PCR.

Table 2: Genes that showed significant expression differences between w^{1118} control and $daw^{1/11}$ mutants.

Gene Name	W^{1118}	$daw^{1/11}$	log2 (Fold change)	*p* Value
Dpt	239.04	0.65	-8.52	0.0017
CG5773	831.08	2.45	-8.41	5.00E-05
CG4288	11.58	0.14	-6.37	0.00065
CG3036	127.56	2.04	-5.97	5.00E-05
CG3868	16.45	0.31	-5.71	0.00025
CG31676	10.47	0.22	-5.55	0.00165
DptB	370.95	8.31	-5.48	5.00E-05
CG42329	91.28	2.08	-5.45	5.00E-05
CG14762	8.89	0.32	-4.81	5.00E-05
CG8654	44.94	1.72	-4.71	5.00E-05
CG3239	3.68	0.15	-4.58	0.0004
CG3513	101.27	4.71	-4.43	5.00E-05
Gpo-1	79.82	4.32	-4.21	5.00E-05
Hsp67Bb	78.54	4.30	-4.19	5.00E-05
Odc1	27.72	1.53	-4.18	5.00E-05
Dro	44.02	2.86	-3.95	0.0044
CG18067	155.15	10.30	-3.91	5.00E-05
CG31100	1.96	0.13	-3.91	0.0008
CG42708	19.73	1.39	-3.83	5.00E-05
r	16.58	1.23	-3.75	5.00E-05
Rab23	2.09	0.16	-3.74	0.0026
CG34034	5.31	0.42	-3.68	0.0048
CG6426	18.93	1.49	-3.67	0.0004
CG8160	995.23	81.25	-3.61	5.00E-05
CG33926	12.76	1.06	-3.59	0.0012
aay	148.70	12.44	-3.58	5.00E-05
CG18278	1.75	0.16	-3.42	0.0028
GstD2	36.96	3.59	-3.36	5.00E-05
rdgC	1.89	0.19	-3.30	0.00085
CG5966	1.45	0.15	-3.30	0.0042
CG17032	15.09	1.59	-3.24	5.00E-05
CG1213	3.52	0.37	-3.24	0.00095
CG34436	145.24	16.86	-3.11	5.00E-05
hebe	5.06	0.60	-3.07	0.00085
Cyp6t1	2.98	0.36	-3.06	0.00345
Cyt-b5-r	1009.56	123.57	-3.03	5.00E-05
CG3292	12.92	1.76	-2.88	5.00E-05
Myo28B1	3.14	0.45	-2.81	0.00035
Drs	57.85	8.74	-2.73	0.0013
CG9372	18.96	2.90	-2.71	0.0001
CG2065	39.49	6.14	-2.68	5.00E-05
CG13315	558.66	90.26	-2.63	5.00E-05
CG9906	6.76	1.14	-2.57	0.0005
CG6908	48.09	8.24	-2.55	5.00E-05
CG4398	29.62	5.19	-2.51	5.00E-05

l(2)41Ab	7.10	1.26	-2.49	5.00E-05
CG4607	3.64	0.69	-2.40	0.00315
Pvf3	3.53	0.69	-2.36	0.00185
CG8086	4.96	0.99	-2.32	0.0014
Cyp9c1	48.61	9.80	-2.31	5.00E-05
regucalcin	1232.29	250.27	-2.30	5.00E-05
CG7384	20.99	4.30	-2.29	5.00E-05
CG11425	82.24	17.17	-2.26	5.00E-05
CG4562	4.50	0.94	-2.25	5.00E-05
kcc	2.80	0.59	-2.25	0.00085
CG15917	31.77	6.73	-2.24	0.0044
Taf12L	22.48	4.77	-2.24	0.0038
Tsp42Ep	379.50	80.90	-2.23	5.00E-05
CG9220	3.98	0.86	-2.20	0.00415
CG4021	11.64	2.53	-2.20	0.00085
Myo61F	6.28	1.39	-2.18	5.00E-05
CG34455	144.89	32.01	-2.18	5.00E-05
CG6045	16.95	3.81	-2.15	5.00E-05
CG2736	376.96	85.56	-2.14	5.00E-05
CG6188	1995.59	458.25	-2.12	5.00E-05
CG12692	5.48	1.27	-2.11	0.00315
sug	43.61	10.21	-2.09	5.00E-05
Gpdh	393.74	92.63	-2.09	5.00E-05
CG31288	29.24	6.89	-2.09	5.00E-05
CG1774	28.33	6.83	-2.05	5.00E-05
roX1	13.38	3.23	-2.05	5.00E-05
CG9396	55.33	13.80	-2.00	5.00E-05
Fmo-1	80.42	20.34	-1.98	5.00E-05
SP1173	32.37	8.19	-1.98	5.00E-05
Gclm	45.49	11.56	-1.98	5.00E-05
CG10916	72.54	18.43	-1.98	5.00E-05
Dh31-R1	6.60	1.69	-1.96	5.00E-05
CG4238	5.56	1.44	-1.95	0.0001
CG32652	28.04	7.47	-1.91	5.00E-05
CR32690	26.80	7.14	-1.91	0.0001
CG5065	4.41	1.18	-1.90	0.0006
Btk29A	8.90	2.40	-1.89	5.00E-05
SpdS	182.74	49.64	-1.88	5.00E-05
CG2955	11.74	3.21	-1.87	5.00E-05
CG4797	8.88	2.43	-1.87	0.0003
Cyp4p1	27.54	7.58	-1.86	5.00E-05
CG18473	24.66	6.79	-1.86	5.00E-05
CG15306	12.14	3.35	-1.86	5.00E-05
Mst87F	36.42	10.06	-1.86	0.0022
CG10841	6.10	1.69	-1.85	0.0001
CG10924	73.78	20.46	-1.85	5.00E-05
t	5.86	1.63	-1.85	0.0034
CG6279	13.96	3.89	-1.84	0.00055
CG17124	78.27	21.80	-1.84	5.00E-05
fra	5.47	1.53	-1.84	5.00E-05
CG8157	1090.65	306.39	-1.83	5.00E-05
CG32548	12.88	3.63	-1.83	0.0001

fbp	639.43	180.29	-1.83	5.00E-05
CG8851	4.28	1.21	-1.83	0.0034
CG8565	13.22	3.74	-1.82	5.00E-05
ssp5	5.68	1.61	-1.82	0.0006
CG15040	2.91	0.83	-1.81	5.00E-05
Mec2	43.92	12.58	-1.80	5.00E-05
CR32658	24.74	7.09	-1.80	0.00015
Dscam	2.19	0.63	-1.80	5.00E-05
CG34434	28.46	8.18	-1.80	5.00E-05
CG34168	41.88	12.04	-1.80	0.0013
CG4907	3.20	0.92	-1.79	0.0034
CG2267	7.34	2.13	-1.78	0.00075
Hsp60B	6.49	1.89	-1.78	0.00025
CR42767	22.29	6.50	-1.78	0.0009
Cyp6g1	131.67	38.46	-1.78	5.00E-05
CG12699	89.43	26.15	-1.77	5.00E-05
AttA	60.86	17.81	-1.77	5.00E-05
CR32661	18.06	5.30	-1.77	0.005
Obp83cd	25.99	7.63	-1.77	0.00025
CG17352	3.90	1.14	-1.77	0.0013
CG3213	15.99	4.69	-1.77	5.00E-05
Mst98Ca	19.96	5.88	-1.76	5.00E-05
Men	511.49	150.71	-1.76	5.00E-05
CG15128	8.16	2.41	-1.76	5.00E-05
Klp59D	5.35	1.59	-1.75	0.00065
TrxT	27.37	8.14	-1.75	5.00E-05
CG18522	25.38	7.55	-1.75	5.00E-05
CG32064	25.45	7.59	-1.75	5.00E-05
CG9284	22.71	6.78	-1.74	0.00015
CG31709	22.31	6.66	-1.74	5.00E-05
Arp53D	7.49	2.24	-1.74	0.00465
CG5840	37.37	11.23	-1.73	5.00E-05
CG3330	13.65	4.11	-1.73	0.00025
CG30148	170.03	51.38	-1.73	5.00E-05
CG4802	100.87	30.62	-1.72	5.00E-05
CG5790	4.88	1.48	-1.72	0.00125
CG15208	7.80	2.37	-1.72	0.00345
CG1324	13.94	4.25	-1.71	0.00015
CG7229	4.82	1.48	-1.70	0.00185
Porin2	9.45	2.91	-1.70	0.0043
CG3323	4.94	1.52	-1.70	0.00085
CG3875	10.34	3.20	-1.69	0.001
Hsp68	53.38	16.60	-1.69	5.00E-05
orb	5.12	1.59	-1.68	5.00E-05
CG18266	6.30	1.96	-1.68	0.0018
TTLL3B	5.10	1.59	-1.68	0.0002
CG32063	20.44	6.37	-1.68	5.00E-05
CG1288	15.13	4.73	-1.68	0.00055
CG15086	3.19	1.00	-1.67	5.00E-05
CG14718	7.63	2.40	-1.67	0.00015
CG4691	11.41	3.59	-1.67	0.0011
CG14540	8.52	2.71	-1.65	5.00E-05

Pkd2	5.61	1.79	-1.65	5.00E-05
CG10252	29.44	9.38	-1.65	5.00E-05
CG5762	14.62	4.66	-1.65	0.0015
CG2750	1.88	0.60	-1.65	0.0012
Atox1	114.84	36.65	-1.65	5.00E-05
CG5111	5.20	1.66	-1.65	0.00325
CG4439	21.55	6.89	-1.65	5.00E-05
CG9920	31.98	10.23	-1.65	5.00E-05
Poc1	7.74	2.48	-1.64	0.00105
CG9389	6.46	2.07	-1.64	0.00065
CG2861	8.52	2.73	-1.64	0.0003
CG6304	8.74	2.80	-1.64	0.0015
ocn	37.65	12.12	-1.63	5.00E-05
CG7309	5.27	1.70	-1.63	0.0021
CG42678	27.21	8.79	-1.63	5.00E-05
CG7886	11.10	3.59	-1.63	5.00E-05
CG4218	9.54	3.09	-1.63	0.00485
SIP2	18.61	6.03	-1.63	5.00E-05
loopin-1	30.42	9.86	-1.62	5.00E-05
CG17098	6.62	2.15	-1.62	0.0003
CG31025	8.74	2.83	-1.62	5.00E-05
Hsc70-2	8.24	2.68	-1.62	0.0001
CG1394	21.06	6.86	-1.62	0.0002
CG7349	9.19	3.00	-1.62	5.00E-05
CG6776	83.34	27.21	-1.61	5.00E-05
CG1340	5.02	1.64	-1.61	0.00465
CG7804	11.23	3.67	-1.61	0.0001
CG13340	23.54	7.71	-1.61	5.00E-05
CG6372	36.73	12.04	-1.61	5.00E-05
CG3124	26.20	8.59	-1.61	5.00E-05
CG31601	5.41	1.78	-1.61	0.00455
CG42666	3.54	1.17	-1.60	0.002
CG30376	11.89	3.94	-1.59	0.00525
fan	12.09	4.01	-1.59	0.00585
CG15109	21.11	7.01	-1.59	5.00E-05
CG8219	4.03	1.34	-1.59	0.0014
CG13991	2.02	0.67	-1.59	0.00115
CG13597	7.72	2.58	-1.58	0.00155
CG8564	7.59	2.54	-1.58	0.00065
CG12861	17.06	5.70	-1.58	0.00025
CG32703	4.49	1.50	-1.58	0.00015
CG4836	32.86	11.03	-1.58	5.00E-05
CG3927	15.46	5.22	-1.57	0.0002
Cyp4d14	17.76	6.00	-1.57	5.00E-05
Tub85D	26.04	8.80	-1.57	5.00E-05
CG9133	20.82	7.03	-1.57	0.0007
CG10859	6.69	2.27	-1.56	0.00025
CG18135	242.81	82.78	-1.55	5.00E-05
Idh	1051.71	358.73	-1.55	5.00E-05
CG5043	6.61	2.27	-1.55	0.00155
CG32081	7.12	2.44	-1.54	0.00275
CG11089	430.81	148.25	-1.54	5.00E-05

ACXC	2.69	0.93	-1.54	0.0041
PGRP-SD	280.36	96.86	-1.53	0.00025
Ppm1	8.54	2.95	-1.53	0.00155
CG13032	5.45	1.88	-1.53	0.00115
AttC	203.20	70.29	-1.53	5.00E-05
CG9975	25.66	8.90	-1.53	5.00E-05
CG16782	9.61	3.34	-1.52	0.0038
bol	11.43	4.00	-1.52	5.00E-05
CG3964	5.78	2.02	-1.52	0.0001
CG8526	4.80	1.68	-1.51	0.0053
dj	13.59	4.77	-1.51	0.0004
CG42820	5.03	1.77	-1.51	0.0019
Hsp60C	14.92	5.24	-1.51	5.00E-05
CG5538	17.93	6.30	-1.51	5.00E-05
lea	5.15	1.81	-1.50	5.00E-05
CG14355	4.92	1.74	-1.50	0.00025
CG10623	14.21	5.05	-1.49	0.00015
CG2893	12.61	4.49	-1.49	5.00E-05
CG7813	4.68	1.67	-1.49	0.0024
Cht3	1.78	0.63	-1.49	0.00305
RpS19b	20.54	7.33	-1.49	0.00305
CG33090	10.73	3.84	-1.48	5.00E-05
sm	46.81	16.77	-1.48	5.00E-05
CG11125	7.70	2.76	-1.48	0.00445
CG3408	13.93	5.03	-1.47	5.00E-05
nonA-l	7.03	2.54	-1.47	0.00015
CG30015	2.79	1.01	-1.47	0.00095
CG12179	2.52	0.91	-1.46	0.0019
Cyp4d1	855.36	311.26	-1.46	5.00E-05
CG7900	28.88	10.52	-1.46	5.00E-05
CG6287	333.14	121.84	-1.45	5.00E-05
mud	4.74	1.74	-1.44	5.00E-05
srpk79D	2.81	1.03	-1.44	0.0024
blot	4.45	1.65	-1.43	0.00085
Pepck	1075.39	399.41	-1.43	5.00E-05
CG15599	4.76	1.77	-1.43	0.0047
Eaat1	40.88	15.24	-1.42	5.00E-05
CG6752	2.57	0.96	-1.42	0.00105
CG30187	100.47	37.56	-1.42	5.00E-05
CG9279	4.26	1.61	-1.40	5.00E-05
CG31029	8.47	3.21	-1.40	5.00E-05
Treh	58.22	22.17	-1.39	5.00E-05
CG13659	6.47	2.48	-1.38	0.0031
CG17734	199.76	76.83	-1.38	5.00E-05
CG12860	12.70	4.89	-1.38	0.0007
Dhc98D	1.04	0.40	-1.38	0.00025
RpL22-like	15.95	6.20	-1.36	0.00025
CG1387	2.85	1.11	-1.36	0.00545
CG10734	8.74	3.42	-1.36	0.0044
Hsp26	46.81	18.33	-1.35	5.00E-05
kuz	11.87	4.66	-1.35	5.00E-05
CG31636	52.23	20.52	-1.35	5.00E-05

CG9344	46.51	18.29	-1.35	0.00375
CG10512	234.74	92.48	-1.34	5.00E-05
CG8136	6.66	2.62	-1.34	0.00435
Rpt3R	7.60	3.00	-1.34	0.0056
CG10960	93.99	37.35	-1.33	5.00E-05
CG1347	18.62	7.41	-1.33	5.00E-05
ana3	1.83	0.73	-1.32	0.00255
exu	63.79	25.79	-1.31	5.00E-05
scf	90.51	36.61	-1.31	5.00E-05
CG6040	4.15	1.68	-1.31	5.00E-05
CG14879	13.47	5.47	-1.30	5.00E-05
Pdk	183.81	74.69	-1.30	5.00E-05
CG10621	1171.47	477.51	-1.29	5.00E-05
orb2	15.47	6.31	-1.29	5.00E-05
ap	17.34	7.08	-1.29	5.00E-05
Tob	4.32	1.77	-1.29	0.0021
CG5987	6.63	2.73	-1.28	0.0007
RpS5b	19.16	7.89	-1.28	0.0009
dpr17	4.53	1.88	-1.27	0.00515
Ih	19.70	8.19	-1.27	5.00E-05
CG5660	3.79	1.58	-1.27	0.005
CG14688	339.22	141.35	-1.26	5.00E-05
CG15343	86.69	36.22	-1.26	5.00E-05
fusl	14.27	5.97	-1.26	5.00E-05
CG30460	9.38	3.93	-1.26	5.00E-05
CG32444	164.43	68.87	-1.26	5.00E-05
GstS1	603.83	253.51	-1.25	5.00E-05
CG30151	42.28	17.78	-1.25	5.00E-05
Klp3A	2.88	1.21	-1.25	0.00155
CG9399	36.43	15.36	-1.25	5.00E-05
hoe1	15.03	6.36	-1.24	5.00E-05
CG5389	7.02	2.98	-1.24	0.00165
Orct	20.99	8.91	-1.24	5.00E-05
sle	6.93	2.95	-1.23	5.00E-05
Ptpmeg	17.20	7.33	-1.23	5.00E-05
l(2)08717	34.03	14.61	-1.22	5.00E-05
CG6201	6.30	2.70	-1.22	0.00375
Ance	59.46	25.53	-1.22	5.00E-05
Nmd3	28.30	12.17	-1.22	5.00E-05
CG17928	31.24	13.50	-1.21	5.00E-05
Cyp310a1	96.37	41.85	-1.20	5.00E-05
CG31324	11.74	5.14	-1.19	0.00065
CG7860	37.58	16.49	-1.19	5.00E-05
yellow-d	135.47	59.66	-1.18	0.00065
GstE3	247.22	109.00	-1.18	5.00E-05
Fim	23.72	10.51	-1.17	5.00E-05
Stat92E	150.23	66.58	-1.17	5.00E-05
CG13822	100.92	44.95	-1.17	5.00E-05
CG4068	27.20	12.18	-1.16	5.00E-05
Rbp4	9.36	4.23	-1.15	0.0028
whd	47.00	21.29	-1.14	5.00E-05
CG9664	65.95	29.90	-1.14	5.00E-05

CG5707	34.27	15.63	-1.13	5.00E-05
CG11883	7.69	3.51	-1.13	0.0001
CG2765	19.76	9.04	-1.13	5.00E-05
CG4686	33.59	15.42	-1.12	5.00E-05
CG4752	90.54	41.66	-1.12	5.00E-05
CG3961	212.48	98.11	-1.11	5.00E-05
CG8369	421.84	194.84	-1.11	5.00E-05
Jheh3	187.14	86.78	-1.11	5.00E-05
GstD4	72.66	33.72	-1.11	5.00E-05
CG17350	35.69	16.58	-1.11	5.00E-05
CG31414	34.26	15.99	-1.10	5.00E-05
eIF4E-3	18.15	8.50	-1.10	0.00155
Pof	17.58	8.24	-1.09	0.0001
CG33099	56.71	26.63	-1.09	5.00E-05
Pen	27.79	13.08	-1.09	5.00E-05
CG5577	151.66	71.83	-1.08	5.00E-05
alpha-Est5	24.20	11.50	-1.07	5.00E-05
CG31988	18.67	8.89	-1.07	0.0017
GIIIspla2	25.85	12.33	-1.07	0.0001
CG33307	1481.95	710.88	-1.06	5.00E-05
Jafrac1	285.69	137.06	-1.06	5.00E-05
CG3714	31.67	15.20	-1.06	5.00E-05
CG11897	5.00	2.40	-1.06	5.00E-05
Spn42Db	48.44	23.29	-1.06	5.00E-05
mthl3	23.83	11.46	-1.06	5.00E-05
CG31523	17.23	8.31	-1.05	5.00E-05
axo	15.08	7.31	-1.04	5.00E-05
CG13868	148.07	71.94	-1.04	5.00E-05
Pvr	28.79	14.06	-1.03	5.00E-05
CG3842	73.80	36.21	-1.03	5.00E-05
Ppat-Dpck	69.38	34.10	-1.02	5.00E-05
polo	8.96	4.42	-1.02	0.00075
CG10031	158.48	78.52	-1.01	5.00E-05
Ady43A	8.57	4.25	-1.01	0.0016
CG31373	29.07	14.41	-1.01	0.0033
Fmo-2	57.17	28.36	-1.01	5.00E-05
sPLA2	200.14	99.43	-1.01	0.0008
Jheh1	59.78	29.80	-1.00	5.00E-05
CG32191	29.02	14.47	-1.00	5.00E-05
gb	10.68	5.33	-1.00	0.0001
CG3226	56.77	28.39	-1.00	5.00E-05
Obp99c	3093.55	1553.12	-0.99	5.00E-05
Jupiter	16.85	8.48	-0.99	0.0005
GstE8	39.13	19.86	-0.98	0.0008
GstD1	2651.77	1350.57	-0.97	5.00E-05
CG4893	34.69	17.71	-0.97	5.00E-05
CG15293	713.05	365.12	-0.97	5.00E-05
nmo	7.96	4.09	-0.96	0.00085
CG9339	4.21	2.17	-0.96	0.00475
GstE7	310.65	160.79	-0.95	5.00E-05
Vago	133.21	69.18	-0.95	5.00E-05
nimB4	46.00	23.96	-0.94	5.00E-05

CG3394	49.49	25.78	-0.94	5.00E-05
CG8026	138.04	72.06	-0.94	5.00E-05
CG4302	25.79	13.59	-0.92	0.0053
Nhe2	5.16	2.73	-0.92	0.00095
CG11284	75.83	40.20	-0.92	5.00E-05
miple2	21.97	11.68	-0.91	0.0011
l(1)G0255	166.49	88.52	-0.91	5.00E-05
CG9444	61.14	32.79	-0.90	5.00E-05
ssp3	6.03	3.24	-0.90	0.00025
LRP1	21.24	11.43	-0.89	5.00E-05
CG40191	108.20	58.44	-0.89	5.00E-05
CG5567	29.40	15.97	-0.88	0.0001
rl	45.73	24.85	-0.88	5.00E-05
CG30344	12.81	6.97	-0.88	5.00E-05
ade2	64.65	35.37	-0.87	5.00E-05
vir-1	522.69	286.69	-0.87	5.00E-05
CG14882	14.09	7.73	-0.87	0.00335
ras	27.32	15.00	-0.87	0.0001
CG11334	174.02	95.58	-0.86	5.00E-05
Tsf1	1129.19	621.67	-0.86	5.00E-05
CG31689	36.77	20.25	-0.86	5.00E-05
CG32103	75.21	41.59	-0.85	5.00E-05
ltd	63.21	35.02	-0.85	5.00E-05
CG14997	85.47	47.57	-0.85	5.00E-05
Spn6	40.44	22.51	-0.85	0.0001
CG13641	452.33	251.98	-0.84	5.00E-05
CG16743	465.53	259.91	-0.84	5.00E-05
CG15093	418.69	233.95	-0.84	5.00E-05
Tsp42Ek	312.47	174.64	-0.84	5.00E-05
CG6574	36.34	20.38	-0.83	5.00E-05
rogdi	12.31	6.90	-0.83	0.0008
armi	4.79	2.69	-0.83	0.0034
CG1532	116.66	65.46	-0.83	5.00E-05
ade5	425.87	240.58	-0.82	5.00E-05
CG14291	48.06	27.17	-0.82	5.00E-05
Nc73EF	69.49	39.38	-0.82	5.00E-05
PGRP-LB	18.19	10.38	-0.81	0.0051
CG10254	9.99	5.70	-0.81	5.00E-05
CG6199	277.47	158.89	-0.80	5.00E-05
CG7692	7.05	4.04	-0.80	0.00075
CG8788	91.54	52.48	-0.80	5.00E-05
CG6654	8.73	5.01	-0.80	0.0042
Yeti	244.65	140.75	-0.80	5.00E-05
Unc-76	21.74	12.51	-0.80	5.00E-05
CG9449	89.10	51.53	-0.79	5.00E-05
Nha2	56.50	32.75	-0.79	5.00E-05
CG1732	9.85	5.71	-0.79	0.00095
CG4078	6.07	3.52	-0.79	0.0037
CG34136	427.16	248.38	-0.78	5.00E-05
CG6404	17.67	10.28	-0.78	0.0007
fal	18.77	10.92	-0.78	0.00035
pst	548.79	319.41	-0.78	5.00E-05

CG13185	3.12	1.82	-0.78	5.00E-05
eIF4G2	13.66	7.98	-0.78	0.00225
CG7737	9.58	5.62	-0.77	0.00375
CG10171	75.41	44.33	-0.77	5.00E-05
CG7255	367.45	216.03	-0.77	5.00E-05
CG10527	628.73	369.87	-0.77	5.00E-05
CG33493	911.57	536.69	-0.76	5.00E-05
l(1)G0289	42.10	24.84	-0.76	5.00E-05
Glt	536.86	318.94	-0.75	5.00E-05
fry	11.20	6.66	-0.75	5.00E-05
Sam-S	522.54	311.08	-0.75	5.00E-05
Obp99a	629.57	375.13	-0.75	5.00E-05
CG4572	58.97	35.42	-0.74	5.00E-05
CG12262	355.57	213.69	-0.73	0.0001
CG1662	38.14	22.93	-0.73	0.0001
Tom70	14.82	8.94	-0.73	0.0008
MRP	42.75	25.78	-0.73	5.00E-05
CG9662	52.30	31.57	-0.73	0.0011
CAH1	26.25	15.85	-0.73	0.00045
CG2200	29.55	17.87	-0.73	0.00215
oaf	15.36	9.40	-0.71	0.00455
CG11737	18.69	11.44	-0.71	0.0006
Tcp-1eta	48.43	29.74	-0.70	5.00E-05
lap	36.01	22.15	-0.70	5.00E-05
Ace	7.08	4.37	-0.70	0.00105
Zip3	13.36	8.29	-0.69	0.0037
CG10741	12.91	8.03	-0.69	0.00475
Top2	11.67	7.27	-0.68	0.00025
rept	14.46	9.01	-0.68	0.00525
CG33494	139.45	87.05	-0.68	5.00E-05
PGRP-SB1	323.17	201.81	-0.68	0.0012
prominin-like	16.95	10.63	-0.67	5.00E-05
att-ORFA	22.49	14.21	-0.66	0.0017
CG7441	13.45	8.54	-0.66	0.00265
Hsp60	154.89	98.30	-0.66	5.00E-05
Tsp42Ed	29.24	18.62	-0.65	0.00555
CG12825	342.71	219.20	-0.64	5.00E-05
CAP	44.43	28.48	-0.64	0.0005
CG3999	323.12	207.32	-0.64	5.00E-05
CG8709	53.92	34.65	-0.64	5.00E-05
DNaseII	364.94	234.73	-0.64	5.00E-05
CG8368	15.96	10.27	-0.64	0.00125
out	16.58	10.69	-0.63	0.00075
CG2982	12.66	8.18	-0.63	0.0041
mdy	147.45	95.55	-0.63	5.00E-05
CG32626	218.56	141.83	-0.62	5.00E-05
Tl	42.67	27.73	-0.62	5.00E-05
CG10639	162.01	105.35	-0.62	5.00E-05
CG32687	298.58	194.41	-0.62	5.00E-05
CG5151	13.35	8.71	-0.62	0.002
CG31778	202.16	132.51	-0.61	5.00E-05
toc	7.11	4.66	-0.61	0.0045

CG33093	65.87	43.29	-0.61	0.00035
Fer1HCH	280.32	184.51	-0.60	0.00155
CG5991	61.08	40.22	-0.60	0.00015
h	23.31	15.37	-0.60	0.0012
SamDC	68.47	45.23	-0.60	0.00015
CG6767	147.82	98.21	-0.59	0.0001
Tif-IA	27.19	18.08	-0.59	0.00085
nudC	41.19	27.40	-0.59	0.0009
Ald	2630.16	1755.92	-0.58	0.0003
Mical	5.99	4.01	-0.58	0.00425
CG4882	24.63	16.54	-0.57	0.0052
CG9616	239.42	160.74	-0.57	0.0004
inx3	52.33	35.17	-0.57	0.0008
nimB5	113.93	76.75	-0.57	5.00E-05
Ubi-p63E	31.98	21.55	-0.57	0.00055
Tps1	509.56	345.59	-0.56	0.0001
CG8206	55.19	37.49	-0.56	0.0023
CG6191	14.43	9.81	-0.56	0.00205
CG10467	123.09	83.75	-0.56	5.00E-05
prc	6.65	4.54	-0.55	0.00505
CG34424	343.06	234.60	-0.55	0.00025
KLHL18	71.23	48.80	-0.55	0.00025
Ndg	35.36	24.24	-0.54	0.0003
CG11811	37.86	25.96	-0.54	0.0018
CG15814	25.51	17.54	-0.54	0.00415
Cdc27	12.86	8.85	-0.54	0.0028
Cct5	64.45	44.33	-0.54	0.00065
CG9153	49.20	33.85	-0.54	0.00015
ACXD	25.43	17.51	-0.54	0.00045
Hn	537.26	371.54	-0.53	0.00015
alphaTub84D	45.58	31.69	-0.52	0.00055
CG9027	106.85	74.34	-0.52	0.00145
CG10638	54.78	38.13	-0.52	0.00305
CG7033	54.63	38.12	-0.52	0.0008
p38c	59.45	41.54	-0.52	0.0023
Uch	52.74	36.87	-0.52	0.0044
Cyp4e2	263.88	186.40	-0.50	0.0004
CG32803	103.54	73.18	-0.50	0.0022
CG8258	41.09	29.05	-0.50	0.002
CG5390	309.83	219.14	-0.50	0.00045
CG3397	124.71	88.58	-0.49	0.00195
Fpps	273.61	194.37	-0.49	0.0003
Cyp4d2	40.63	28.94	-0.49	0.00505
CG13654	22.71	16.22	-0.49	0.00345
CG8449	75.14	53.69	-0.48	0.0027
CG5525	53.08	37.94	-0.48	0.00205
NTPase	51.00	36.48	-0.48	0.00425
CG34215	1039.29	744.22	-0.48	0.00035
CG17331	170.56	122.17	-0.48	0.00195
Trc8	26.78	19.25	-0.48	0.004
CG1516	541.96	389.64	-0.48	0.00285
CG1468	962.19	692.17	-0.48	0.0011

Cctgamma	34.90	25.12	-0.47	0.00285
CG4673	33.90	24.48	-0.47	0.00435
skap	145.96	105.52	-0.47	0.0014
CG4774	58.35	42.28	-0.46	0.0058
CG6330	76.27	55.47	-0.46	0.00285
CG9894	249.60	181.78	-0.46	0.0016
CG33120	94.65	69.08	-0.45	0.00165
CG16935	101.73	74.26	-0.45	0.0046
Nsf2	29.25	21.36	-0.45	0.0054
Itp-r83A	33.90	24.78	-0.45	0.00155
CG32521	233.24	170.70	-0.45	0.00145
CG3597	97.92	71.71	-0.45	0.00415
gem	72.77	53.49	-0.44	0.00165
gp210	14.59	10.79	-0.44	0.00525
Droj2	114.60	84.91	-0.43	0.00245
CG8029	72.61	54.16	-0.42	0.00375
Vha100-1	70.73	52.76	-0.42	0.0027
CG5590	308.03	229.81	-0.42	0.00235
CG11594	287.04	214.76	-0.42	0.0028
CG16718	57.00	42.67	-0.42	0.00345
Idgf3	285.61	215.67	-0.41	0.00345
CG17244	895.83	677.78	-0.40	0.00425
CG11395	414.42	316.37	-0.39	0.00555
CG14629	578.33	441.56	-0.39	0.0051
awd	1806.62	2357.86	0.38	0.0061
ATPsyn-d	509.60	665.72	0.39	0.0045
Nurf-38	316.57	413.91	0.39	0.00545
CG7461	148.52	195.73	0.40	0.0044
CG7181	607.69	800.98	0.40	0.005
CG31769	217.97	287.48	0.40	0.00405
GRHR	70.69	93.26	0.40	0.0057
growl	145.67	192.29	0.40	0.003
CG32230	938.60	1239.71	0.40	0.00445
CG3321	520.82	690.48	0.41	0.00345
ced-6	97.83	129.79	0.41	0.004
CG10664	649.57	862.13	0.41	0.003
Xbp1	248.79	331.80	0.42	0.00265
Ent2	57.97	77.33	0.42	0.0057
Oat	804.93	1074.74	0.42	0.0051
CG5010	148.25	198.13	0.42	0.004
sec31	108.60	145.29	0.42	0.00275
CG14767	62.92	84.22	0.42	0.0042
prel	54.79	73.36	0.42	0.0056
Pmm45A	95.25	127.64	0.42	0.0021
Cyp1	655.39	881.47	0.43	0.00305
CG2846	58.71	79.00	0.43	0.0061
Atg8a	160.56	216.74	0.43	0.0024
Pgm	284.52	384.62	0.43	0.00175
fs(1)h	9.76	13.20	0.43	0.00575
sesB	891.44	1206.25	0.44	0.0038
CG17508	107.29	145.54	0.44	0.0029
CG7834	484.92	658.59	0.44	0.00165

CG10962	1190.55	1617.30	0.44	0.0048
Vha13	131.40	178.54	0.44	0.00465
CG5315	93.04	126.46	0.44	0.00225
arg	313.40	426.08	0.44	0.002
Syb	160.65	218.57	0.44	0.0035
porin	422.01	574.57	0.45	0.0014
Sod2	136.89	186.65	0.45	0.0027
ATPsyn-	1453.11	1982.70	0.45	0.00445
spirit	109.29	149.13	0.45	0.00165
Mtp	245.23	334.83	0.45	0.0016
Surf4	270.20	369.56	0.45	0.001
CG31548	117.17	160.36	0.45	0.00255
l(2)37Cc	114.49	156.79	0.45	0.00165
SdhC	128.19	175.91	0.46	0.0041
CrebA	27.22	37.35	0.46	0.0021
Prx5037	148.79	204.51	0.46	0.00135
T3dh	115.82	159.37	0.46	0.0013
for	89.62	123.40	0.46	0.0006
CG9577	151.14	208.25	0.46	0.0023
Vinc	25.73	35.51	0.46	0.00145
Cyp28d1	201.58	278.55	0.47	0.00115
l(3)neo18	151.48	209.44	0.47	0.0016
CG6206	38.93	53.87	0.47	0.0016
NP15.6	165.31	228.76	0.47	0.00365
kdn	51.10	70.86	0.47	0.00145
CG3560	401.67	557.18	0.47	0.00215
Ucrh	377.60	524.08	0.47	0.00145
CG14621	27.71	38.56	0.48	0.0057
CG10672	88.60	123.33	0.48	0.00245
Dcr-2	19.38	27.08	0.48	0.0052
tud	60.30	84.30	0.48	0.0006
CG10320	290.22	406.21	0.49	0.00375
CG7320	216.14	302.53	0.49	0.00055
l(1)G0230	539.05	754.97	0.49	0.00035
CG1458	203.63	285.28	0.49	0.001
CG3731	281.52	394.70	0.49	0.00075
CG6910	517.60	726.68	0.49	0.00085
CG33936	60.78	85.48	0.49	0.00055
CG9467	25.59	36.00	0.49	0.002
CG42593	24.07	33.88	0.49	0.0017
CG32425	162.65	228.93	0.49	0.00065
Sply	46.77	65.89	0.49	0.001
CG6359	60.76	85.84	0.50	0.0011
Tal	1019.23	1443.71	0.50	0.0005
Hsc70-3	1360.11	1929.17	0.50	0.00475
CG11357	17.31	24.56	0.50	0.0027
CG15203	268.74	381.73	0.51	0.00075
CG13887	152.58	216.78	0.51	0.0002
lama	34.94	49.66	0.51	0.0006
Cat	1672.69	2377.88	0.51	0.0033
CG9306	140.58	199.99	0.51	0.00135
CG9691	549.56	782.59	0.51	0.00025

CG2118	36.67	52.27	0.51	0.0008
Hsromega	32.65	46.55	0.51	0.0048
CG9436	35.19	50.23	0.51	0.0026
CG9914	178.68	255.02	0.51	0.00015
CG5002	31.58	45.11	0.51	0.00125
tai	13.04	18.64	0.51	0.00025
TRAM	395.74	565.83	0.52	0.0003
CG10219	62.31	89.12	0.52	0.0038
cu	49.86	71.33	0.52	0.0005
Oatp74D	50.14	71.78	0.52	0.00035
CG1105	79.88	114.45	0.52	0.00095
Atg9	10.70	15.35	0.52	0.0057
l(2)k09913	161.36	231.47	0.52	0.0001
CG8726	28.95	41.57	0.52	0.0038
CG1161	56.09	80.61	0.52	0.0015
atl	71.65	102.98	0.52	0.0001
CG9044	12.33	17.75	0.53	0.00145
Egfr	35.10	50.65	0.53	0.00045
CG4390	122.30	176.63	0.53	0.00035
cdi	7.41	10.71	0.53	0.0012
CG10660	20.58	29.75	0.53	0.003
fru	11.18	16.17	0.53	0.0058
CG30104	25.24	36.52	0.53	0.0017
CG14715	244.75	354.19	0.53	0.00085
CG4769	209.91	303.91	0.53	5.00E-05
chic	461.36	668.11	0.53	0.00015
CG6084	711.65	1032.24	0.54	0.00015
schlank	59.72	86.65	0.54	0.00045
CG7322	863.29	1253.61	0.54	0.0001
CG8680	108.84	158.10	0.54	0.0019
Rab7	82.33	119.63	0.54	0.0003
Gie	44.57	64.77	0.54	0.003
CG32000	31.39	45.76	0.54	0.00015
alt	106.66	155.59	0.54	0.0001
Las	30.23	44.11	0.55	0.00175
Pdsw	203.85	297.86	0.55	0.00025
CG15828	74.63	109.07	0.55	0.00015
Atg13	14.46	21.14	0.55	0.001
CG30492	46.36	67.77	0.55	0.0045
Hydr2	63.02	92.31	0.55	0.00015
CG14073	7.26	10.65	0.55	0.0028
Pfrx	36.47	53.60	0.56	0.0002
CG9319	49.20	72.36	0.56	0.00035
Nedd8	95.24	140.10	0.56	0.0042
CG7998	846.21	1244.82	0.56	0.0002
Got2	783.44	1152.72	0.56	0.0003
aralar1	68.91	101.52	0.56	0.0001
l(2)35Di	127.91	188.48	0.56	0.00055
CG18815	80.90	119.55	0.56	0.0001
PH4alphaEFB	74.85	111.03	0.57	5.00E-05
Lmpt	8.19	12.17	0.57	0.00495
Pdi	3306.27	4915.83	0.57	0.0056

CG11015	294.92	438.62	0.57	5.00E-05
Aats-val	31.55	46.95	0.57	5.00E-05
RFeSP	261.63	389.50	0.57	0.0001
CG3621	129.77	193.56	0.58	0.00075
CG7430	190.56	284.41	0.58	0.0001
Pde11	3.64	5.45	0.58	0.0055
CG14200	5.53	8.29	0.58	0.0011
CG40006	8.32	12.47	0.58	0.00515
PMCA	33.96	50.95	0.59	5.00E-05
CG13298	54.86	82.41	0.59	0.00065
CG5059	52.74	79.24	0.59	0.0001
Spn	3.91	5.88	0.59	0.00295
CG12140	151.74	228.18	0.59	5.00E-05
Acon	92.19	138.64	0.59	5.00E-05
CG42258	15.07	22.74	0.59	0.00135
LKR	88.66	133.81	0.59	5.00E-05
vkg	263.62	398.27	0.60	0.00015
CG16926	1597.43	2414.91	0.60	5.00E-05
cpb	24.82	37.54	0.60	0.0006
CG4335	155.06	234.66	0.60	5.00E-05
Mitf	15.21	23.02	0.60	0.0005
CG12272	11.54	17.47	0.60	0.00055
CG3683	143.91	217.97	0.60	5.00E-05
mnd	13.66	20.71	0.60	0.0009
CG5599	23.23	35.22	0.60	0.0006
ppl	704.36	1069.36	0.60	5.00E-05
tobi	86.92	132.11	0.60	0.0001
CG4729	123.80	188.17	0.60	5.00E-05
CG15771	12.05	18.32	0.61	0.00135
CG7149	28.20	42.91	0.61	0.0001
Cyp4d8	51.30	78.07	0.61	5.00E-05
flr	24.77	37.97	0.62	0.0002
CG32529	5.64	8.65	0.62	0.0005
CG3829	18.79	28.83	0.62	0.0002
CG33144	5.93	9.11	0.62	0.00095
ATPsyn-Cf6	657.43	1009.50	0.62	5.00E-05
Hel89B	6.68	10.27	0.62	0.00025
Spn77Ba	35.32	54.27	0.62	0.0001
CG15369	903.73	1388.75	0.62	5.00E-05
sda	5.00	7.69	0.62	0.00155
Zyx102EF	38.36	59.16	0.62	5.00E-05
Sps2	17.65	27.22	0.62	0.002
CG6028	219.74	338.92	0.63	5.00E-05
CG1702	55.82	86.14	0.63	0.0004
CG17896	294.31	454.50	0.63	5.00E-05
CG11309	165.99	256.60	0.63	5.00E-05
CG33774	192.20	297.43	0.63	0.0046
Cyp6a23	186.52	288.91	0.63	5.00E-05
Trl	20.62	31.98	0.63	0.00025
CG4630	12.48	19.38	0.63	0.00295
alpha-Est3	11.72	18.20	0.63	0.0029
CG12130	102.06	158.44	0.63	5.00E-05

CG18624	240.64	373.90	0.64	5.00E-05
CG31075	3113.78	4842.14	0.64	0.00075
CG12581	11.42	17.76	0.64	0.0004
mfas	24.93	38.78	0.64	5.00E-05
Cct1	99.46	154.72	0.64	5.00E-05
CG6067	131.21	204.25	0.64	5.00E-05
CG30359	276.34	430.92	0.64	5.00E-05
CG11652	27.71	43.31	0.64	0.00015
eIF-2	277.93	434.56	0.64	5.00E-05
CG14196	40.69	63.69	0.65	5.00E-05
stv	11.39	17.84	0.65	0.00025
galectin	66.08	103.50	0.65	5.00E-05
Mnt	11.80	18.48	0.65	0.0002
PKD	31.13	48.85	0.65	5.00E-05
LanA	90.59	142.25	0.65	5.00E-05
CG9331	1076.32	1690.29	0.65	5.00E-05
CG42351	364.81	573.69	0.65	5.00E-05
CG9547	129.20	203.32	0.65	5.00E-05
CG2254	337.06	531.31	0.66	5.00E-05
Acox57D-d	41.62	65.63	0.66	5.00E-05
SdhB	125.42	197.83	0.66	5.00E-05
SCAP	23.38	36.96	0.66	5.00E-05
CG30091	63.90	101.28	0.66	5.00E-05
CG9953	57.14	90.73	0.67	5.00E-05
CG3267	34.68	55.26	0.67	5.00E-05
wnd	4.75	7.58	0.67	0.00225
CG10824	21.17	33.82	0.68	0.0059
CG7220	9.27	14.80	0.68	0.00315
dob	43.76	69.97	0.68	5.00E-05
Ets98B	13.96	22.39	0.68	5.00E-05
CG33460	37.91	60.85	0.68	0.00025
Gp150	45.46	72.96	0.68	5.00E-05
CG10026	103.41	166.01	0.68	5.00E-05
CG32486	9.88	15.87	0.68	0.0004
CG9238	87.33	140.31	0.68	5.00E-05
CG1021	7.92	12.72	0.68	0.0006
CG15438	19.28	31.01	0.69	0.0003
Reg-2	845.94	1361.77	0.69	5.00E-05
ClC-a	14.09	22.70	0.69	5.00E-05
Eno	892.63	1443.08	0.69	5.00E-05
ox	425.87	688.68	0.69	0.0001
CG5205	7.97	12.89	0.69	5.00E-05
Cyp6v1	21.79	35.26	0.69	0.0001
CG1968	11.06	17.95	0.70	0.0018
scu	511.47	831.90	0.70	5.00E-05
by	5.47	8.91	0.70	0.00235
LanB1	53.36	86.94	0.70	5.00E-05
Lsd-2	536.59	875.32	0.71	5.00E-05
CG3061	44.23	72.16	0.71	5.00E-05
bmm	21.90	35.72	0.71	5.00E-05
CG32699	12.74	20.84	0.71	5.00E-05
CR42862	129.76	212.35	0.71	5.00E-05

CG6325	6.71	10.98	0.71	0.00065
Gli	7.73	12.67	0.71	5.00E-05
dl	9.20	15.09	0.71	0.0004
SelG	45.51	74.78	0.72	0.0001
C3G	5.76	9.48	0.72	0.0001
CG32850	9.58	15.76	0.72	0.0008
CG5532	57.63	94.90	0.72	0.00015
Acsl	92.96	153.10	0.72	5.00E-05
CG30069	4.39	7.24	0.72	5.00E-05
Spn42Dc	39.91	65.91	0.72	5.00E-05
Oda	293.72	485.95	0.73	5.00E-05
CG15658	9.89	16.36	0.73	0.00215
Pu	9.97	16.54	0.73	0.00175
Rala	18.30	30.39	0.73	5.00E-05
ImpL2	33.72	56.18	0.74	5.00E-05
CG6115	98.67	164.41	0.74	5.00E-05
GstE6	24.55	40.95	0.74	0.00215
grass	103.17	172.11	0.74	5.00E-05
CG8586	43.45	72.51	0.74	5.00E-05
CG32068	157.38	262.91	0.74	5.00E-05
hfw	18.92	31.66	0.74	5.00E-05
IP3K2	9.59	16.05	0.74	0.00015
CG30273	25.71	43.15	0.75	0.00405
CG5362	1322.49	2220.43	0.75	5.00E-05
CG1291	32.01	53.75	0.75	5.00E-05
Thor	354.04	594.87	0.75	5.00E-05
su(r)	133.33	224.28	0.75	5.00E-05
4GalNAcTA	20.78	34.99	0.75	5.00E-05
kraken	33.21	55.92	0.75	5.00E-05
CG14787	47.34	79.78	0.75	5.00E-05
CG7878	9.70	16.36	0.75	0.00035
CG1275	33.59	56.69	0.75	5.00E-05
CG2083	3.48	5.88	0.76	0.00015
CG34417	21.92	37.08	0.76	0.0002
CG6543	812.56	1375.99	0.76	5.00E-05
CG32666	4.69	7.95	0.76	0.00035
Ac13E	3.24	5.51	0.76	0.0003
Cyp9b1	57.82	98.32	0.77	5.00E-05
CG2493	102.44	174.42	0.77	5.00E-05
smp-30	242.44	413.22	0.77	5.00E-05
CG30288	56.25	96.08	0.77	5.00E-05
CG31674	14.01	24.07	0.78	0.0008
fu12	27.85	47.94	0.78	5.00E-05
CG2862	307.03	528.73	0.78	5.00E-05
Hex-A	40.14	69.17	0.79	5.00E-05
Sp7	35.19	60.88	0.79	5.00E-05
Gs1l	13.96	24.21	0.79	0.00365
CG9629	188.55	328.41	0.80	5.00E-05
CG14872	61.68	107.43	0.80	5.00E-05
CG9542	148.00	258.50	0.80	5.00E-05
Dhfr	28.53	49.90	0.81	0.0016
CG14225	20.07	35.12	0.81	5.00E-05

Fdh	252.21	441.27	0.81	5.00E-05
CG6770	813.42	1425.07	0.81	5.00E-05
CG6746	63.62	111.60	0.81	5.00E-05
CG1943	21.82	38.36	0.81	5.00E-05
cp309	6.54	11.51	0.81	5.00E-05
alpha-Est8	13.15	23.18	0.82	5.00E-05
if	11.45	20.21	0.82	5.00E-05
CG5044	93.59	165.63	0.82	5.00E-05
CG3603	111.38	197.47	0.83	5.00E-05
CG2991	15.63	27.78	0.83	5.00E-05
CG5261	168.65	299.96	0.83	5.00E-05
Msp-300	5.39	9.60	0.83	5.00E-05
casp	29.37	52.25	0.83	5.00E-05
CG8475	27.12	48.32	0.83	5.00E-05
eIF2B-epsilon	13.74	24.49	0.83	0.00525
CG17597	95.64	170.58	0.83	5.00E-05
CG12025	38.34	68.43	0.84	5.00E-05
CG32407	75.75	135.45	0.84	5.00E-05
CG30269	25.51	45.65	0.84	0.00475
mav	4.15	7.42	0.84	0.0046
CG2911	12.45	22.34	0.84	0.00495
CG2444	201.92	362.55	0.84	5.00E-05
CG42806	45.29	81.69	0.85	0.00115
CD98hc	60.51	109.23	0.85	5.00E-05
bor	25.28	45.72	0.85	5.00E-05
CG11474	44.79	81.44	0.86	5.00E-05
scrib	5.58	10.17	0.87	5.00E-05
CG13004	13.35	24.35	0.87	5.00E-05
CG42694	12.56	23.00	0.87	5.00E-05
CG30431	35.96	65.91	0.87	5.00E-05
CG11791	9.14	16.77	0.88	0.0014
Lac	25.90	48.02	0.89	5.00E-05
MSBP	140.96	261.44	0.89	5.00E-05
CG32369	15.46	28.74	0.89	5.00E-05
Aats-thr	68.18	126.90	0.90	5.00E-05
CG6912	143.08	266.76	0.90	5.00E-05
Ate1	19.26	36.03	0.90	5.00E-05
CG42846	754.20	1411.23	0.90	5.00E-05
Acer	78.18	146.48	0.91	5.00E-05
Spn43Ab	437.52	821.61	0.91	5.00E-05
CG3609	176.01	330.79	0.91	5.00E-05
tok	23.72	44.75	0.92	5.00E-05
HspB8	149.56	282.24	0.92	5.00E-05
Tsp42Eq	10.77	20.34	0.92	0.0022
Thd1	12.52	23.75	0.92	5.00E-05
CG12159	20.87	39.61	0.92	0.00035
CG1969	17.34	33.09	0.93	5.00E-05
Ance-4	178.24	340.47	0.93	5.00E-05
PyK	286.60	547.79	0.93	5.00E-05
mRpL28	59.37	113.75	0.94	5.00E-05
ry	25.76	49.38	0.94	5.00E-05
v	138.56	268.00	0.95	5.00E-05

Kr	99.32	192.23	0.95	5.00E-05
CG34437	71.06	138.03	0.96	5.00E-05
CG31937	67.48	131.28	0.96	5.00E-05
ATPCL	471.67	919.22	0.96	5.00E-05
bnl	2.54	4.97	0.97	0.0011
CG1637	83.31	163.05	0.97	5.00E-05
CG5999	41.98	82.23	0.97	5.00E-05
CG10932	178.01	349.69	0.97	5.00E-05
yellow-f2	33.20	65.25	0.98	5.00E-05
CG18812	6.90	13.61	0.98	0.0002
CG1307	16.66	32.90	0.98	0.0002
Socs36E	3.63	7.19	0.98	0.00015
CG31793	8.18	16.28	0.99	5.00E-05
CG1092	37.20	74.01	0.99	5.00E-05
Ncc69	4.29	8.55	0.99	5.00E-05
ScpX	188.00	374.48	0.99	5.00E-05
CG32412	35.49	70.80	1.00	5.00E-05
Mlc2	8.26	16.51	1.00	5.00E-05
CG3270	40.19	80.35	1.00	5.00E-05
CG9536	41.40	82.91	1.00	5.00E-05
CG10376	5.23	10.48	1.00	0.00065
CG6357	5.77	11.59	1.01	0.0046
Lip4	57.51	116.31	1.02	5.00E-05
Act57B	25.45	51.50	1.02	5.00E-05
CG8501	11.88	24.05	1.02	0.0015
CG18343	92.75	188.03	1.02	5.00E-05
Aats-his	91.15	185.48	1.02	5.00E-05
CG5793	596.58	1215.06	1.03	5.00E-05
Ugt35a	48.76	99.38	1.03	5.00E-05
cbt	48.18	98.44	1.03	5.00E-05
CG4592	27.75	56.81	1.03	5.00E-05
Est-6	19.13	39.49	1.05	5.00E-05
Cyp9b2	264.00	548.09	1.05	5.00E-05
CG14375	99.08	205.86	1.05	5.00E-05
CG6834	41.05	85.31	1.06	5.00E-05
Herp	66.89	139.37	1.06	5.00E-05
up	6.54	13.66	1.06	0.00095
CG3168	13.75	28.80	1.07	5.00E-05
CG9989	6.62	13.89	1.07	0.00465
Ser	1.39	2.93	1.08	0.00205
CG14131	5.98	12.66	1.08	0.00035
rho-4	3.49	7.43	1.09	0.00485
CG3775	57.84	123.18	1.09	5.00E-05
CG16713	689.44	1468.57	1.09	5.00E-05
CG6805	7.20	15.36	1.09	0.0001
Spec2	5.95	12.74	1.10	0.00025
CG12883	28.05	60.32	1.10	5.00E-05
CG32115	27.79	59.87	1.11	5.00E-05
Odc2	18.02	39.46	1.13	5.00E-05
CG31974	14.36	31.46	1.13	5.00E-05
CG6503	137.01	300.35	1.13	5.00E-05
Jhl-1	7.38	16.24	1.14	5.00E-05

CG8745	242.13	534.70	1.14	5.00E-05
Mhc	5.09	11.24	1.14	5.00E-05
retm	9.02	19.95	1.15	5.00E-05
CG18249	16.86	37.36	1.15	5.00E-05
CG11241	96.13	213.36	1.15	5.00E-05
CG8249	12.28	27.38	1.16	5.00E-05
CG2064	17.60	39.31	1.16	5.00E-05
CG3770	18.60	41.63	1.16	5.00E-05
CG4594	54.79	122.63	1.16	5.00E-05
GM130	19.44	43.52	1.16	5.00E-05
Prm	4.16	9.32	1.16	5.00E-05
Glycogenin	14.58	32.81	1.17	5.00E-05
CG9380	2.27	5.12	1.17	0.00445
FucTB	11.50	25.93	1.17	5.00E-05
Mlc1	7.07	16.00	1.18	0.00555
CG16712	4239.41	9600.83	1.18	5.00E-05
Cyt-c-p	196.81	447.29	1.18	5.00E-05
Pect	90.25	206.41	1.19	5.00E-05
CG13751	60.27	138.41	1.20	0.0003
GstD10	494.55	1137.03	1.20	5.00E-05
CG33691	4.95	11.42	1.21	5.00E-05
htt	3.89	9.00	1.21	5.00E-05
CG18347	18.75	43.41	1.21	5.00E-05
Nplp2	15518.10	35937.90	1.21	5.00E-05
CG4793	16.41	38.18	1.22	5.00E-05
CG33123	25.22	58.80	1.22	5.00E-05
scyl	31.36	73.21	1.22	5.00E-05
Yp3	347.88	814.03	1.23	5.00E-05
CG1600	113.75	266.48	1.23	5.00E-05
wts	5.30	12.41	1.23	5.00E-05
CG9674	14.76	34.83	1.24	5.00E-05
CG9231	14.14	33.48	1.24	5.00E-05
CG5953	1.78	4.23	1.25	0.0017
CG7224	398.74	948.39	1.25	5.00E-05
CG17681	5.45	13.32	1.29	0.00175
Ect3	70.22	172.71	1.30	5.00E-05
CG32280	66.97	164.88	1.30	5.00E-05
CG8034	11.91	29.32	1.30	5.00E-05
CG3568	3.65	9.02	1.31	0.0023
CG32335	7.88	19.56	1.31	0.0005
trbl	15.90	39.67	1.32	5.00E-05
CG1640	73.01	182.62	1.32	5.00E-05
shf	6.04	15.14	1.33	5.00E-05
CG42345	2.28	5.71	1.33	0.00035
kek1	6.54	16.46	1.33	5.00E-05
CG11198	137.92	349.10	1.34	5.00E-05
CG11784	30.58	77.42	1.34	0.00025
Ahcy89E	9.40	23.81	1.34	5.00E-05
CG33785	8.40	21.33	1.34	5.00E-05
Got1	149.36	379.73	1.35	5.00E-05
LpR2	1.15	2.94	1.35	0.00275
iPLA2-VIA	24.44	62.62	1.36	5.00E-05

RhoGDI	26.22	67.26	1.36	5.00E-05
Sodh-1	113.67	292.11	1.36	5.00E-05
pyd3	41.85	108.74	1.38	5.00E-05
Aats-ile	34.09	89.10	1.39	5.00E-05
CG18619	10.29	26.94	1.39	0.0055
CG11313	44.93	118.68	1.40	5.00E-05
CG33459	30.68	81.63	1.41	5.00E-05
Act5C	637.59	1713.69	1.43	5.00E-05
kal-1	49.16	132.17	1.43	5.00E-05
Acf1	1.07	2.90	1.43	0.00065
veil	3.82	10.37	1.44	5.00E-05
CG13962	452.80	1233.00	1.45	5.00E-05
lig3	10.50	28.61	1.45	5.00E-05
CG7763	230.37	628.20	1.45	5.00E-05
Aats-asn	104.60	285.69	1.45	5.00E-05
btsz	2.06	5.64	1.45	5.00E-05
CG16758	189.14	520.26	1.46	5.00E-05
Zw	51.77	143.42	1.47	5.00E-05
CG2611	67.67	187.71	1.47	5.00E-05
CG5704	4.58	12.81	1.49	0.00305
oys	33.43	93.93	1.49	5.00E-05
ppa	1.72	4.85	1.50	0.0008
JhI-26	75.34	212.97	1.50	5.00E-05
GstD7	125.00	353.44	1.50	5.00E-05
Tsp42El	23.68	67.26	1.51	5.00E-05
CG8229	24.79	70.49	1.51	5.00E-05
CG34348	65.74	188.01	1.52	5.00E-05
Kaz1-ORFB	73.42	211.87	1.53	5.00E-05
CG3902	718.98	2077.11	1.53	5.00E-05
Ubi-p5E	13.12	38.31	1.55	5.00E-05
CG17816	1.60	4.75	1.57	0.00265
CG12224	12.75	37.94	1.57	5.00E-05
stg	1.51	4.51	1.58	0.0019
CG11882	4.21	12.58	1.58	0.0043
CG9837	72.61	219.41	1.60	5.00E-05
Gs1	124.13	376.13	1.60	5.00E-05
lectin-28C	115.06	349.35	1.60	5.00E-05
CG2964	1.80	5.48	1.60	0.0041
Eip63F-1	2.11	6.42	1.60	0.00035
spir	3.54	10.78	1.61	5.00E-05
CG6830	1.30	3.97	1.61	0.0041
CG33226	15.54	47.80	1.62	0.0034
Dif	5.62	17.32	1.62	5.00E-05
CG10444	15.79	48.80	1.63	5.00E-05
lpp	2.82	8.83	1.65	0.00475
CG1607	1.89	5.93	1.65	0.0005
CG31248	25.82	81.44	1.66	5.00E-05
CG33199	42.26	134.10	1.67	5.00E-05
CG2017	29.23	93.02	1.67	5.00E-05
CG17278	14.61	46.97	1.69	5.00E-05
Sodh-2	141.58	455.79	1.69	5.00E-05
Ac78C	0.88	2.84	1.69	0.0002

Alas	59.77	198.72	1.73	5.00E-05
Cyp9f2	10.10	33.70	1.74	5.00E-05
Hex-C	5.54	18.53	1.74	5.00E-05
CG5288	81.05	272.10	1.75	5.00E-05
CG9505	9.12	30.74	1.75	5.00E-05
p24-2	6.45	21.76	1.75	0.0009
Epac	1.71	5.89	1.79	5.00E-05
CG17221	12.62	43.64	1.79	5.00E-05
CG3700	12.69	44.07	1.80	5.00E-05
Sip1	3.10	10.75	1.80	0.0005
Dgp-1	35.46	123.30	1.80	5.00E-05
slow	5.69	20.15	1.82	5.00E-05
Hexo1	2.25	8.03	1.83	0.0006
CG7433	1.51	5.47	1.86	0.0022
Tina-1	109.71	400.53	1.87	5.00E-05
Zasp52	4.24	15.54	1.87	5.00E-05
CG9119	38.98	142.79	1.87	5.00E-05
CG42868	128.98	474.35	1.88	5.00E-05
CG5618	2.73	10.06	1.88	0.0001
dnr1	1.33	5.03	1.92	0.0005
alpha-Est1	52.33	200.11	1.93	5.00E-05
daw	44.22	171.90	1.96	5.00E-05
Cyp4p3	4.79	18.63	1.96	5.00E-05
CG13936	3.75	14.60	1.96	5.00E-05
CG1140	73.24	287.66	1.97	5.00E-05
MtnA	92.47	364.25	1.98	5.00E-05
CG4250	9.35	37.97	2.02	0.0004
CG33510	4.33	17.85	2.04	5.00E-05
CG18622	1.94	8.10	2.06	0.00585
bgm	226.62	950.01	2.07	5.00E-05
Hmgs	23.28	97.59	2.07	0.0002
Tepl	6.89	28.91	2.07	5.00E-05
CG4259	9.41	39.97	2.09	5.00E-05
Cpr11A	2.70	11.80	2.13	0.0008
CG34232	5.63	24.66	2.13	0.00065
CG3921	0.38	1.71	2.19	5.00E-05
CG2641	9.97	47.58	2.25	5.00E-05
CG9928	6.39	31.46	2.30	0.00455
jp	0.30	1.51	2.33	0.00335
CG6812	0.78	3.93	2.34	0.0041
CG34054	10.93	55.40	2.34	5.00E-05
CG9512	65.23	331.82	2.35	5.00E-05
nrv3	0.67	3.41	2.35	0.00455
Cyp6d5	20.60	106.08	2.36	5.00E-05
CG11370	1.66	8.54	2.37	0.0024
CG14400	23.51	122.31	2.38	5.00E-05
Cyp309a1	30.65	167.14	2.45	5.00E-05
CG18431	0.95	5.21	2.46	0.0013
Dab	0.23	1.30	2.50	0.00125
CG9766	1.00	5.71	2.51	0.00525
Cyp6d2	2.63	15.47	2.56	0.0001
Jhl-21	10.81	64.37	2.57	5.00E-05

CG5321	24.97	152.49	2.61	5.00E-05
Inos	27.34	168.36	2.62	5.00E-05
Tsp96F	1.01	6.26	2.64	5.00E-05
CG4928	0.78	4.92	2.65	0.00065
l(2)01289	2.00	12.63	2.66	5.00E-05
CG10764	1.77	11.26	2.67	0.0003
CG32647	2.47	15.72	2.67	5.00E-05
CG32352	0.14	0.91	2.68	0.00455
Cyp12a4	11.34	72.78	2.68	5.00E-05
dally	1.80	12.10	2.75	5.00E-05
pncr009:3L	5.45	36.61	2.75	5.00E-05
melt	0.34	2.37	2.80	0.0046
CG33225	9.95	69.75	2.81	5.00E-05
asparagine-synthetase	178.17	1266.13	2.83	5.00E-05
CG15861	1.79	12.77	2.83	0.0008
CG14292	3.07	21.94	2.84	0.0034
Rbp6	0.29	2.16	2.92	0.00155
CG10814	1.65	12.78	2.96	5.00E-05
v(2)k05816	0.58	4.64	2.99	5.00E-05
CG14964	0.10	0.78	2.99	0.00485
CG11961	1.68	14.37	3.10	5.00E-05
GstD3	78.75	678.89	3.11	5.00E-05
CG17549	31.46	281.79	3.16	5.00E-05
Muc11A	3.81	35.15	3.21	5.00E-05
CadN	1.19	11.10	3.23	5.00E-05
dgo	0.12	1.17	3.23	0.00255
CG2663	0.13	1.26	3.26	0.0052
CG12974	0.27	2.60	3.27	0.00395
CG12520	1.16	11.22	3.27	0.00045
CG1358	0.07	0.68	3.30	0.00075
CG8665	50.87	533.87	3.39	5.00E-05
CG13077	0.86	9.48	3.47	0.0005
Tsp42Eg	10.69	118.23	3.47	5.00E-05
CG30438	0.17	1.90	3.51	0.00095
CG42335	0.52	5.92	3.51	0.00115
NaPi-T	0.57	6.56	3.51	0.00045
CG16727	0.82	9.53	3.54	0.0003
CG11892	1.88	22.36	3.57	5.00E-05
CG33511	0.27	3.23	3.59	0.0037
W	0.17	2.18	3.65	0.00025
Or83b	0.92	11.79	3.68	5.00E-05
Ipod	0.86	11.23	3.70	0.0015
Npc2f	41.49	560.92	3.76	5.00E-05
CG32284	0.88	12.06	3.77	0.00265
dpr12	0.20	2.80	3.82	0.00025
CG11236	2.68	38.23	3.83	5.00E-05
Mur18B	3.53	51.35	3.86	5.00E-05
Scp2	4.48	65.84	3.88	5.00E-05
CG10514	1.66	24.69	3.90	5.00E-05
CG42390	0.56	8.66	3.95	5.00E-05
CG6125	0.31	4.72	3.95	0.0024
Tehao	0.28	4.45	3.97	5.00E-05

CG14669	0.21	3.45	4.02	0.0054
Cyp12d1-p	0.20	3.64	4.17	0.0009
Mipp1	0.42	7.68	4.18	0.0002
CG15406	0.52	9.56	4.21	0.00245
CG5697	0.20	4.13	4.37	0.0043
Rhp	0.26	6.05	4.56	0.0043
CG42807	7.21	183.39	4.67	5.00E-05
CG9259	1.13	31.47	4.80	5.00E-05
kar	8.52	248.33	4.87	5.00E-05
CG5853	3.19	94.92	4.90	5.00E-05
CG42256	0.01	0.35	5.21	0.00015
Uro	1.62	62.58	5.27	5.00E-05
Cyp6a2	1.11	43.43	5.29	5.00E-05
TepIV	21.06	943.37	5.49	5.00E-05
Glut1	0.49	24.15	5.63	5.00E-05
Sox21a	0.21	10.39	5.64	5.00E-05
CG4716	5.62	287.76	5.68	5.00E-05
CG8539	0.21	11.00	5.73	0.00045
CG10073	0.22	12.27	5.82	5.00E-05
CG42784	0.03	1.88	5.84	0.00395
CG18088	0.05	32.37	9.24	0.00555

Appendix II

Metabolomic analysis of *daw* mutant, control and rescued animals

Table 3: Metabolites that changed significantly in *daw* mutants

Metabolite	w^{1118}	$daw^{1/+}$	$daw^{1/11}$	p Value (w^{1118} vs $daw^{1/11}$)	p Value ($daw^{1/+}$ vs $daw^{1/11}$)
2-KETOGLUTARIC ACID	165.03	227.88	731.41	6.84304E-07	2.3088E-06
FUMARIC ACID	1094.78	2120.88	4391.50	4.57759E-12	6.93251E-10
KYNURENIC ACID	6.73	2.69	23.24	2.89739E-07	4.3031E-09
PYRUVIC ACID	47.20	50.91	152.00	9.4797E-08	2.02032E-07
2-HYDROXYGLUTARATE	170.83	254.95	459.58	0.000518535	0.013292859
LACTIC ACID	108.80	127.19	286.43	1.61058E-05	0.000125954
PROLINE	259.63	355.80	654.81	4.23399E-05	0.00044123
MALEIC ACIDD	10.94	8.79	27.52	0.042996267	0.007334776
SUCCINIC ACID	417.66	548.13	908.66	9.08981E-05	0.000995913
MALIC ACID	678.70	1107.54	1350.83	4.04794E-07	0.003442133
PHOSPHOGLYCEROL	18348.18	26150.13	33752.32	6.00909E-06	0.003010881
SARCOSINE	249.96	148.00	452.48	0.009411255	0.000319751
GLUTAMIC ACID	1232.52	1730.63	2220.60	0.001308593	0.034461765
GLUCOSE-1-PHOSPHATE	503.10	665.75	901.69	0.000248519	0.005738014
GLUCOSE-6-PHOSPHATE	1036.26	1303.71	1819.48	0.000488572	0.005079255
ALANINE	59.77	43.78	91.30	0.004365965	9.83012E-05
THREONINE	445.01	451.77	670.52	0.001140642	0.001322886
N-ACETYLGLUTAMATE	5.53	5.15	7.56	0.009520861	0.005961834
CHLOROGENIC ACID	8.04	8.22	10.33	0.029237344	0.025451283
SERINE	1329.05	1332.89	1070.75	0.038814879	0.014492513
2-METHYLCITRATE	20.77	23.01	13.41	0.001231365	6.46623E-05
UREA	468.52	425.21	293.29	0.017772342	0.039009571
ADENOSINE	56.10	46.88	35.05	0.006407944	0.006543595
SORBITOL	502.24	319.96	242.16	0.016528562	0.012549088
TRYPTOPHAN	2981.49	3076.08	1430.40	1.67651E-05	1.90177E-05
PHOSPHOETHANOLAMINE	389.90	227.78	165.95	0.000310896	0.011857815
TYROSINE	1578.20	1567.60	655.08	2.86271E-07	1.18003E-07
MANNITOL	115.47	80.01	46.58	9.37004E-07	5.01032E-05
RIBITOL/XYLITOL	43.69	22.12	16.60	1.68726E-06	0.001140791
METHIONINE	748.48	627.50	248.57	4.84584E-06	0.00029275
ORNITHINE	2778.49	1756.96	669.53	3.60723E-08	3.79136E-07
HOMOSERINE	516.41	73.75	99.05	5.16287E-09	0.006127233
2-AMINOADIPIC ACID	141.31	95.55	27.10	8.26712E-06	2.83578E-07
HOMOCYSTEINE	143.75	74.31	20.30	7.1423E-05	2.21825E-05
PANTOTHENIC ACID	49.83	47.79	3.84	4.27548E-08	9.57413E-14
URIC ACID	2710.83	536.01	88.74	1.09577E-05	2.73697E-06

P.S: Values shown are normalized to total mass of the samples in mg. Orange: metabolies that were up-regulated, Purple: metabolites that were down-regulated. *n = 8* samples per genotype with each sample containing 15 mid third instar larvae.

Table 4: Metabolites that changed significantly in FB-Gal4>*babo*^{CA} rescued animals.

Metabolite	*daw*^{11}; *UAS-babo*^{CA}/+	*daw*^{11}; *FB-Gal4>babo*^{CA}	p Value
FUMARIC ACID	1886.56	341.47	3.32307E-11
2-KETOGLUTARIC ACID	206.96	49.92	7.81026E-09
2-HYDROXYGLUTARATE	87.72	21.97	1.50896E-07
MALIC ACID	1405.20	385.31	1.57752E-12
PYRUVIC ACID	364.60	113.63	3.13668E-07
PHOSPHOGLYCEROL	3314.64	1209.84	1.05466E-10
SEDOHEPTULOSE-7-P	742.05	279.29	3.55323E-06
HOMOSERINE	101.49	39.04	0.000481617
LACTIC ACID	79.81	32.98	1.13081E-05
GLUCONIC ACID	2.39	1.04	0.000625109
SUCCINIC ACID	284.59	154.08	6.4534E-07
PROLINE	294.18	188.93	0.034875365
CITRIC ACID	298.45	202.02	8.06185E-07
GLYCEROL	446.50	302.42	0.000480892
ISOCITRIC ACID	41.32	28.19	0.036800303
GLUTAMIC ACID	505.32	357.26	0.000545458
URIC ACID	47.77	33.86	0.032087711
1-MONOPALMITOLYLGLYCEROL	5.54	4.07	0.002802307
THREONINE	1424.67	1078.76	6.36175E-05
GLUCOSE-6-PHOSPHATE	380.35	293.79	0.032640246
PHOSPHATE	1528.38	1314.62	0.001464929
LYSINE	3459.28	3841.44	0.03647346
MANNITOL	20.69	25.87	0.03588341
2-PHOSPHOGLYCERATE	2.65	3.34	0.034457672
UREA	894.30	1132.65	0.030001039
B-ALANINE	2201.86	2804.23	0.000397703
GLYCERIC ACID	3.33	4.64	5.74706E-05
4-AMINOBUTYRATE	60.36	85.67	0.014917927
URACIL	15.25	22.12	0.045411202
DHAP	4.04	6.10	0.004575078
ADENOSINE	11.52	17.45	0.035677386
GLYCINE	164.09	264.88	3.90927E-05
PHOSPHOETHANOLAMINE	53.57	87.23	2.26782E-05
3-PHOSPHOGLYCERATE	54.44	95.09	0.000117853
TRYPTOPHAN	448.06	958.17	0.000217579
PHENYLALANINE	206.79	527.19	4.12385E-06
TYROSINE	188.14	550.50	3.84241E-09
PANTOTHENIC ACID	2.55	8.16	2.09619E-06
ORNITHINE	189.86	656.00	0.000392143
2-AMINOADIPIC ACID	17.27	80.96	3.78091E-05
METHIONINE	103.26	1176.98	6.36852E-09
HOMOCYSTEINE	3.36	46.07	1.55419E-07

P.S: Values shown are normalized to total mass of the samples in mg. Orange: metabolites that were up-regulated, Purple: metabolites that were down-regulated. *n = 8* samples per genotype with each sample containing 15 mid third instar larvae.

Appendix III

Smox is required for dFOXO nuclear localization in starved larval fatbody

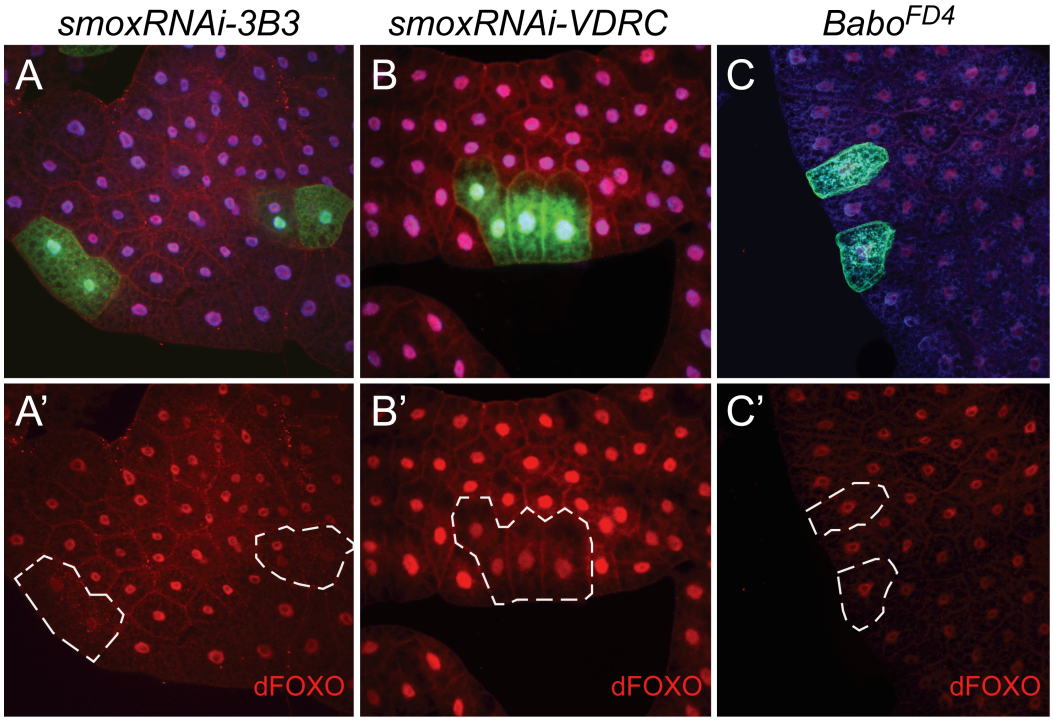

Figure 38: Smox is required for dFOXO nuclear localization

To test the role of TGF-β signaling in dFOXO nuclear localization Smox-RNAi or babo null clones were generated in larval fatbody. The larvae were grown to mid third instar stages and starved to induce nuclear localization of dFOXO. Fatbody were subsequently stained with anti-dFOXO (Red) antibodies and localization in the clones were compared to surrounding control cells. Cones were identified as GFP positive cells. (A-A') dFOXO nuclear localization is inhibited in fatbody cells expressing a Smox-RNAi construct generated in our laboratory. (B-B') dFOXO nuclear localization is inhibited in fatbody cells expressing a Smox-RNAi construct generated by VDRC. (C-C') dFOXO nuclear localization is not affected in fatbody cells that are mutant for the type-I receptor Babo.

Appendix IV

Genes & Development

From: Arpan Ghosh <ghos0056@umn.edu>
Sent: Friday, August 16, 2013 9:35 AM
To: Genes & Development
Subject: Copyright permission

Hi,

I am preparing my doctoral thesis at the University of Minnesota and would like to include the materials (Figures, Tables and Text) from the following publication:

Ghosh A, McBrayer and O'Connor MB. (2010). The Drosophila gap gene giant regulates ecdysone production through specification of the PTTH-producing neurons. Dev Biol. 2010 Nov 15;347(2):271-8.

How can I get the official permission document to use the material from this paper?

Thank you.
Arpan Ghosh
****

Grad Student
Dr. Michael O'connor lab
University of Minnesota, Twin Cities
5-235 Moos Tower
515 Delaware St. SE
Minneapolis, MN-55455